TIME DOMAIN METROLOGY FOR DIELECTRIC SPECTROSCOPY OF PARTICULATES

by

Robert Bruce Stafford

Dissertation submitted to the Faculty of the
Virginia Polytechnic Institute and State University
in partial fulfillment of the requirements for the degree
of
DOCTOR OF PHILOSOPHY
in
Electrical Engineering

APPROVED:

S. M. Riad, Chairman

I. A. Besieris

G. E. Brown

T. C. Poon

N. S. Nahman

September, 1992

Blacksburg, Virginia

TIME DOMAIN METROLOGY FOR DIELECTRIC SPECTROSCOPY OF PARTICULATES

by

Robert Bruce Stafford

Committee Chairman: Sedki M. Riad
Electrical Engineering

(ABSTRACT)

Several methods for evaluating the permittivity of soil samples using measurements in the time domain were studied. A number of algorithms for inverting the measured data to obtain epsilon were investigated and three different types of sampling devices were examined.

The investigation examined the positive and negative aspects of three different types of sample holders to determine a method of obtaining dielectric information from in-situ time domain measurements. A scheme using a twin lead balun driven ground probe was proposed and analysed with regard to accuracy and sensitivity to measurement error.

ACKNOWLEDGEMENTS

In the course of this work I have received aid and encouragement from a large number of people. I would first like to thank my advisor, Dr. Sedki Riad, who not only stood by me during the days of my master's work but has exhibited nearly infinite patience with my difficult progress in this investigation. Indeed, it is precisely this quality which drew me to him originally and I hope that he feels his investment of time in me to be worthwhile.

I must also thank another person who has contributed more than generously of his time and resources, my advisor's advisor and my committee member and 'local advisor', Dr. Norris Nahman. I truly believe that I would not have been able to carry this work to its conclusion without the many hours of talks and explanations that he has provided me.

My committee members, Doctors Besieris, Brown, and Poon have been very patient with me and I thank them for their indulgence. I was assisted by the use of laboratory facilities kindly provided by William Gans of the National Institute of Standards and Technology, and also received assistance from Picosecond Pulse Labs and Dr. James Andrews. Several friends also offered help and encouragement, among

them Dr. Douglas Hopkins, Dr. Mark Nelms, both of Auburn University, Dr. Arun Majumdar and Nicholas Paulter of the National Institute of Standards and Technology, and Dale Severance of the University of Colorado at Boulder.

Finally I must thank my staunchest supporter and ally, my wife Suzanne, who I think must have often felt herself in the position of a passenger in a car driven by a madman. She has seen me through the highs and numerous lows of this research and has always maintained her faith that it would eventually reach a conclusion. To her, my son Christopher, and my family who thought that this work would never end I offer my love and thanks.

TABLE OF CONTENTS

LIST OF FIGURES

Figure

LIST OF TABLES

Table

CHAPTER I

INTRODUCTION

Dielectric characterization reached its peak shortly after World War II with the classic works of Von Hipple and Westphall. Interest in this research fell off during the decades of the 60's and 70's but has experienced a resurgence in the 80's due to digital technology, the stealth program, and advances in radar technology, to name a few influences.

On the other hand, time domain metrology got its first real beginning during the testing of the first transatlantic cable in 1858 when it was found that telegraph pulses ran together and became indistinguishable from one another above a very small repetition rate.

In this work, several time domain methods for characterizing dielectric permittivity have been investigated. Various types of sample holders and probes as well as the mathematical models describing them are presented. A balanced line twin lead probe which may be used for in-situ measurements of soil samples is characterized and measurements made with this probe of several types of soils are performed.

In this dissertation, the investigation results of three different types of soil measurement systems are provided. Experimental results as well as mathematical analysis and error investigation of these systems from a time domain metrology viewpoint are presented. Finally, conclusions and recommendations for future work will be presented.

This chapter begins with a short history of time domain metrology, particularly as it applies to dielectric measurements. Some of the difficulties implicit in time domain schemes as opposed to frequency domain, as well as some of the advantages, are discussed. The chapter also describes the particular dielectric characterization problem with a review of various previous techniques.

TIME DOMAIN GENERAL HISTORY

The earliest true application of time domain metrology was probably at the time of the first transatlantic cable. It was noticed that telegraph pulses at even moderate rates would become hopelessly garbled and indistinguishable from one another at the receiving end. This early transmission line was quite dispersive and the pulses were losing so much of their high frequency content that they were overlapping one another. Effects of this nature eventually lead to

Heaviside's formulation of the telegrapher's equations and Heaviside's Operational Calculus.

In order to make a step response characterization one must be able to produce transient waveforms whose transition duration is considerably shorter than the transient response of the system under investigation. Although the transition duration of those early pulses was of the order of milliseconds, the response time of the system under investigation was longer and so these conditions were met. For a long time following this period repeatable short transition duration pulses of the order of microseconds and therefore suitable for high frequency structures were difficult or impossible to produce. Therefore, time domain metrology was restricted to the study of large structures having slow response times such as cables or large networks either by studying reflected (time domain reflectometry) or transmitted pulses in those structures.

Today, broadband sampling oscilloscopes provide the technology for observing transition durations of tens of picoseconds. In a sampling oscilloscope, the value displayed at any given sampling time is proportional to the signal being sampled integrated over the sampling aperture time. Long sampling apertures mean long integration period and loss of fine structure and time resolution of the oscilloscope.

Thus, today's sampling oscilloscopes have extended time domain metrology to 20 GHz. and up.

Sampling oscilloscopes are equivalent time sampling systems. Equivalent time sampling requires a repeatable signal and a trigger signal which is precisely time locked to that signal (sometimes derived from the signal itself). A sample is first taken at the time of the trigger signal. During the next repetition a precise delay is inserted between the time of the trigger signal and the time the sample is taken. This delay is increased incrementally on each succeeding signal repetition until the whole waveform has been sampled at which time the process repeats itself. In this fashion, a modern equivalent time sampling oscilloscope allows a time base resolution of 0.25 picoseconds although the sampling rate is 500 kilo samples per second or less. However, the aperture time is roughly two orders larger - about 10 ps.

PRIOR WORK ON DIELECTRIC CHARACTERIZATION

The majority of techniques used for dielectric characterization do not differentiate between data which was originally obtained using frequency domain methods such as a network analyzer, and data derived from time domain measurements. In general, the time domain derived data is

Fourier transformed into the frequency domain before it is used. This is logical, since the parameter usually sought, complex permittivity, is a function of frequency. However, a few schemes either actually take place in the time domain or depend upon special characteristics of time domain metrology such as windowing or the ability to observe transients rather than steady state effects.

Another common thread in time domain dielectric characterization, as well as dielectric characterization in general, is the use of coaxial lines as integral parts of the measurement system. Coaxial lines are often used as sample holders, where the sample is in the shape of an annular ring which forms the dielectric for some portion of the line, and where the line may be matched terminated (in its original characteristic impedance) or it may be terminated in an open or a short. Another possibility is the lumped capacitance configuration, where the sample provides the connection between the inner conductor and a short circuit termination on the outer conductor. Alternatively, the line may be open-ended and simply pressed against the sample. Each of these schemes as well as others using other geometries, will be discussed in the following paragraphs.

The match terminated line was the earliest sample holder used in time domain work. Fellner-Feldegg [1] used it in a scheme which evaluated reflection information directly in the

time domain to derive Debye parameters (high and low frequency permittivity and relaxation time). The author pointed out in a later work [2] that the earlier work was not accurate for dispersive dielectrics, and he corrected this work using several terms of a Taylor series expansion of the Laplace Transform of the sample time domain response.

This approach, known as the total reflection method, has also been used by several authors who have used improved Taylor series expansions of either the time domain dielectric response [3,4,5], or a Taylor series expansion of the frequency domain response [4,6,7,8] to solve for the permittivity analytically. The original equation for S_{11}

$$S_{11}(\omega) = \frac{(1-e^{-2\gamma l})\,\rho}{1-\rho^2 e^{-2\gamma l}}$$
$$\text{where} \quad \rho = \frac{1-\sqrt{\epsilon_R(\omega)}}{1+\sqrt{\epsilon_R(\omega)}} \qquad (1.1)$$
$$\text{and} \quad \gamma(\omega) = j\frac{\omega\sqrt{\epsilon_R(\omega)}}{c}$$

may also be solved numerically [9,10], but the presence of multiple roots imposes some restrictions on this method.

A paper by Nicholson [11] showed how to evaluate the S-parameters through time domain measurements and the Fourier transform and in a later work [12], Nicholson and Ross gave a scheme which used both reflection and transmission time domain measurements to produce a closed form solution for

both the permittivity and the permeability. This method was later used by Fellner-Feldegg [13] to evaluate Debye parameters and by Weir [14] who used frequency domain measurements and phase information to remove an ambiguity in the original scheme. More recently, Baker-Jarvis has used the same frequency domain information with a numerical root finding scheme which removes instabilities in the analytical expression but is limited to non-magnetic materials [15].

Another geometry that is quite commonly used for dielectric characterization is the open circuited coaxial sample holder. This is a coaxial line which is open (and therefore unterminated) at one end to allow it to be filled with the sample of interest. The center conductor is typically recessed to allow any evanescent fields to dissipate within the sample. Investigators who have used this type of probe to advantage include Bussey [16], Scott and Smith [17], and Cahine and Bose [18].

If the outer conductor of the open circuited probe is degenerated to zero length, one is left with the open ended probe. This probe is very popular with investigators making biological measurements but must be calibrated very carefully to characterize the complex end fields of the abruptly terminated coaxial line. This geometry has been used quite extensively by several researchers [19,20,21,22,23,24,25,26,27,28,29,30,31,32].

The short circuit terminated coaxial sample holder has been used extensively by investigators working directly in the frequency domain. It is known as the Roberts-Von Hipple method, but it is not popular with researchers working in the time domain. An analysis by Cole using an admittance model for the short circuit terminated holder [8] indicates that the measured waveform is nearly independent of the sample permittivity at low frequencies. Time domain analysis places an emphasis on baseband information, so this effect may account for the unpopularity of this configuration [23,33,34,35,36,37].

If the coaxial center conductor is slightly shorter than the length of the outer conductor, the sample may be used to capacitively bridge the gap between the center conductor and a short circuit termination. This method is known as the lumped capacitance or sample terminated cell and has been used with some success in both the time domain and the frequency domain to study the properties of very small volumes of liquid samples such as liquid crystals [3,5,7,21,23,38,39,40,41,42].

It is also possible to use non-coaxial geometries for dielectric characterization, although such geometries are not often used in time domain work. Cavity resonators are often used in frequency domain studies to achieve very precise measurements at high frequencies. In these devices, the

introduction of the sample perturbs the resonant frequency of the cell, an effect which can be measured and characterized with high accuracy. Unfortunately, their inability to be used for baseband measurements makes them unattractive for time domain work. Non-coaxial waveguides suffer from the same limitation.

Two non-coaxial geometries which have seen somewhat limited use in this type of work are the monopole probe and the dipole probe. The complex field configuration of the monopole makes it less attractive for this type of study than the dipole, but at least two researchers have reported good results using this method [43,44]. It's mechanical characteristics are well suited to in-situ measurements, since only one borehole needs to be drilled in ice or frozen soil, but mathematical manipulation of the resulting measurement requires the use of analytical continuation and may become somewhat involved.

The dipole probe, typically configured as a two-pronged fork, has been used to study soils and ice. It appears to have been generally used with frequency domain measurements [45,46,47], but has also seen limited use in the time domain [48]. It may be driven in either a balanced or unbalanced mode, and is sometimes short circuited at one end as part of the procedure.

PROBLEM STATEMENT

The purpose of this study is to analyze and implement a dielectric probe which may be used for time domain in-situ studies of soils. The need for this device grew from a study funded by the U.S. Army which attempted to characterize landmine detectors accurately and in a repeatable manner. In the course of the army study, it became clear that no efficient method for making in-situ measurements of soil dielectric parameters existed.

A number of laboratory schemes for dielectric measurements may be applied to soil samples, but these methods require disturbing the medium and transporting the sample, with the subsequent danger of changing its moisture content and the virtual certainty that the sample measured will not have the same packing characteristics and moisture gradient as the original environment. The choice of time domain over frequency domain methods was dictated by the necessity that any in-situ scheme be rugged and able to withstand at least moderate variation in temperature and other environmental parameters. Precisely tuned oscillators and systems such as those found in a frequency domain network analyzer tend to lose calibration rapidly under these conditions.

Time domain instrumentation is inherently simpler in design and is intrinsically 'calibration resistant' to environmental constraints because of the use of digital circuitry and a much stronger dependance upon digital signal processing techniques to evaluate the signal being measured. The equipment used is also less expensive and is simpler in design.

Arguably, time domain measurements of this type do not as yet produce the accuracy of some frequency domain methods. This is probably due to the inherently wide bandwidth of time domain measurements (12-20 GHz) which allows much more noise in the measurements as compared to the 10 to 20 kHz bandwidth used by modern frequency domain network analyzers. This wide bandwidth characteristic of time domain measurements is also what makes measurements over a wide frequency range so rapid, and, in any case, is inherent in the measurement philosophy itself. Furthermore, for this particular application of a bulk half-space measurement, the accuracy is much more strongly constrained by other factors, such as limits on the homogeneity of the sample medium.

In this study, three different dielectric measurement configurations have been examined. Initial investigations began with a match terminated coaxial system in order to identify problems associated with the use of time domain. The match terminated system is unique among the systems

discussed since it allows both reflection and transmission measurements and this extra information was felt to be useful in characterizing the technique.

The open ended coaxial holder was investigated next, in an attempt to simulate the in-situ probe while maintaining the coaxial structure and the field confinement it provides. This scheme was also useful in the development of the numerical algorithms needed to extract dielectric information from a pure reflection measurement.

The in-situ probe was designed as a twin lead transmission line driven in a balanced configuration through the use of a balun transformer which also matched the impedance of the twin lead probe to the 50 ohm impedance of the line. The balun provided a major obstacle to clean measurements in the time domain, but this type of probe was the only one available to the author at the time of the study.

The next chapter will cover the mathematical basis for this type of time domain measurements. It will also detail some of the experimental considerations required in the implementation of these measurements.

CHAPTER II

MATHEMATICAL BASIS AND EXPERIMENTAL CONSIDERATIONS

In this chapter the mathematical basis for these measurements is presented as well as a discussion of some of the experimental considerations involved in this type of measurement. Initially the mathematical theory of transmission lines will be presented, followed by a discussion of scattering and impedance parameters. This will lead to an investigation of some of the analysis tools used to derive permittivity information from the raw time domain data. The latter portion of this chapter describes how the samples were prepared and what steps were taken to evaluate and assure repeatability in these measurements.

MATHEMATICAL BASIS
TRANSMISSION LINE THEORY

As all three measurement systems to be discussed in this thesis will be modeled as transmission lines, a brief review of transmission line theory will be given.

A transmission line may be modeled (after Heaviside) as a ladder network consisting of an infinite series of

identical lumped-parameter elements. Each of these elements is composed of a series inductance L, a series resistance R, a shunt capacitance C, and a shunt conductance G. Normally the values of the lumped parameter elements are given on a per-unit-length basis. Evaluating the differential change in voltage and current versus distance for one element gives:

$$\frac{\partial v(z,t)}{\partial z} = -R*i(z,t) - L*\frac{\partial i(z,t)}{\partial t} \qquad (2.1)$$

$$\frac{\partial i(z,t)}{\partial z} = -G*v(z,t) - C*\frac{\partial (v(z,t)}{\partial t} \qquad (2.2)$$

For steady-state sinusoidal excitation, these equations can be expressed in terms of phasor notation as:

$$\frac{dV(z)}{dz} = -(R+j\omega L)*I(z) \qquad (2.3)$$

$$\frac{dI(z)}{dz} = -(G+j\omega C)*V(z) \qquad (2.4)$$

Each of these equations may be differentiated and substituted into the other to yield:

$$\frac{d^2V(z)}{dz^2} - (R+j\omega L)(G+j\omega C)*V(z) = 0 \qquad (2.5)$$

$$\frac{d^2I(z)}{dz^2} - (R+j\omega L)(G+j\omega C)*I(z) = 0 \qquad (2.6)$$

The general solutions to these second-order linear differential equations are:

$$V(z) = V_1 e^{-\gamma z} + V_2 e^{+\gamma z} \tag{2.7}$$

$$I(z) = I_1 e^{-\gamma z} + I_2 e^{+\gamma z} \tag{2.8}$$

where

$$\gamma = \sqrt{(R+j\omega L)(G+j\omega C)} \tag{2.9}$$

is the transmission coefficient of the line. The two exponential functions represent traveling waves propagating in opposite directions, $\exp(-\gamma z)$ corresponding to a wave propagating in the positive z direction, while $\exp(+\gamma z)$ corresponds to wave propagation in the negative z direction.

Consider the case for wave propagation only in the positive direction i.e., $V_2=I_2=0$. This represents a line terminated in it's characteristic impedance, Z_0. An expression for Z_0 may be derived using the above equations.

$$\begin{aligned} V(z) &= V_1 e^{-\gamma z} \\ I(z) &= -\frac{dV(z)}{dz} / (R+j\omega L) \\ &= \gamma V(z) / (R+j\omega L) \\ &= \sqrt{(R+j\omega L)(G+j\omega C)} \cdot V(z) / (R+j\omega L) \\ &= \sqrt{\frac{G+j\omega C}{R+J\omega L}} \cdot V(z) \end{aligned} \tag{2.10}$$

From this follows

$$Z_0 = \frac{V(z)}{I(z)} = \sqrt{\frac{R+j\omega L}{G+j\omega C}} \qquad (2.11)$$

Under the assumption of TEM propagation and perfect conductors in the line (R=0) the parameters become

$$\gamma = \pm j\omega\sqrt{LC} = \pm j\omega\sqrt{\mu\epsilon} \qquad (2.12)$$

$$Z_0 = \sqrt{\frac{L}{C}} = \sqrt{\frac{\mu}{\epsilon}} \qquad (2.13)$$

The equivalence between the lumped circuit representation and the material parameter representation occurs because the inductance per unit length of the line (L) is directly proportional to the permeability of the medium in which the transmission line conductors are embedded and the same holds true for the capacitance per unit length (C) and the material permittivity.

Next the line impedance Z(z) and reflection coefficient $\rho(z)$ will be defined. From equation 2.10 I(z) may be defined as

$$
\begin{aligned}
I(z) &= -\frac{1}{R-j\omega L}\frac{dV(z)}{dz} \\
&= -\frac{\gamma}{R+j\omega L}\left(-V_1 e^{-\gamma z}+V_2 e^{+\gamma z}\right) \\
&= \sqrt{\frac{G+j\omega C}{R+j\omega L}}\left(V_1 e^{-\gamma z}-V_2 e^{+\gamma z}\right) \\
&= \frac{1}{Z_0}\left(V_1 e^{-\gamma z}-V_2 e^{+\gamma z}\right)
\end{aligned}
\qquad \textbf{(2.14)}
$$

Now the impedance at any point on the line may be evaluated

$$
Z(z) = \frac{V(z)}{I(z)} = Z_0 \frac{\left(V_1 e^{-\gamma z}+V_2 e^{+\gamma z}\right)}{\left(V_1 e^{-\gamma z}-V_2 e^{+\gamma z}\right)} \qquad \textbf{(2.15)}
$$

The reflection coefficient $\rho(z)$ is defined as the ratio of the reflected voltage to the incident voltage:

$$
\rho(z) = \frac{V_2 e^{+\gamma z}}{V_1 e^{-\gamma z}} \qquad \textbf{(2.16)}
$$

Algebraic manipulation yields

$$
Z(z) = Z_0 \frac{1+\rho(z)}{1-\rho(z)} \qquad \textbf{(2.17)}
$$

$$\rho(z) = \frac{\left(\frac{Z(z)}{Z_0} - 1\right)}{\left(\frac{Z(z)}{Z_0} + 1\right)} \qquad (2.18)$$

A number of parametric two-port transmission line representations exist. These may be based on power measurements (S and T parameters) or on measurements of voltages and currents (Z and Y parameters). The scattering parameter representation will be examined first, followed by the transmission parameter model, which is similar. Impedance and admittance parameters will then be discussed.

The basic S parameter model is given in figure 2.1 where a_1 and b_1 are defined as:

$$a_1 = V_1 \frac{e^{-\gamma z}}{\sqrt{Z_0}} \qquad (2.19)$$

$$b_1 = V_1 \frac{e^{+\gamma z}}{\sqrt{Z_0}} \qquad (2.20)$$

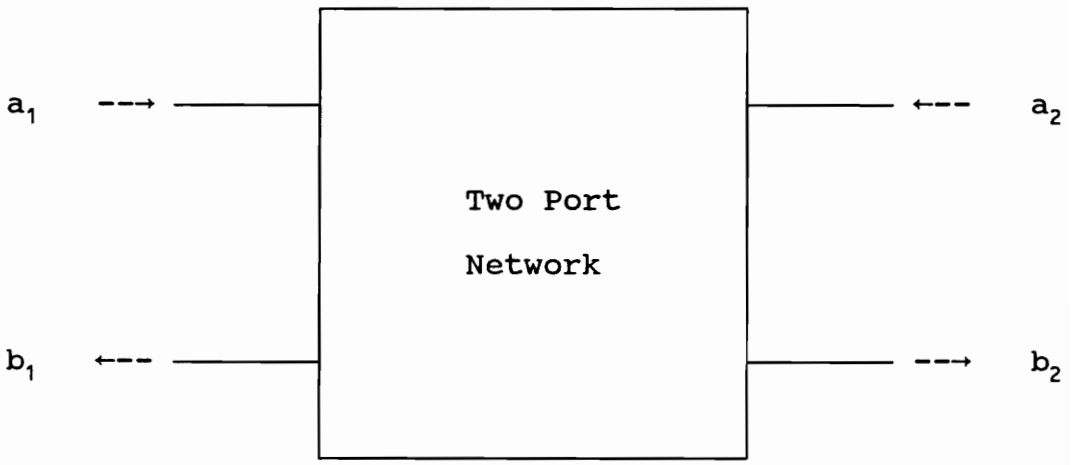

Figure 2.1: The Scattering Parameter Model

and a_2 and b_2 are similarly defined:

$$a_2 = V_2 \frac{e^{-\gamma z}}{\sqrt{Z_0}} \qquad (2.21)$$

$$b_2 = V_2 \frac{e^{+\gamma z}}{\sqrt{Z_0}} \qquad (2.22)$$

Note that z is measured from the right hand end of the line in these definitions.

The S parameter matrix equation is

$$\begin{bmatrix} b_1 \\ b_2 \end{bmatrix} = \begin{bmatrix} S_{11} & S_{12} \\ S_{21} & S_{22} \end{bmatrix} \begin{bmatrix} a_1 \\ a_2 \end{bmatrix} \qquad (2.23)$$

and the T parameter equation is

$$\begin{bmatrix} a_2 \\ b_2 \end{bmatrix} = \begin{bmatrix} T_{11} & T_{12} \\ T_{21} & T_{22} \end{bmatrix} \begin{bmatrix} a_1 \\ b_1 \end{bmatrix} \qquad (2.24)$$

It is clear that the T parameter matrix for a network of series connected transmission lines may be found by multiplying together the T matrices of the constituent individual networks.

The impedance and admittance models for transmission lines are illustrated in figure 2.2. Note that the output

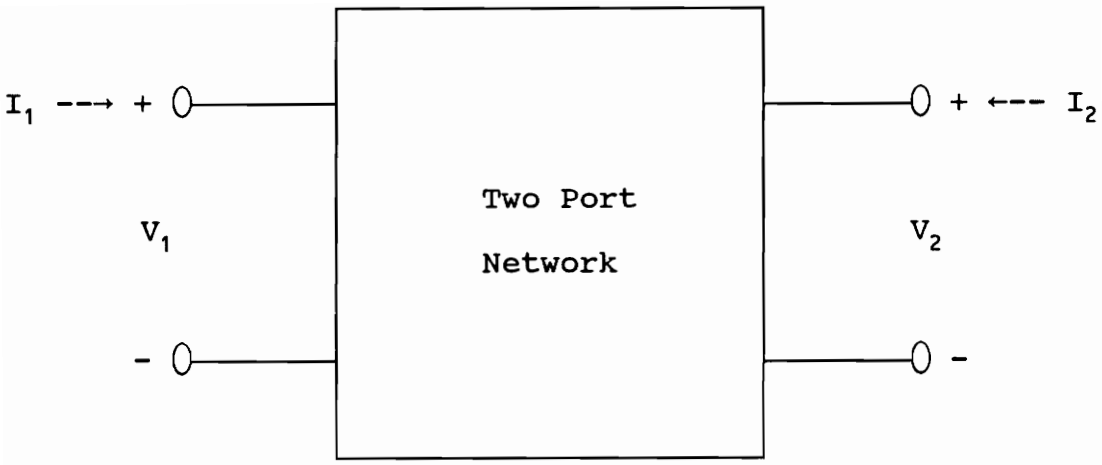

Figure 2.2: The Impedance and Admittance Model

current I_2 is defined positive entering the network. The relevant matrix equations are:

$$\begin{bmatrix} V_1 \\ V_2 \end{bmatrix} = \begin{bmatrix} Z_{11} & Z_{12} \\ Z_{21} & Z_{22} \end{bmatrix} \begin{bmatrix} I_1 \\ I_2 \end{bmatrix} \qquad (2.25)$$

and

$$\begin{bmatrix} I_1 \\ I_2 \end{bmatrix} = \begin{bmatrix} Y_{11} & Y_{12} \\ Y_{21} & Y_{22} \end{bmatrix} \begin{bmatrix} V_1 \\ V_2 \end{bmatrix} \qquad (2.26)$$

The final conceptual tool which has proved useful in this work is the *bounce diagram*. (This is called the reflection-transmission diagram in [49]). This device helps to clarify the effects caused by the finite propagation velocity of the wavefront in the transmission line and also produces a mathematical description of the reflected and transmitted signals in terms of ρ and γ.

The bounce diagram, which graphically depicts the action of a wavefront traveling through and reflecting from regions of different characteristic impedances and propagation constants, is easily constructed through the application of three rules.

1. A wavefront which encounters a region of different characteristic impedance from that in

which it is traveling is split into two wavefronts, one of which is reflected back towards the source.

2. The reflected portion of the wavefront is multiplied by ρ and the transmitted portion of the wavefront is multiplied by $(1+\rho)$.

3. A wavefront traveling through a region of length l with propagation constant γ is multiplied by $\exp(-\gamma l)$.

The application of these rules is shown in figures 2.3 and 2.4. The case of a transmission line with a central section of unknown characteristic impedance and propagation constant is given in figure 2.3, and that of a transmission line terminated in a perfect open circuit is given in figure 2.4.

From figure 2.3 it is clear that the total reflection (S_{11}) from a line with an unknown, centrally located dielectric section is:

$$\begin{aligned} S_{11} &= \rho + (1-\rho^2)(-\rho)e^{-2\gamma l} + (1-\rho^2)(-\rho)^3 e^{-4\gamma l} + (1-\rho^2)(-\rho)^5 e^{-6\gamma l} + \ldots \\ &= \rho\left[1 - (1-\rho^2)e^{-2\gamma l}\left[1 + (\rho^2 e^{-2\gamma l}) + (\rho^2 e^{-2\gamma l})^2 + \ldots\right]\right] \\ &= \rho\left[1 - \frac{(1-\rho^2)e^{-2\gamma l}}{1-\rho^2 e^{-2\gamma l}}\right] \\ &= \frac{(1-e^{-2\gamma l})\rho}{1-\rho^2 e^{-2\gamma l}} \end{aligned} \qquad \textbf{(2.27)}$$

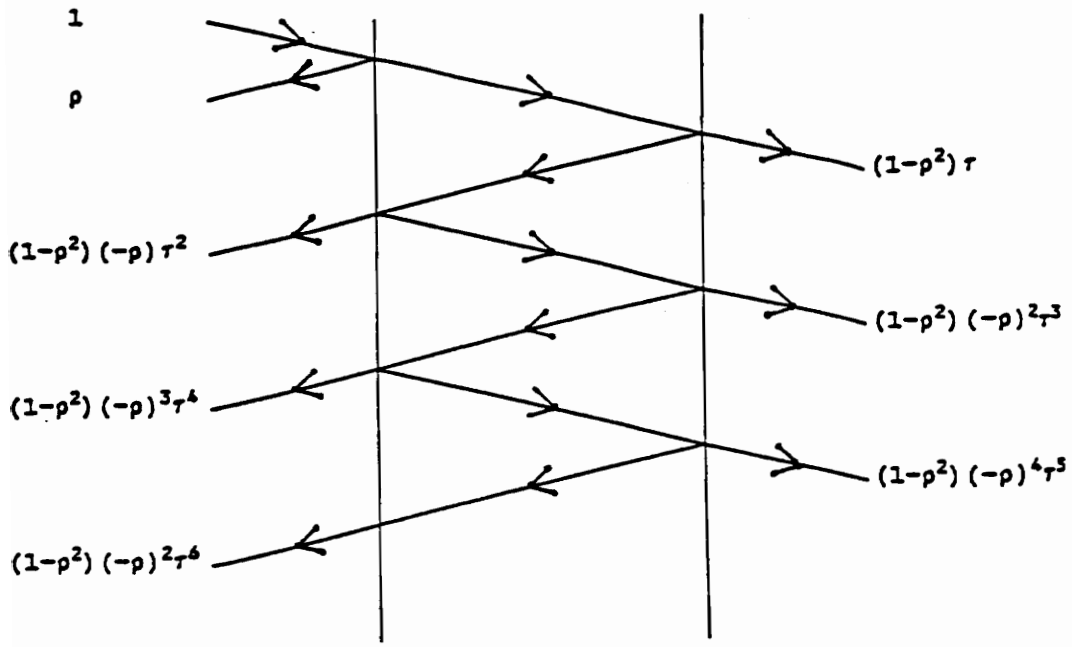

Figure 2.3: Bounce Diagram for the Terminated Coaxial Cell

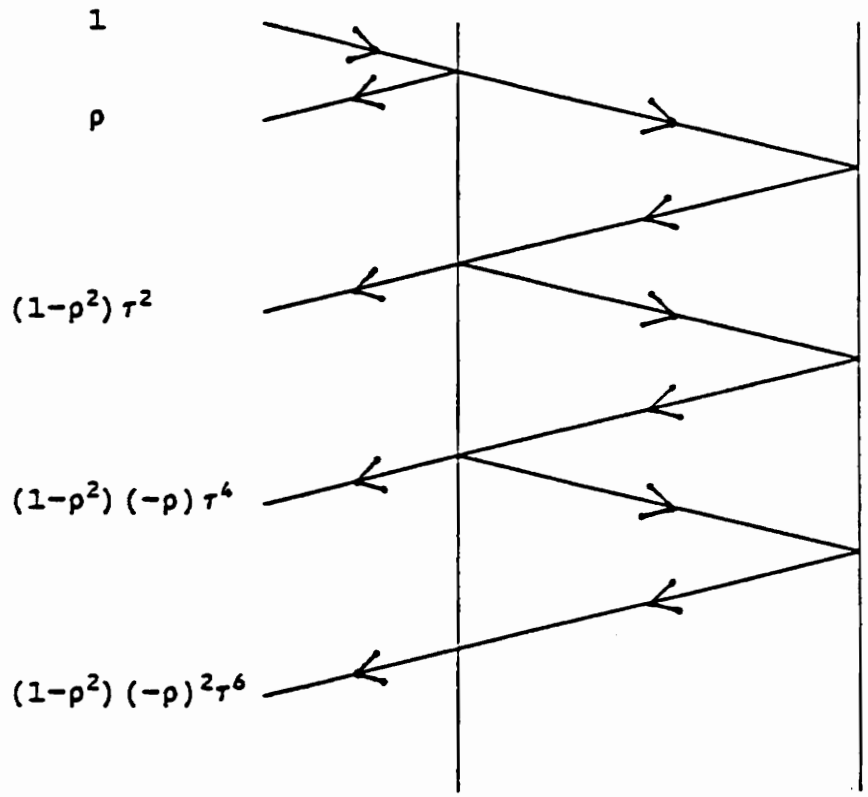

Figure 2.4: Bounce Diagram for the Open Circuit Coaxial Cell

Similarly, the total transmitted signal (S_{21}) is:

$$S_{21} = (1-\rho^2)\, e^{-\gamma l}[1 + (\rho^2 e^{-2\gamma l}) + (\rho^2 e^{-2\gamma l})^2 + \ldots]$$
$$= \frac{(1-\rho^2)\, e^{-\gamma l}}{1-\rho^2 e^{-2\gamma l}} \qquad (2.28)$$

Note that these equations describe the signals seen at the sample planes and also note that ρ here refers to the reflection coefficient looking into the sample at the sample plane.

Another type of sample holder is illustrated by figure 2.4. In this situation the sample once again forms the dielectric for a transmission line, but here the line is terminated in an open circuit. The bounce diagram shows that S_{11} for this case is:

$$S_{11} = \rho + (1-\rho^2)\, e^{-2\gamma l}[1 + (-\rho e^{-2\gamma l}) + (-\rho e^{-2\gamma l})^2 + \ldots]$$
$$= \rho + \frac{(1-\rho^2)\, e^{-2\gamma l}}{1+\rho e^{-2\gamma l}} \qquad (2.29)$$
$$= \frac{\rho + e^{-2\gamma l}}{1+\rho e^{-2\gamma l}}$$

Once again ρ refers to the reflection coefficient seen at the sample plane while looking into the sample from the sampling oscilloscope.

The above equations relate to the closed cell coaxial sample holder and the open circuit terminated coaxial sample holder respectively. The third type of sampling sensor used in this research, the balun transformer driven twin lead probe, required a different analysis tool to facilitate its use.

The balun driven twin lead probe (figure 2.5) is seen by the sampling scope as a twin lead line whose characteristics are to be determined, preceded by an unknown two port network (the balun transformer and connection circuitry). Although this could be analyzed through the use of the bounce diagram, the large number of internal reflections makes this a very tedious process. For this reason, a frequency domain approach was selected to model the effects of the balun transformer by utilizing the signal flow graph method.

Analysis of the signal flow graph (figure 2.6) indicates that the signal seen at the sampling oscilloscope may be expressed as

$$V_R = V_I \left(1+\frac{\rho_1(1+\rho_g)+\rho_L B}{(1-\rho_g\rho_1)(1-\rho_L\rho_b)}\right)$$

$$B = (1+\rho_g)(\tau_1\tau_2-\rho_1\rho_2) \qquad \textbf{(2.30)}$$

$$\rho_b = \rho_2+\left(\frac{\rho_g\tau_1\tau_2}{1-\rho_g\rho_1}\right)$$

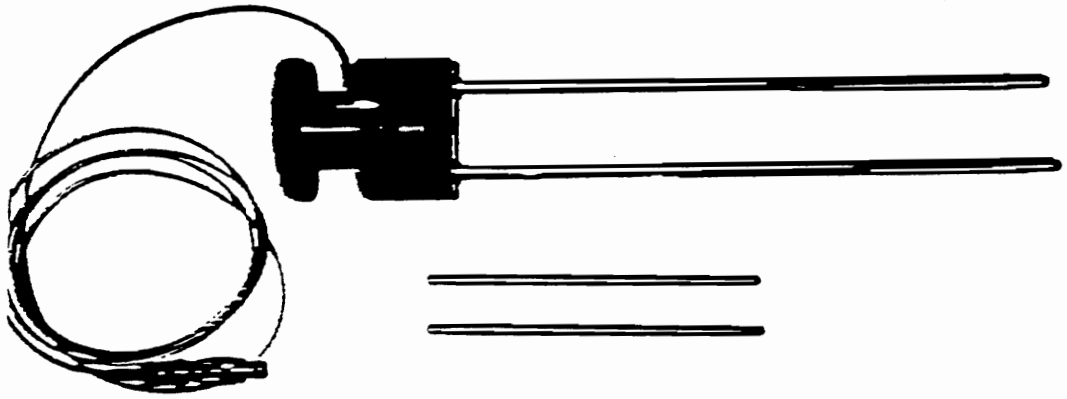

Figure 2.5: The Balun Driven Twin Lead Ground Probe

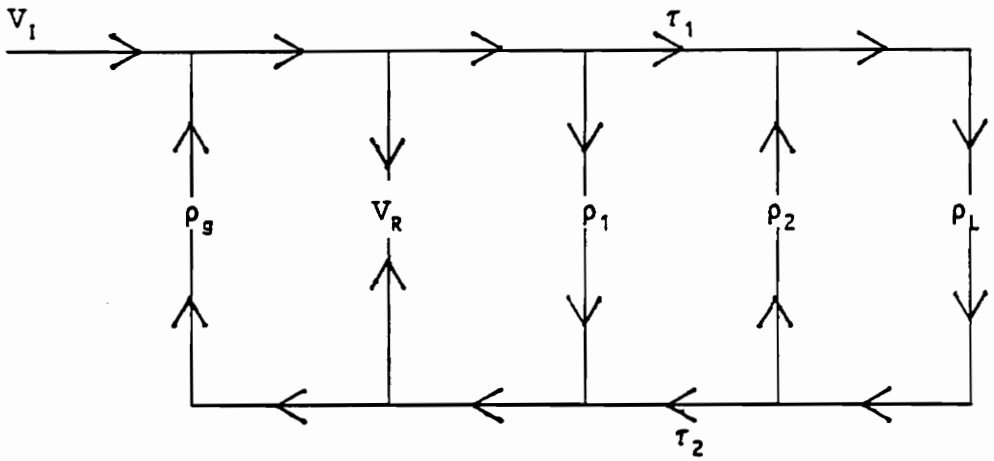

Figure 2.6: Twin Lead Probe Signal Flow Graph

where the reflection coefficient of the sample is ρ_L, the reflection coefficient looking into the sampling oscilloscope is ρ_g , and the scope/balun network reflection coefficient which is seen by the sample is ρ_b.

Evaluating the previous expression for the cases where the sample is a short circuit, a known reflection coefficient k, and an open circuit, leads to

$$V_{R_{short}} = V_I \left(1+\frac{\rho_1(1+\rho_g)-B}{(1-\rho_g\rho_1)\ (1+\rho_b)}\right) \qquad (2.31)$$

$$V_{R_k} = V_I \left(1+\frac{\rho_1(1+\rho_g)+kB}{(1-\rho_g\rho_1)\ (1-k\rho_b)}\right) \qquad (2.32)$$

$$V_{R_{open}} = V_I \left(1+\frac{\rho_1(1+\rho_g)+B}{(1-\rho_g\rho_1)\ (1-\rho_b)}\right) \qquad (2.33)$$

which may be combined to produce

$$\frac{V_R-V_{R_k}}{V_{R_{short}}-V_{R_k}} = \frac{k-\rho_L}{k+1}\ \frac{1+\rho_b}{1-\rho_L\rho_b} \qquad (2.34)$$

$$\frac{V_{R_{open}} - V_{R_k}}{V_{R_{short}} - V_{R_k}} = \frac{k-1}{k+1} \frac{1+\rho_b}{1-\rho_b} \qquad (2.35)$$

The second expression is used to find ρ_b which is then substituted into the first expression to solve for ρ_L and subsequently the permittivity of the sample.

SAMPLE PREPARATION

The sand samples were taken from a bag of standard construction-type sand. The sand was cleaned of any organic material but was not changed in any other way. Since the intent of the research was to investigate the ground probe for eventual use as an in-situ type of probe, it was felt that the implicit inhomogeneities regarding particle size, etc. of the sand should be left undisturbed. The wet samples were prepared with ordinary room temperature tap water and the saltwater saturated samples used a one Normal solution (58.5 grams NaCl/1 liter H_2O) of table salt in tap water. The ambient temperature was kept within 1 degree of 22 degrees C. All wet samples were thoroughly saturated with solution until the first trace of free standing solution appeared on the top of the sample. This procedure was used in an attempt to maintain the same degree of water saturation

in all wet samples without regard to changes in dry sand density and packing factor due to particle size inhomogeneity.

Packing technique varied considerably as a function of sample holder and type of sample. The 14 mm closed cell coaxial sample holder required very small samples, but the particulate samples alone would not have been adequate to maintain the coaxial alignment of the center conductor. Two teflon washers were precision machined to act as end plates for the sample. The first washer was put in place slightly recessed from the end of the sample holder and a measured volume of sample was placed into the recess. If the sample was a wet sample, the solution was now introduced using a hypodermic syringe. The second teflon washer was pressed into place and a GR-900 short was attached to the end of the sample holder. A hollow tube was then introduced into the far side of the coaxial line and was used to press the teflon washer/sample combination tightly against the short. The depth from the far end of the coaxial line to the face of the teflon washer was then measured and recorded. The teflon washers were each 2 mm thick and the length of the coaxial air line (10 cm) was known, so this process gave the sample thickness, typically 8 mm for the dry samples and 4 mm for the wet samples. The entire setup is diagrammed in figure 2.7.

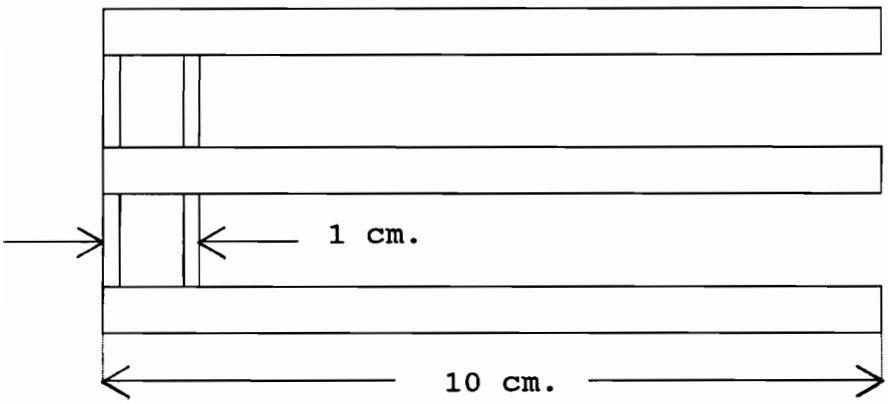

Figure 2.7: Terminated Coaxial Sample Holder Setup

The open circuit shielded coaxial sample holder required a different method to assure even packing. The 14 mm holder was approximately 14 cm long with a recessed inner conductor 9.2 cm in length and a sample volume of 19.55 cc. The possibility of voids in the sample over the length of the sample holder dictated the use of a vibrating table to help insure even packing of the sample. In addition, wet samples were filled in stages to assure that the solution was evenly distributed throughout the sample. The components of the sample were weighed before filling to help assure repeatability.

The sample 'cell' for the twin lead balun driven ground probe was formed by a cylindrical plastic bucket 28 cm in diameter and 33 cm deep. The plastic was used to reduce the possibility of spurious ground plane reflections which might have existed in a metal container. Experiments with the containers resting horizontally rather than vertically did not indicate any difference in results with regard to orientation. It was feared that percolation might have produced a depth gradient in the water saturation level, but this phenomena was not evident so measurements were taken with the probe inserted vertically down into the sample. Although three probe lengths were available (15 cm, 30 cm, and 45 cm) the longest probe exceeded the cell dimensions and so was not used.

All waveforms were acquired with an HP-54120T sampling oscilloscope using a 1024 point sampling window over a time regime of 5 ns. Waveforms were acquired 2048 times and averaged automatically by the sampling oscilloscope to reduce noise effects to an absolute minimum. The oscilloscope was calibrated and periodically rechecked against a known stable signal source to assure that long term drift was not a factor in the acquisitions. All acquisitions were made using channel 1 of the oscilloscope and it's internal 200 mv, 35 ps step generator.

The acquired waveforms were steplike in nature and would have produced severe aliasing and leakage errors if Fourier transformed in their initial forms, so the Nahman-Gans technique [50] of appending an inverted, time and level shifted version of the original waveform to the end of that waveform (in effect turning it off the same way it was turned on) was used to assure that the first and last point in the waveform had the same value. This doubles the time window, halving the frequency spacing between samples in the spectral domain, but the symmetry of the new waveform causes all even numbered frequency domain samples to evaluate to zero so that information is conserved. The net effect of this action was to produce frequency domain information at 200 MHz intervals starting at 100 MHz. A restricted bandwidth was used for

these measurements leading to an upper frequency bound of 5 GHz.

The closed cell coaxial measurements were initially taken to assure that useful information could indeed be derived for these particulate samples. It was felt that the greater constraints implicit in the match terminated closed cell coaxial environment would lead to a more accurate assessment of the true electrical characteristics of the samples. The shielded open circuit sample holder was next used to investigate what types of difficulties would be experienced due to longer sample lengths and the inherent ambiguities of the open circuit termination. Finally the techniques developed using the previous two sample holders were applied to the balun driven twin lead ground probe in an attempt to develop a useful and reasonably accurate in-situ probe for permittivity measurement.

The next three chapters discuss the specifics of each of these measurement schemes, detailing the mathematical methods used to extract permittivity information from the measurements and giving actual results.

CHAPTER III

THE COAXIAL SAMPLE HOLDER

This chapter discusses experiments conducted using a coaxial sample holder with a known termination. The coaxial geometry is attractive because of its well constrained fields and thus these experiments will be used to provide baseline values against which the later work on the unterminated coaxial sample holder and the twin lead ground probe will be compared.

A description of the experimental setup will be presented first, showing how a series of single port time domain measurements may be used to derive values for S_{11} and S_{21} under the assumption of reciprocity in the sample. This is followed by a discussion of several equations which may be used to invert the scattering parameters or measured impedance information to resolve the permittivity of the sample. Actual experimentally derived values for several materials are presented and the chapter concludes with an analysis of possible error sources.

EXPERIMENTAL SETUP

Consider a system such as that shown in figure 3.1 in which Region 1 represents a coaxial line with an air dielectric, Region 2 represents the same line filled with a sample of unknown permittivity, and Region 3 is like Region 1. The characteristic impedances of Regions 1 and 3 will be assumed to be Z_0 and the characteristic impedance of Region 2 will be $Z_0*(\mu_R/\epsilon_R)^{1/2}$ where μ_R is the relative complex permeability of the sample and ϵ_R is the relative complex permittivity of the sample. The reflection coefficient of a wave incident on the air/sample boundary is given by

$$\rho = \frac{Z-Z_0}{Z+Z_0} = \frac{\sqrt{\frac{\mu_R}{\epsilon_R}}-1}{\sqrt{\frac{\mu_R}{\epsilon_R}}+1} \qquad (3.1)$$

Similarly, the reflection coefficient for a wave passing out of the sample into the air filled portion of the line is

$$\frac{Z_0-Z}{Z_0+Z} = -\rho \qquad (3.2)$$

The transmission coefficient through the material is given by

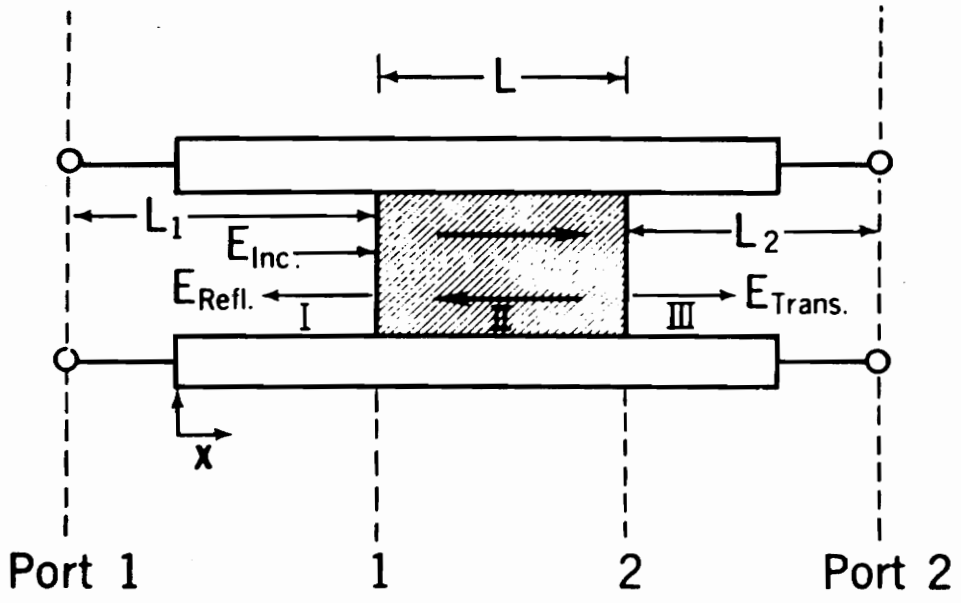

Figure 3.1: The Coaxial Sample Holder

$$\tau = \exp(-j\omega l\sqrt{\mu\epsilon}) = \exp\left(-\frac{j\omega l\sqrt{\mu_R\epsilon_R}}{c}\right) \qquad (3.3)$$

Using these expressions a transmission/reflection diagram may be constructed as in figure 3.2. This shows that the total reflection coefficient, which is equivalent to $S_{11}(\omega)$ is

$$S_{11}(\omega) = \frac{(1-\tau^2)\rho}{(1-\rho^2\tau^2)} \qquad |\rho\tau|<1 \qquad (3.4)$$

The total transmission, $S_{21}(\omega)$, becomes[1]

$$S_{21}(\omega) = \frac{(1-\rho^2)\tau}{(1-\rho^2\tau^2)} \qquad |\rho\tau|<1 \qquad (3.5)$$

The previous section assumes that $S_{11}(\omega)$ and $S_{21}(\omega)$ are available over the frequency range of interest. To evaluate these from time domain measurements, four waveforms were acquired and massaged through the use of the fast Fourier

---

[1]Some care must be taken with the assumption that the magnitude of the ρ τ product is less than unity. Although τ must have a magnitude less than one for passive materials, the magnitude of ρ may exceed one if the substances under test are lossy and if $X_0 \bullet X_s < 0$ where X_0 represents the reactance of the empty line and X_s is the reactance of the sample [51,52]. The samples examined in this study are assumed to be non-magnetic, so this condition should not apply.

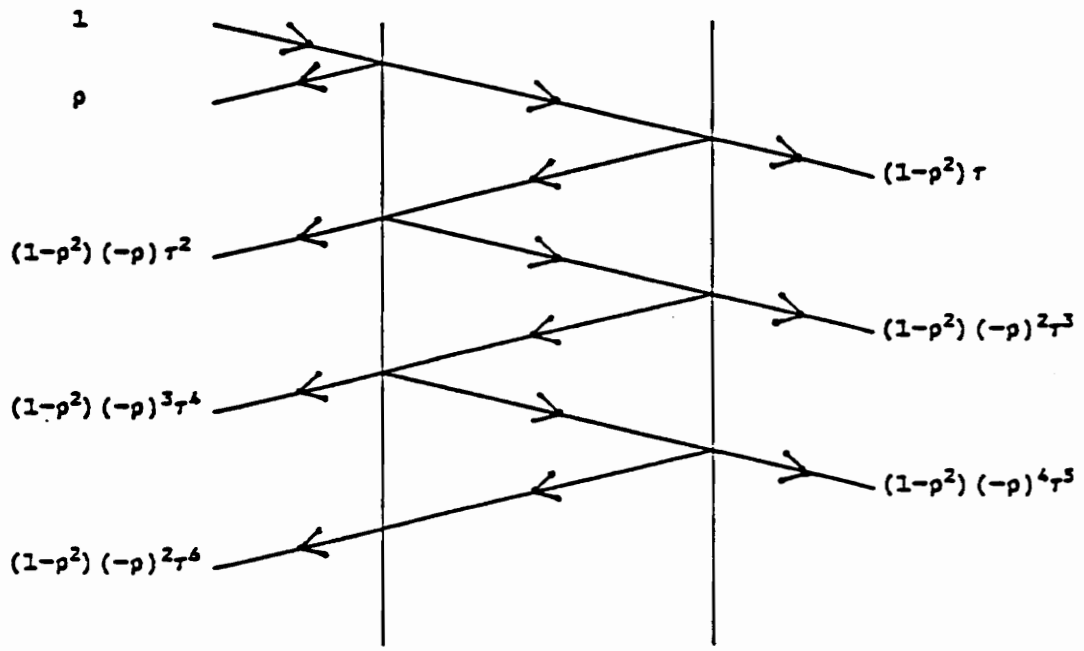

Figure 3.2: Bounce Diagram for the Terminated Coaxial Cell

transform. The details of this method and some results are given below.

The actual experimental layout is diagrammed in figure 3.3. Four waveforms were acquired. The first, which represents the $S_{11}(\omega)$ information, was acquired at the sample plane closest to the sampling head. This represents a voltage $V_A(t-t_0)$ where t_0 is the time required for the step to traverse the round trip distance between the sampling head and the sample. The purpose for this delay will be discussed below.

The sample is now removed and replaced by a short circuit. The waveform acquired $V_S(t-t_0)$ is an inverted version of the incident step voltage, including any effects produced by imperfections in the transmission lines used. The inversion occurs because the reflection coefficient of a perfect short circuit is -1. From the ratio of the Fourier transforms of these two waveforms one derives

$$\frac{\mathcal{F}(V_A(t-t_0))}{\mathcal{F}(V_s(t-t_0))} = \frac{\mathcal{F}(V_I(t-t_0)\otimes s_{11}(t))}{\mathcal{F}(-V_I(t-t_0))} = -S_{11}(\omega) \qquad \textbf{(3.6)}$$

where V_I represents the incident step voltage waveform and $\otimes$ is the convolution operator.

In order to evaluate $S_{21}(\omega)$ the sample is assumed to be reciprocal i.e. $S_{12}(\omega) = S_{21}(\omega)$. A waveform is acquired at the

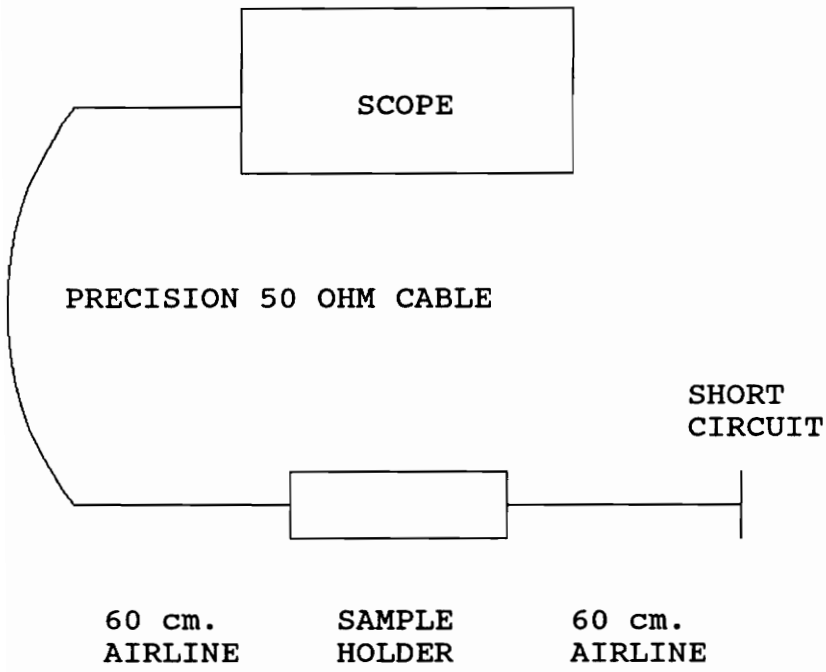

Figure 3.3: Experimental Layout for the Coaxial Sample Holder

proximal sample plane, as in the first waveform acquired, but at a later time which represents a complete transversal of the incident step through the sample, reflecting off the short circuit at the end of the transmission line system with the subsequent inversion that is implied, and back through the sample in the reverse direction i.e. towards the sampling head. This is $V_B(t-t_0-2t_s-t_1)$ where t_0, as before, represents the round trip time between the sampling head and the sample, t_1 represents the round trip time between the far end of the sample and the short circuit, and t_s is the one way transit time through the sample.

The sample is removed and the fourth waveform is acquired over exactly the same time window as the third waveform giving $V_{S_2}(t-t_0-2t_d-t_1)$ where t_d represents the one way transit time for the signal to traverse a distance equal to the sample thickness in the empty sample holder. This is c/l, where c is the speed of light, 2.9979×10^{10}cm/sec and l is the thickness of the sample.

This waveform once again represents an inverted version of the incident step including any non sample induced effects of the transmission path traversed by the third waveform. The ratio of the Fourier transforms of these two waveforms gives

$$\frac{\mathcal{F}(V_B(t-t_0-2t_s-t_1))}{\mathcal{F}(V_{S_2}(t-t_0-t_d-t_1))}=\frac{\mathcal{F}(-V_I(t-t_0-t_1)\otimes s_{12}(t)\otimes s_{21}(t))}{\mathcal{F}(-V_I(t-t_0-t_1))\cdot e^{-j2\omega t_d}} \quad (3.7)$$
$$=S_{12}(\omega)\cdot S_{21}(\omega)\cdot e^{-j2\omega t_d}$$

Note that both waveforms have encountered an inversion of the incident step and that these two inversions cancel one another out in the ratio of the transforms.

It is clear that, under the assumption of reciprocity of the sample[2], this ratio represents $S^2_{21}(\omega)$ retarded in phase by the effect of two transitions through the sample. Multiplying the resulting values by $\exp(-j2\omega t_d)$ removes this effect, yielding $S^2_{21}(\omega)$.

The reasoning behind the choice of a 2l/l ratio for the delay lines may now be made clear. If the transit time through the sample is small compared to the delay through the first delay line, then $t_s \ll t_1 < t_0$ and, for the above ratio of lengths, $t_0 = 2t_1$.

This choice allows a time window of t_1 for the measurement of the waveforms associated with $S_{11}(\omega)$ and allows the same time window for the measurement of waveforms associated with $S_{21}(\omega)$. In particular, if the sampling head is not properly back-matched, then a signal which represents

---

[2]Although reciprocity in the strict sense may not hold for small samples and coarse granularity, the measurement is intended to provide information about the *bulk* characteristics of the sample material, as opposed to the characteristics of the individual sample, so this assumption is justifiable.

the portion of the incident step which has been reflected off of the front face of the sample, has then been reflected from the improperly back-matched sampler, and has then been reflected again from the sample will appear at the sampling head at $t=t_0+t_1+t_1=2t_0$ allowing an uncorrupted sampling window for the $S_{21}(\omega)$ related waveforms from $t=t_0+t_1$ to $t=t_0+2t_1=2t_0$.

The sample holder is formed from a 10 cm. length of 14 mm. beadless airline which has GR-900 connectors on both ends. The particulate samples are held in position by means of two thin (2 mm.) teflon washers which seal tightly against both the inner and the outer conductor surfaces. Teflon was chosen for this purpose because it is easily machined, it provides a tight fit without marring the inner surfaces of the sample holder, and it is similar in dielectric properties to dry sand.

The sampling oscilloscope used is an HP-54120. This oscilloscope contains an internal step generator with a transition time of approximately 35 ps. which was used in these experiments to provide the excitation voltage. The use of the internal generator provides greater stability in the measurement (against jitter) than an external source would due to the characteristics of the oscilloscopes internal triggering circuitry.

In order to provide the necessary time delay both before and after the sample, a combination of several types of

coaxial lines was used. The direct mechanical connection to the precision 3.5 mm connectors of the scope was made through the use of a flexible 50 ohm cable which was 1 meter in length. This was attached through an adapter to a series network composed of two 7 mm airlines with a total length of 60 cm. The sample holder was attached to these and two 30 cm long 14 mm airlines were used to provide the final delay period, thus approximating the desired 2 to 1 length ratio.

The presence of the teflon washers produces internal reflections within the sample which are not accounted for by equations 3.6 and 3.7. The permittivity of teflon (ϵ_R=2.03) is similar to that of dry sand, but is quite different from the permittivity of the wet samples. This produces a high dielectric contrast with a large reflection coefficient which must be considered in the model. This effect is removed through the use of transmission parameters (sometimes called chain matrices).

The transmission parameter expression for the teflon-sample-teflon portion of the coaxial transmission line is given by

$$\begin{bmatrix} T_{11_{teflon}} & T_{12_{teflon}} \\ T_{21_{teflon}} & T_{22_{teflon}} \end{bmatrix} \begin{bmatrix} T_{11_{sample}} & T_{12_{sample}} \\ T_{21_{sample}} & T_{22_{sample}} \end{bmatrix} \begin{bmatrix} T_{11_{teflon}} & T_{12_{teflon}} \\ T_{21_{teflon}} & T_{22_{teflon}} \end{bmatrix} \qquad (3.8)$$

Since the teflon is nonmagnetic, it's μ_R is unity, and the relative permittivity of teflon is known to be 2.03 over the bandwidth used for these measurements. These two values may be substituted into equations 3.6 and 3.7 to evaluate S_{11} and S_{21} of the reciprocal, teflon-filled coaxial line segments at any given frequency. The conversion between S parameters and T parameters is defined as

$$\begin{bmatrix} T_{11} & T_{12} \\ T_{21} & T_{22} \end{bmatrix} = \begin{bmatrix} -\frac{S_{11}S_{22}-S_{12}S_{21}}{S_{21}} & \frac{S_{11}}{S_{21}} \\ -\frac{S_{22}}{S_{21}} & \frac{1}{S_{21}} \end{bmatrix} \qquad (3.9)$$

and

$$\begin{bmatrix} S_{11} & S_{12} \\ S_{21} & S_{22} \end{bmatrix} = \begin{bmatrix} \frac{T_{12}}{T_{22}} & \frac{T_{11}T_{22}-T_{12}T_{21}}{T_{22}} \\ \frac{1}{T_{22}} & -\frac{T_{21}}{T_{22}} \end{bmatrix} \qquad (3.10)$$

The complete algorithm for deembedding the teflon washer effects may now be described.

1. The S-parameters of the teflon-sample-teflon composite are evaluated using the process described above involving the acquisition of four waveforms and calculating the ratios of the Fourier transforms of pairs of those waveforms. This yields values for $S_{11}(\omega)$ and $S_{21}^2(\omega)$.

2. The $S_{21}^2(\omega)$ information is converted to $S_{21}(\omega)$. The choice of the positive vs. the negative square root is ambiguous and was resolved by writing a small simulation program using an assumed value for ϵ_R to evaluate $S_{21}(\omega)$ for low frequencies. The signs of the real and imaginary parts of $S_{21}(\omega)$ from this program indicated the correct choice of roots, and for higher frequencies the root was chosen which made $S_{21}(\omega)$ a continuous function.

3. Using the known values for the S-parameters of the teflon filled sections of the line, the teflon T parameters are calculated. The T matrix for the measured composite sample is evaluated (again assuming reciprocity and unity μ_R) using equation 3.9 and this matrix is pre- and post-multiplied by the inverse of the teflon T-matrix. This yields the T parameters of the particulate sample with the teflon washer effects deembedded.

4. The T parameters are then transformed to S parameters using equation 3.10.

Although the process seems involved on paper, it is in fact quite easily accomplished using the short computer program given in Appendix A.

MATHEMATICAL ALGORITHMS

Given the measured S parameters, a number of techniques exist to solve for permittivity information, assuming a non-magnetic sample. For the purpose of this study three S parameter methods and two methods which depend upon impedance measurements were chosen. All five methods required iterative solution of an equation which specified the measured quantity as a function of ϵ_R.

The first method involved solving the S_{11} equation (equation 3.4) for ϵ_R. This was an attempt to investigate the difficulties associated with using strictly reflection derived information. Experience gained from this work could logically be expected to be applicable to work on the other two sample systems, both of which were one ports and would allow only reflection measurements.

The second method required the iterative solution of equation 3.5, given a measured value for S_{21}. This transmission measurement was expected to yield better results than the previous technique since it seemed more dependent upon the physical parameters of the entire sample and less dependent upon the dielectric contrast at a particular measurement plane. Both schemes fall under the category of total reflection measurements (i.e. both include the effects of internal reflections as well as front face effects) so the

derived values were not expected to be radically different from one another.

The third measurement technique was used with great success by Baker-Jarvis [15] who was, however, working strictly in the frequency domain with automatic network analyzer measurements and was measuring solid samples. This procedure is a natural extension of the first two schemes as it utilizes both S_{11} and S_{21} measurements in an attempt to iteratively solve for permittivity values. This method was expected to produce the best results since it used all of the available information. The equations for all three of the S-parameter dependant schemes are shown below.

$$\frac{(1-\tau^2)\rho}{1-\rho^2\tau^2} - S_{11_{measured}} = 0 \quad S_{11} \text{ equation} \qquad \textbf{(3.11)}$$

$$\frac{(1-\rho^2)\tau}{1-\rho^2\tau^2} - S_{21_{measured}} = 0 \quad S_{21} \text{ equation} \qquad \textbf{(3.12)}$$

$$\frac{\tau^2-\rho^2}{1-\rho^2\tau^2} - S^2_{21\,measured} + S^2_{11\,measured} = 0 \quad \text{Baker-Jarvis equation} \qquad \textbf{(3.13)}$$

where

$$\rho = \frac{Z-Z_0}{Z+Z_0} = \frac{(Z_0/\sqrt{\epsilon_R}) - Z_0}{(Z_0/\sqrt{\epsilon_R}) + Z_0} = \frac{1-\sqrt{\epsilon_R}}{1+\sqrt{\epsilon_R}} \qquad (3.14)$$

and

$$\tau = e^{-j\frac{\omega l\sqrt{\epsilon_R}}{c}} \qquad \mu_R = 1 \qquad (3.15)$$

The last two methods used to derive permittivity information were quite different from the first three as they did not depend upon the measurement of scattering parameters but rather utilized impedance information. One technique, devised by Cole [7,8], was used in an attempt to (in some sense) cross check the other three schemes. It required a completely different algorithm to remove the effect of the teflon washers (which will be explained below) but was attractive for two reasons. First, impedance measurements are quite often used by investigators working in the frequency domain with one-port measurements and, indeed, were used by Bussey [16] using the same sample holder upon which the second series of measurements were based. The fact that Cole performed his measurements in the time domain was also considered to be a positive feature of this technique. A slight modification of Cole's derivation is given in Appendix B, and the steps necessary to eliminate the effect of the

teflon washers are given below. The second of these techniques involved a simple impedance measurement. This was used to verify the results from Cole's method and to further investigate the rigors of inverting the impedance formulation to find epsilon.

Both of the last two methods require knowledge of the impedance terminating the sample, as well as measurement of the impedance at the proximal sample plane. The impedance at the sample termination is no longer equal to the Z_0 of the line, but, because of the presence of the teflon washer, is instead the line impedance transformed by the effect of the teflon filled portion of the line. This is calculated by

$$Z_I = Z_0 \frac{Z_T + Z_0 \tanh(\gamma l)}{Z_0 + Z_T \tanh(\gamma l)}$$

where

Z_I = input impedance
Z_T = terminating impedance (here 50Ω)
Z_0 = line impedance (here $\frac{50}{\sqrt{2.03}}\Omega$)
$\gamma = \frac{j\omega\sqrt{2.03}}{c}$

(3.16)

In a similar fashion, the previous equation may be solved for Z_T to give

$$Z_T = Z_0 \frac{Z_I - Z_0 \tanh(\gamma l)}{Z_0 - Z_I \tanh(\gamma l)} \qquad \textbf{(3.17)}$$

where Z_I in this case is the measured impedance and Z_T is the effective impedance at the proximal sample plane. The measured impedance is derived from the acquired waveforms by solving equation 3.14 for Z

$$\rho = \frac{Z-Z_0}{Z+Z_0} \Rightarrow Z = Z_0\frac{1+\rho}{1-\rho} \qquad \textbf{(3.18)}$$

where ρ is taken as the ratio of the Fourier transforms of the reflected and incident waveforms. The equations for the modified Cole's method and the impedance method are

$$\epsilon_R = \frac{\sqrt{\epsilon_R}}{\tanh(\gamma l)}\,(Y_L - Y_{MT}) + Y_L \cdot Y_{MT} \qquad \text{Modified Cole's Equation}$$

(3.19)

$$Z_{MT} = \frac{Z_0}{\sqrt{2.03}}\;\frac{Z_L - \dfrac{Z_0}{\sqrt{2.03}}\tanh(\gamma l)}{Z_0 - Z_L\tanh(\gamma l)} \qquad \text{Impedance Equation}$$

(3.20)

$$\gamma = j\,\frac{\omega\sqrt{\epsilon_R}}{C} \quad \text{and} \quad Z_0 = 50\Omega$$

where Z_{MT} is derived from equation (3.17), Y_{MT} is the reciprocal of Z_{MT}, Z_L is derived from equation (3.16) and Y_L is it's associated admittance.

EXPERIMENTAL RESULTS

The five algorithms previously mentioned were applied to experimental data acquired from three different material compositions. The materials selected for examination were chosen in an attempt to explore the entire range of possible permittivity/conductivity combinations which might be encountered in a normal field environment. In all three cases the results from the Cole equation precisely matched those from the impedance formulation, so only the Cole results are graphed. It should also be noted that five sets of acquisitions were taken for each material, and the graphed results represent the average values of those five experiments with error bars indicating the maximum and minimum excursions from those average values.

The first material was ordinary dry sand. This sand was not a laboratory grade product of constant grain size or shape but was instead sandbox sand purchased from a local construction company. No attempt was made to increase the homogeneity of the sand beyond removing any obvious organic material (leaves, twigs, etc.) present in the sample. This material was low loss and had a relatively low permittivity with very little frequency dependence.

The experimental results shown in figures 3.4 through 3.7 indicate that the pure reflection measurements using the

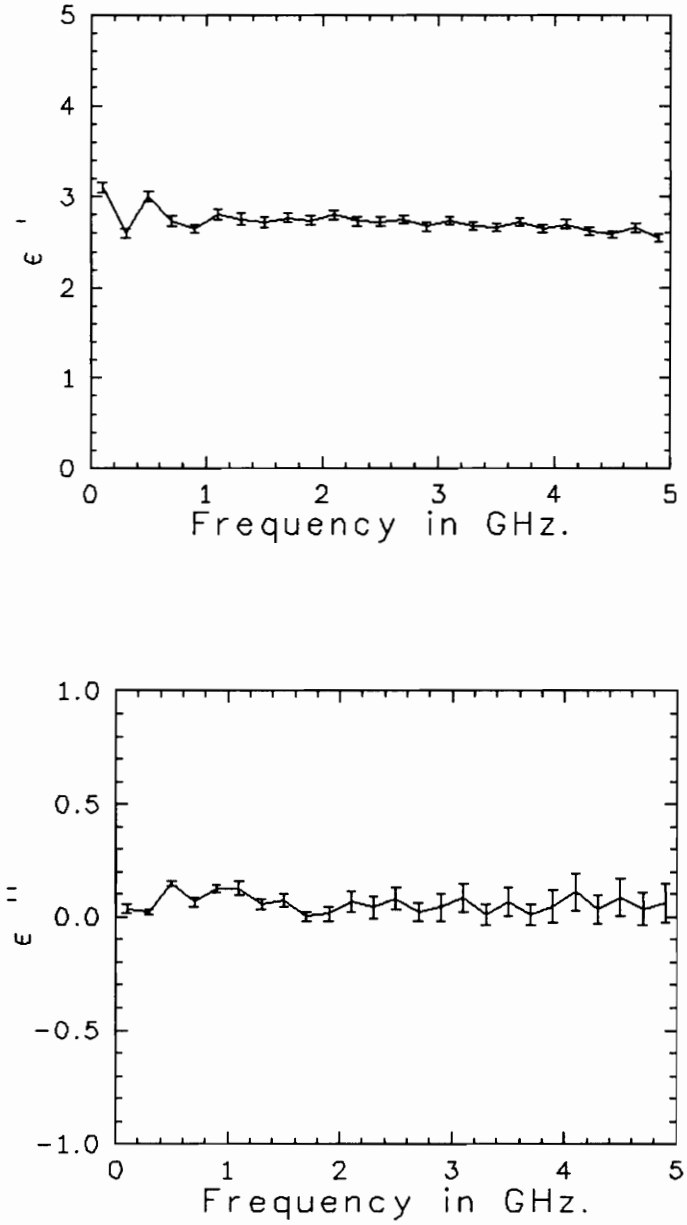

Figure 3.4: Permittivity of Dry Sand Using the S_{11} Equation Experimental Spread

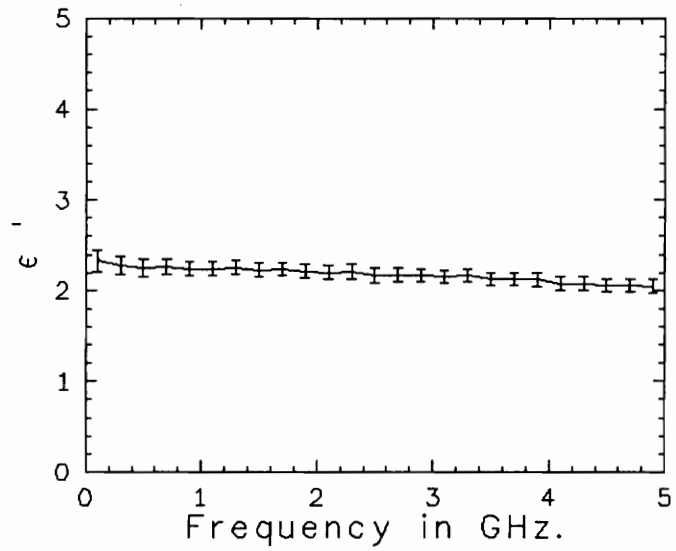

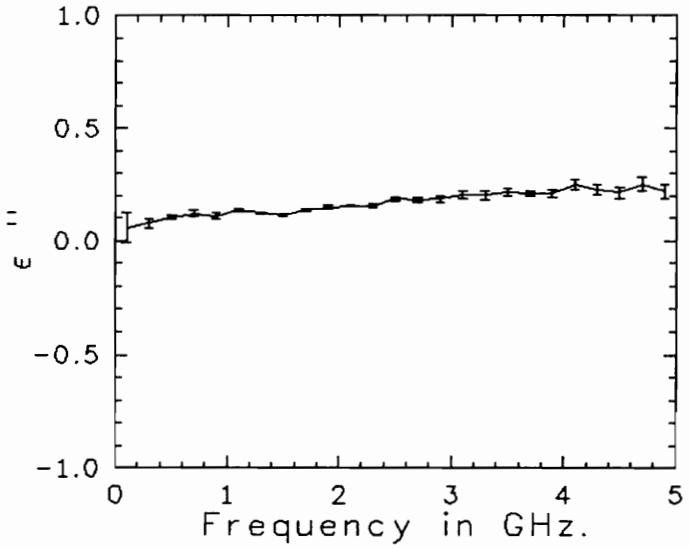

Figure 3.5: Permittivity of Dry Sand Using the S_{21} Equation Experimental Spread

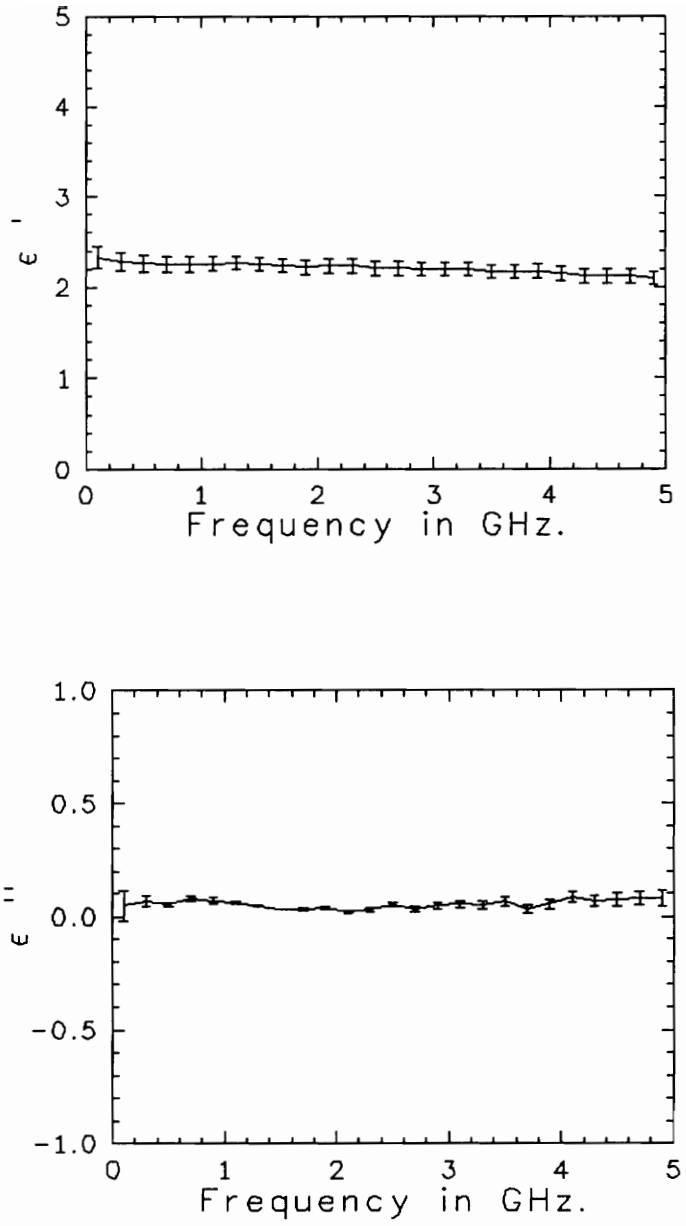

Figure 3.6: Permittivity of Dry Sand Using the Baker-Jarvis Equation -- Experimental Spread

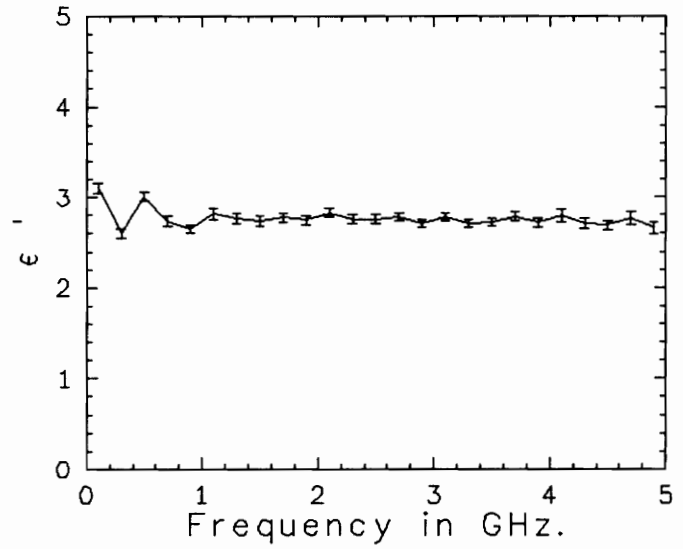

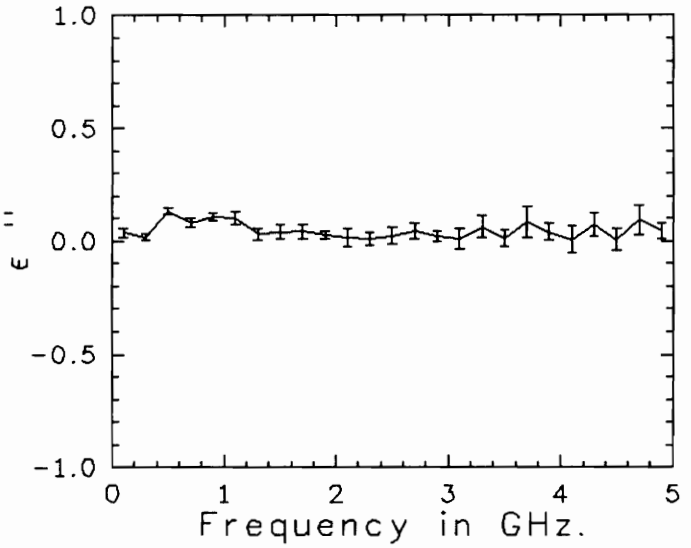

Figure 3.7: Permittivity of Dry Sand Using Cole's Equation Experimental Spread

S_{11} equation produce very similar results to those derived using impedance information. This is not surprising since both results are derived from the same pair of acquired waveforms. The instability at the lower frequencies is apparently not an artifact since it exceeds the error bar range considerably, but may represent some residual effect of the teflon washers. The fact that the transmission derived values (S_{21} equation) and those produced by the Baker-Jarvis equation (3.13 which combines transmission and reflection information) are lower than the other results seems unusual, but all four sets of these results do not differ greatly from those reported for dry sand by previous investigators (i.e. 2.7 [53], 2.55 [54], 2.5 [55]).

The permittivities calculated for sand saturated with water are graphed in figures 3.8 through 3.11. In this frequency range ϵ_R' for water is about 76 and that of 1 Normal saline solution is about 61, and the permittivity of the composite mixtures is subsequently much higher than that of dry sand. A number of interesting features are evident upon examination of these data. First, a subtle effect appears at the lowest frequency datum, where the calculated permittivity is slightly higher than the value at nearby frequencies. This is explained by one investigator [56] as being "attributed to various mechanisms at the particle level."

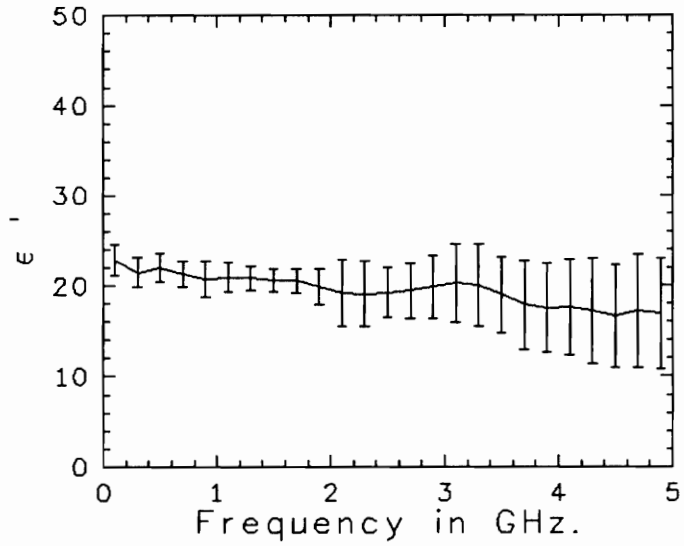

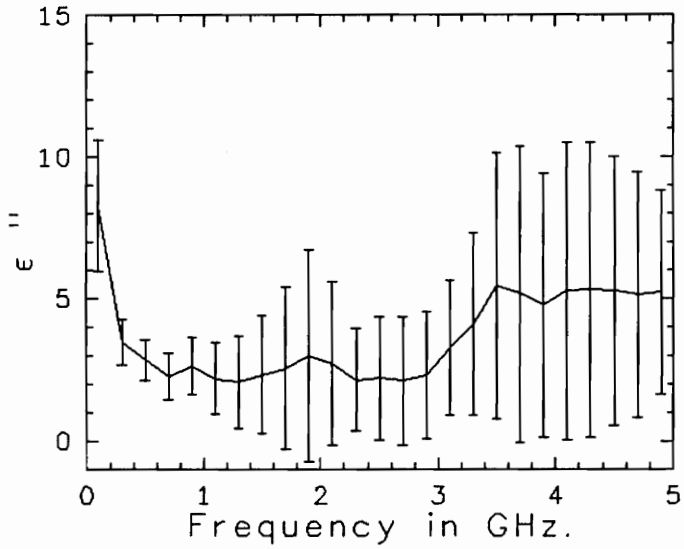

Figure 3.8: Permittivity of Wet Sand Using the S_{11} Equation Experimental Spread

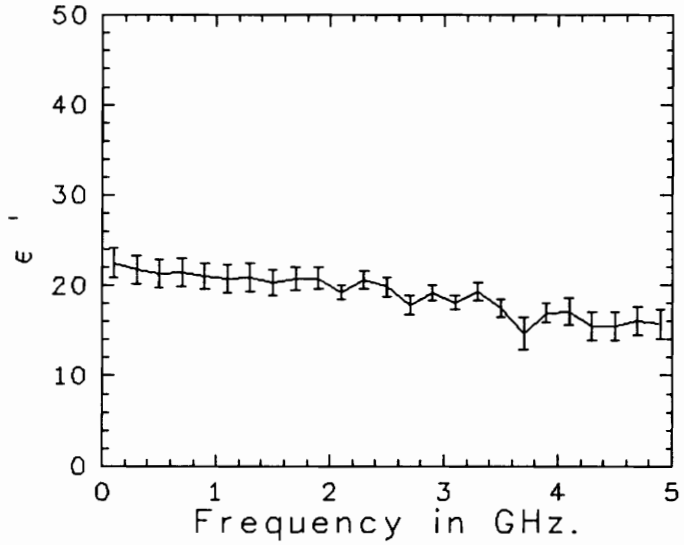

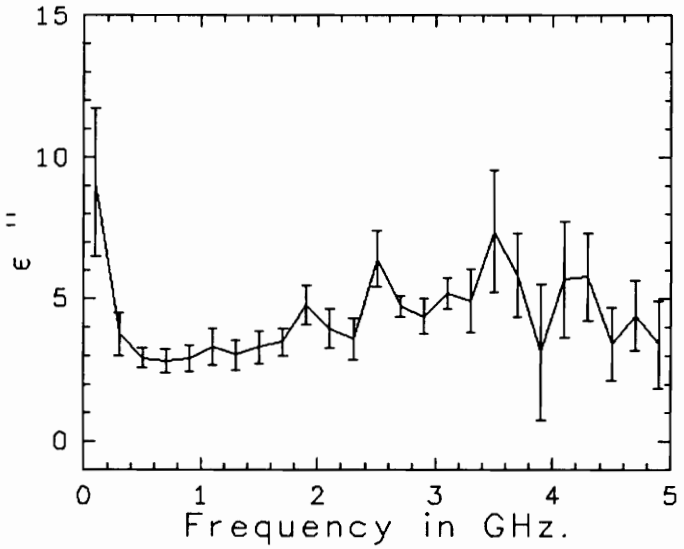

Figure 3.9: Permittivity of Wet Sand Using the S_{21} Equation Experimental Spread

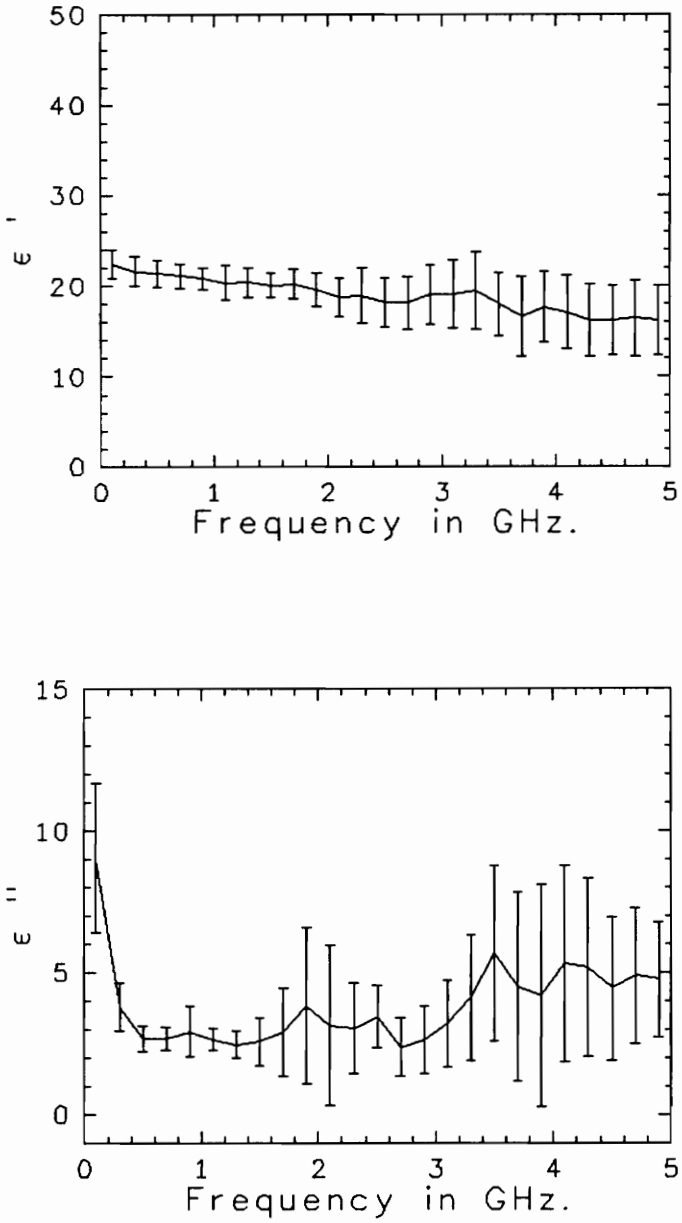

Figure 3.10: Permittivity of Wet Sand Using the Baker-Jarvis Equation -- Experimental Spread

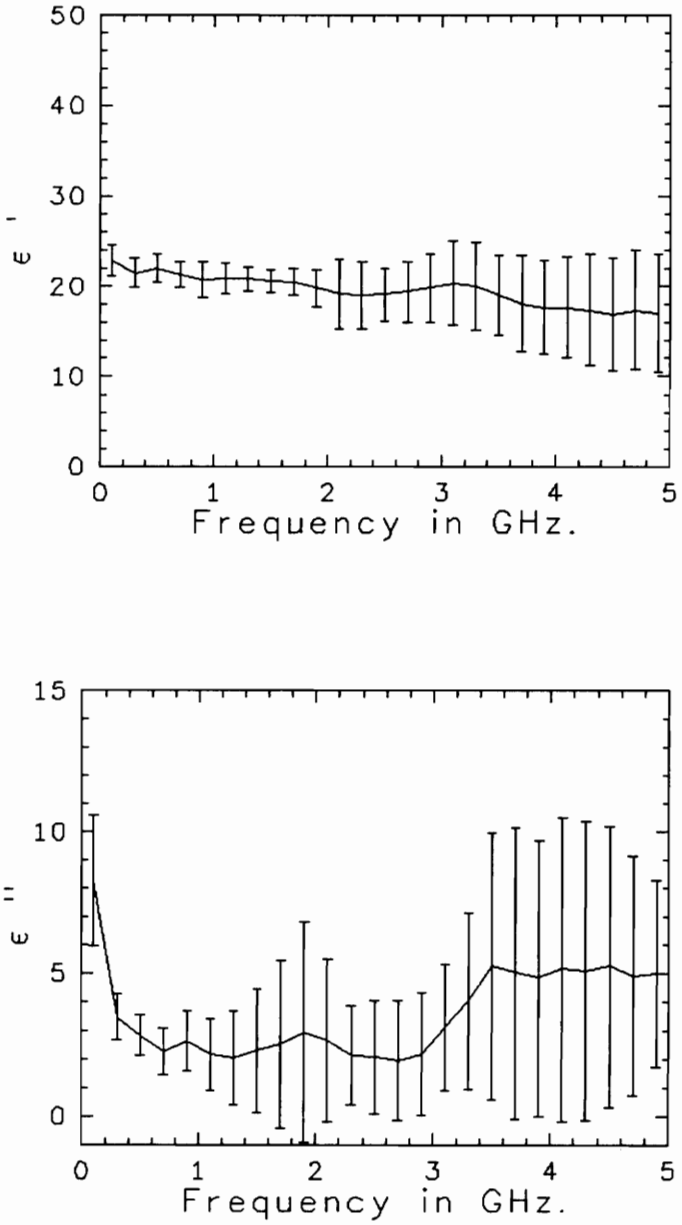

Figure 3.11: Permittivity of Wet Sand Using Cole's Equation -- Experimental Spread

The error bounds for the reflection based measurements (S_{11} and Cole) and, to some extent, the Baker-Jarvis combined algorithm, become rather large at approximately 2.1 GHz. and remain large thereafter. This may possibly be attributed to the onset of TE_{11} mode propagation and will be discussed further in the error analysis portion of this chapter.

Finally, a sharp drop in the value of ϵ_R' and a concomitant rise in $\epsilon_R''$is evident at about 3.5 GHz. This is midway between 3.01 GHz., the frequency where the composite sample including the teflon washers (.829 cm. in length with ϵ_R'=9.01) represents a quarter wavelength, and the frequency where the sand sample alone is equal to $\lambda/4$ (3.9 GHz).

It is very difficult to locate corroborating data in the literature because the measured permittivities are a complex function involving soil type, particle geometry and size, packing density, moisture level, and frequency of measurement. The problem is further complicated by the fact that many of these studies are done versus soil moisture level at just a few frequencies. However, at least one investigator [56] presents evidence that the measured permittivities are not strong functions of soil type and, with this in mind, selected results from several studies with different soil types but similar moisture levels are presented for comparison in figure 3.12.

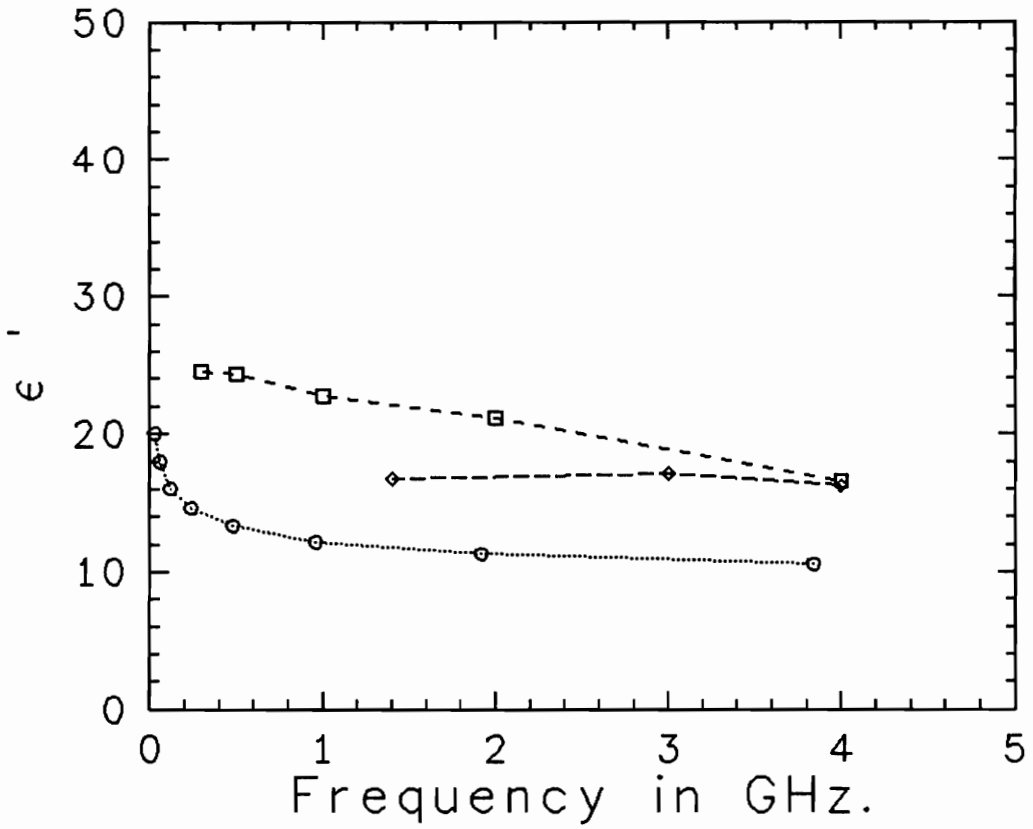

Figure 3.12: Permittivity of Wet Sand - Other Investigators
Jesch,Sandy Loam 24% - □;Hallikainen/Ulaby,Loam 26.9% - ◇
Hipp,San Antonio Clay Loam 20% - ○

The next series of graphs, figures 3.13 through 3.16, represents measurements of sand saturated with a 1 Normal solution (56.5 grams NaCl per 1 liter of water) of saltwater. The reflection based methods (S_{11} and Cole's equation) here produce a much smoother result than those based on transmission information, and this is probably due to the large ionic conduction and the strong attenuation it creates i.e. very little of the original signal is present after passing through the sample once. The low frequency jump in permittivity is clearly evident in these figures, but the sudden drop at 3.5 GHz. is not nearly so prominent, again suggesting that attenuation effects are reducing the destructive interference which normally occurs in quarter wave resonance.

The error bounds on these measurements are considerably smaller than those of the sand and water group, suggesting that the high degree of attenuation swamps any effects due to physical differences between the samples used for successive acquisitions. This also may indicate a large reduction in TE_{11} mode propagation. The ϵ_R'' curves show the correct 1/f characteristic shape which is caused by conductivity being the dominant factor in this quantity.

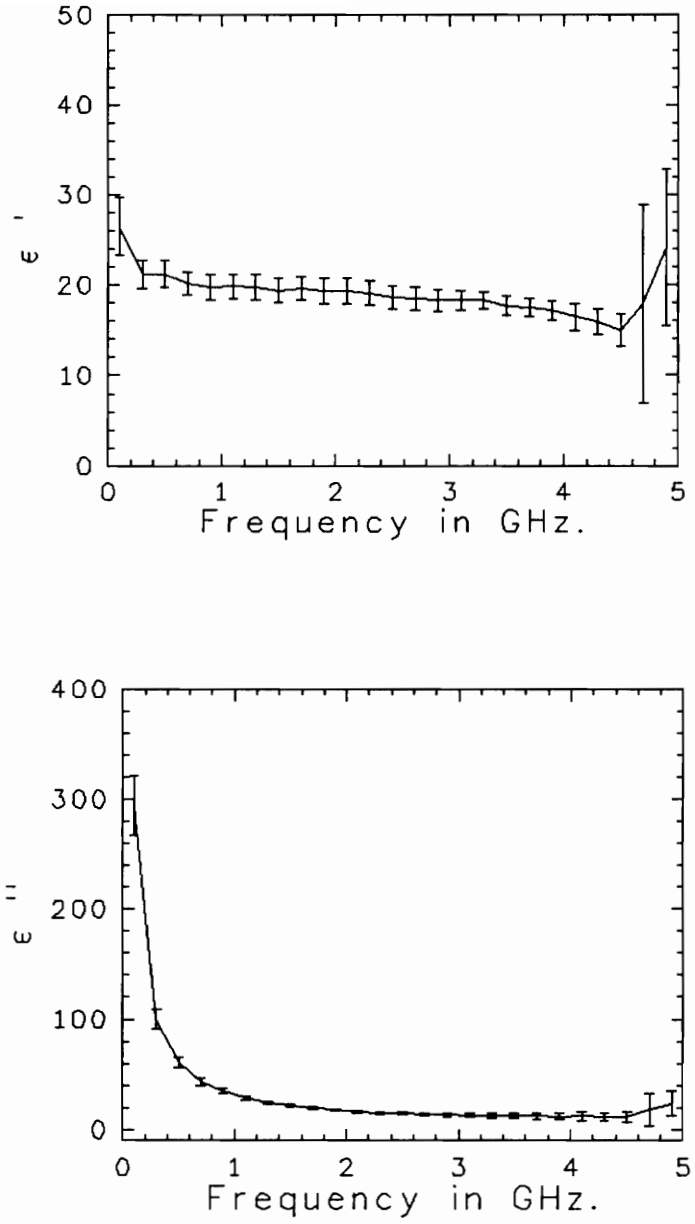

Figure 3.13: Permittivity of Saltwater Sand Using the S_{11} Equation -- Experimental Spread

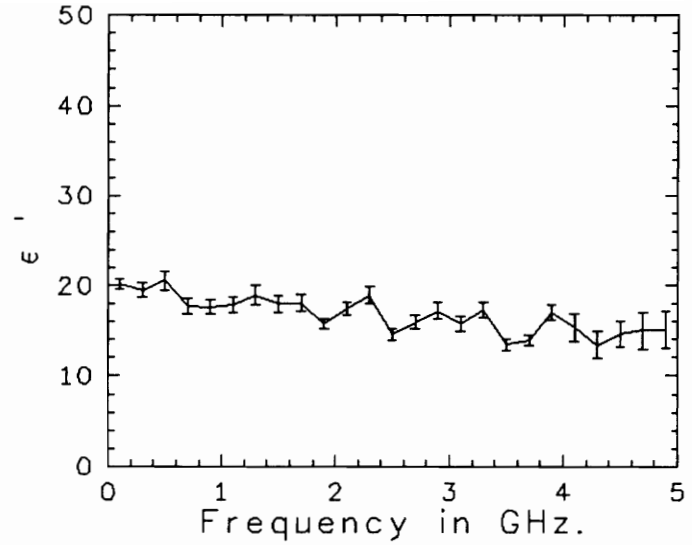

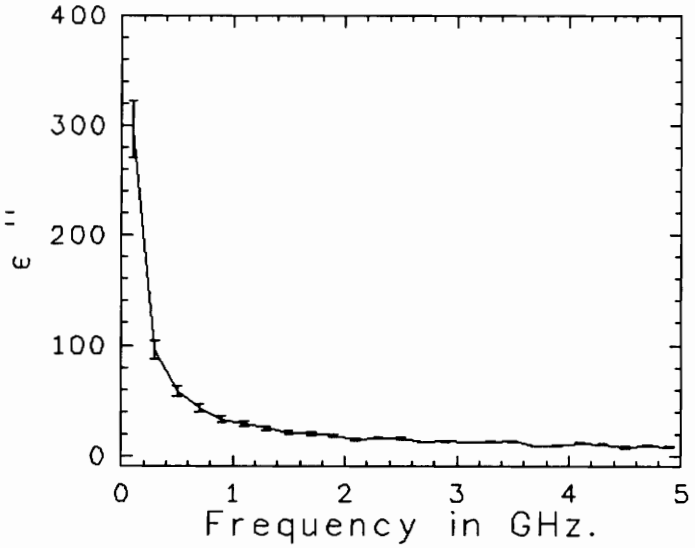

Figure 3.14: Permittivity of Saltwater Sand Using the S_{21} Equation -- Experimental Spread

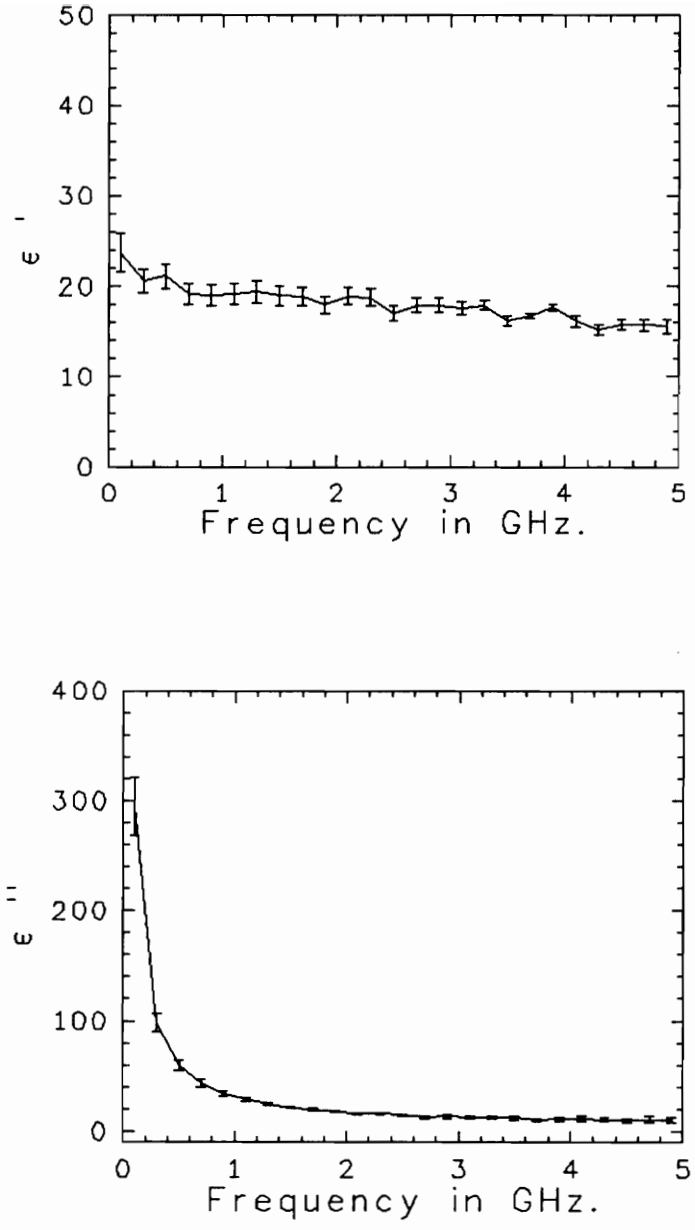

Figure 3.15: Permittivity of Saltwater Sand Using the Baker-Jarvis Equation -- Experimental Spread

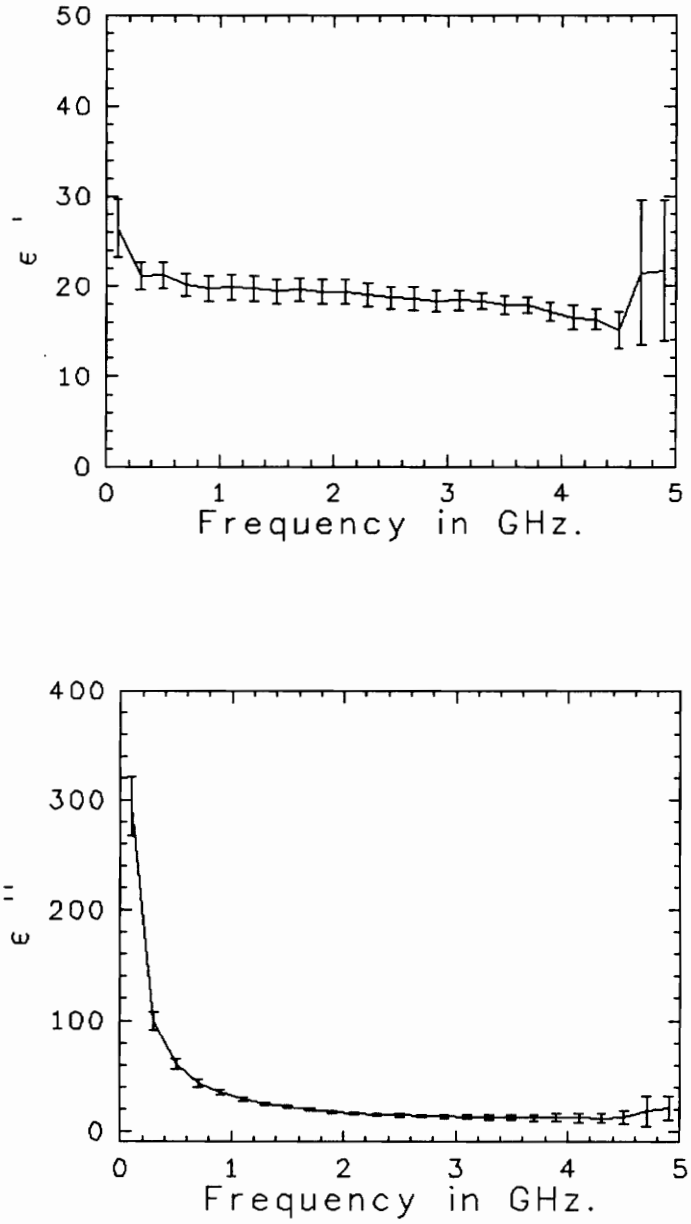

Figure 3.16: Permittivity of Saltwater Sand Using Cole's Equation -- Experimental Spread

ERROR ANALYSIS

Any analysis of experimental error must necessarily address two issues - the accuracy of each individual measurement and the repeatability of the experimental setup from one measurement to the next. Some indication of repeatability is shown in the ϵ_R' graphs of figures 3.4 through 3.16 where the graphed data represents the mean values obtained from five experimental observations using each technique and the error bars indicate the maximum excursions from those mean values within each group of five measurements. It is not surprising to note that maximum variability occurs in the sand and water samples where attenuation is relatively low but epsilon is relatively large. This point will be returned to later, but the first portion of this section will discuss quantitative estimates of experimental accuracy and parameter sensitivity.

The fundamental parameters observed by the sampling oscilloscope are amplitude and time, and error bounds for these parameters are given by the manufacturer. The waveforms observed may be thought of as a time domain version of the reflection coefficient of the network under test insofar as the excitation waveform is known. In this study the experimental setup is varied between acquisitions and the Fourier transform is applied to the waveforms obtained to

evaluate the frequency domain scattering parameters S_{11} and S_{21} and the network impedance Z. It is very difficult to translate the stated error bounds for the sampling oscilloscope through the effect of the Fourier transformation into error bounds on the scattering parameters and network impedance. The only recourse is to estimate the accuracies of these quantities and use the estimated accuracies to compute error bounds for the evaluated permittivities.

The step generator of the HP-54120T oscilloscope has a specified transition duration of 35 ps. Application of the time domain equation $BW=0.35/t_d$ indicates that the 3 dB point for this generator lies at 10 GHz which shows that the excitation waveform is not a limiting factor in this investigation. Similarly, the acquisition accuracy of the sampling oscilloscope is specified as 14 bits of dynamic range when the waveform is averaged 2048 times as was done here. This translates to amplitude errors less than or equal to one-half the least significant bit, or one part in 32,768. The Fourier transform spreads any localized error in the time domain across the full calculated spectrum in the frequency domain, so a maximum error in each of the sampled points of the 1024 point waveform would produce an error of 1024/32768 or just over 3 percent. An error of this magnitude is very unlikely as this assumes that each acquired point is in error and that these errors all act unidirectionally through the

Fourier transform so, for this analysis, a more conservative figure of 1 percent will be used. Note that the scattering parameters and the impedance are computed as the ratio of two Fourier transforms each of which, from the above rough estimation, may be 1 percent in error. This gives a worst case error estimate of (1.01/0.99)-1.0 or very close to 2 percent, so this figure will be used in the subsequent calculations. Finally, the calculated values are also a function of the measured sample length, and this will be assumed to be correct to within 1 percent.

It should be noted at this point that earlier time domain investigators were hampered by significant problems with short term time base variations ('jitter') and long term variations of the same type ('drift'). The HP-54120T timebase generator is exceptionally stable and these effects were found to be negligible and will not be discussed further.

A differential uncertainty analysis will be used to reduce the assumed measurement inaccuracies to error bounds on epsilon. An example for the S_{11} equation is shown in it's entirety - the other cases are similar.

The uncertainty in the solution of the S_{11} equation is assumed to be a function of two independent parameters - the errors in S_{11} and 1. A first order Taylor series

approximation, assuming small differential errors and a well behaved function for ϵ gives

$$\Delta\epsilon_R = \sqrt{\left(\frac{\partial\epsilon_R}{\partial S_{11}}\,\Delta S_{11}\right)^2 + \left(\frac{\partial\epsilon_R}{\partial l}\,\Delta l\right)^2} \qquad (3.21)$$

The differential errors have been estimated in the above paragraphs, and the derivatives may be evaluated through the use of the total differential, leading to

$$\begin{aligned} f &= \frac{(1-\tau^2)\,\rho}{1-\rho^2\tau^2} - S_{11} = 0 \\ \frac{\partial f}{\partial\epsilon_R}\,\frac{\partial\epsilon_R}{\partial S_{11}} &+ \frac{\partial f}{\partial S_{11}} = 0 \\ \frac{\partial\epsilon_R}{\partial S_{11}} &= -\frac{\dfrac{\partial f}{\partial S_{11}}}{\dfrac{\partial f}{\partial\epsilon_R}} \end{aligned} \qquad (3.22)$$

Evaluating the derivatives

$$\begin{aligned} -\frac{\partial f}{\partial S_{11}} &= 1 \\ \frac{\partial f}{\partial\epsilon_R} &= \frac{\tau^2}{1-\rho^2\tau^2}\left[\frac{1+\rho}{\sqrt{\epsilon_R}+\epsilon}\left(\frac{1}{2}-\rho S_{11}\right) + \frac{\rho\gamma l}{\epsilon}\,(1-\rho S_{11})\right] \\ \text{where}\quad \gamma &= j\frac{\omega\sqrt{\epsilon_R}}{c} \end{aligned} \qquad (3.23)$$

so that

$$\frac{\partial\epsilon_R}{\partial S_{11}} = \left(\frac{\partial f}{\partial\epsilon_R}\right)^{-1} \qquad (3.24)$$

The length dependence is evaluated in the same way to give

$$\frac{\partial S_{11}}{\partial l} = \frac{2\gamma\rho\tau^2}{1-\rho^2\tau^2}\ (1-\rho S_{11}) \qquad (3.25)$$

and

$$\frac{\partial \epsilon_R}{\partial l} = -\frac{\frac{\partial S_{11}}{\partial l}}{\frac{\partial S_{11}}{\partial \epsilon_R}} \qquad (3.26)$$

The other equations may be manipulated in exactly the same fashion to produce

$$\frac{\partial S_{21}}{\partial \epsilon_R} = \frac{\rho\tau}{1-\rho^2\tau^2}\left[\frac{1+\rho}{\sqrt{\epsilon_R}+\epsilon}\ (1-\tau S_{21}) + \frac{\rho\gamma l}{\epsilon}\left(\frac{1}{2}-\tau S_{21}\right)\right] \qquad (3.27)$$

$$\frac{\partial \epsilon_R}{\partial S_{21}} = \left(\frac{\partial S_{21}}{\partial \epsilon_R}\right)^{-1} \qquad (3.28)$$

$$\frac{\partial S_{21}}{\partial l} = \frac{\gamma\rho^2\tau}{1-\rho^2\tau^2}\ (1-2\tau S_{21}) \qquad (3.29)$$

for the S_{21} equation,

$$\frac{\partial \epsilon_R}{\partial l} = -\frac{\frac{\partial S_{21}}{\partial l}}{\frac{\partial S_{21}}{\partial \epsilon_R}} \tag{3.30}$$

$$\frac{\partial BJ}{\partial \epsilon_R} = \frac{1}{1-\rho^2\tau^2}\left[\frac{\rho(1+\rho)}{\sqrt{\epsilon_R}+\epsilon}(1-BJ\,\tau^2) - \frac{\tau^2\gamma l}{\epsilon}(1+BJ\,\rho^2)\right] \tag{3.31}$$

$$\frac{\partial \epsilon_R}{\partial S_{11}} = \left(-\frac{2S_{11}}{\frac{\partial BJ}{\partial \epsilon_R}}\right) \quad \frac{\partial \epsilon_R}{\partial S_{21}} = \left(\frac{2S_{21}}{\frac{\partial BJ}{\partial \epsilon_R}}\right) \tag{3.32}$$

$$\frac{\partial BJ}{\partial l} = -\frac{2\gamma\tau^2}{1-\rho^2\tau^2}(1+BJ\,\rho^2) \tag{3.33}$$

$$\frac{\partial \epsilon_R}{\partial l} = -\frac{\frac{\partial BJ}{\partial l}}{\frac{\partial BJ}{\partial \epsilon_R}} \quad \text{where} \quad BJ = \frac{(\tau^2-\rho^2)}{1-\rho^2\tau^2} \tag{3.34}$$

for the Baker-Jarvis equation,

$$\frac{\partial \epsilon_R}{\partial Y_I} = \frac{2\,(\epsilon_R \coth(\gamma l) - \sqrt{\epsilon_R}\,Y_L)}{(\coth(\gamma l) - (\gamma l)\operatorname{csch}^2(\gamma l))(Y_L - Y_I) - 2\sqrt{\epsilon_R}} \tag{3.35}$$

$$\frac{\partial \epsilon_R}{\partial l} = -\frac{\gamma\sqrt{\epsilon_R}(Y_L - Y_I)\,\mathrm{csch}^2(\gamma l)}{\left(\frac{1}{2\sqrt{\epsilon_R}}[\coth(\gamma l) - (\gamma l)\,\mathrm{csch}^2(\gamma l)](Y_L - Y_I) - 1\right)} \quad (3.36)$$

for the modified Cole equation, and

$$\frac{\partial \epsilon_R}{\partial Z} = \frac{\left[2\sqrt{\epsilon_R} + \frac{2\epsilon_R Z_L}{Z_0}\tanh(\gamma l)\right]}{\left[\left(\frac{Z_0}{\epsilon_R} - \frac{Z_I Z_L}{Z_0}\right)(\gamma l)\,\mathrm{sech}^2(\gamma l) - \left(\frac{Z_0}{\epsilon_R} + \frac{Z_I Z_L}{Z_0}\right)\tanh(\gamma l)\right]} \quad (3.37)$$

$$\frac{\partial f_z}{\partial l} = \frac{\gamma\,\mathrm{sech}^2(\gamma l)}{1 + \frac{Z_L\sqrt{\epsilon_R}}{Z_0}\tanh(\gamma l)}\left[\frac{Z_0}{\sqrt{\epsilon_R}} - Z_I Z_L\right] \quad (3.38)$$

for the impedance equation.

The error bounds resulting from these equations are graphed in figures 3.17 through 3.28. Note that the assumption of independence fails to some extent in the case of the Baker-Jarvis equation which depends on both S_{11} and S_{21}. However, for small errors in the scattering parameters this is still a valid first approximation. Also, comparison of the error bounds for the modified Cole equation and the impedance equation showed that they agreed to within 10^{-2}, so only one result is graphed in each case for these two schemes.

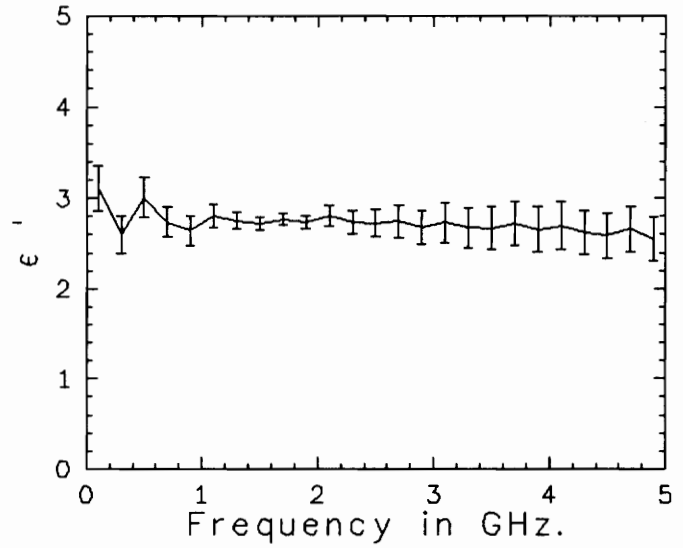

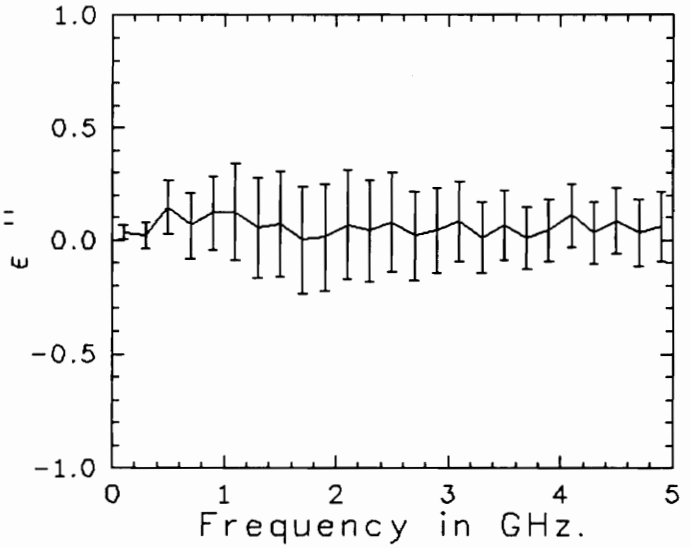

Figure 3.17: Permittivity of Dry Sand Using the S_{11} Equation -- Experimental Error

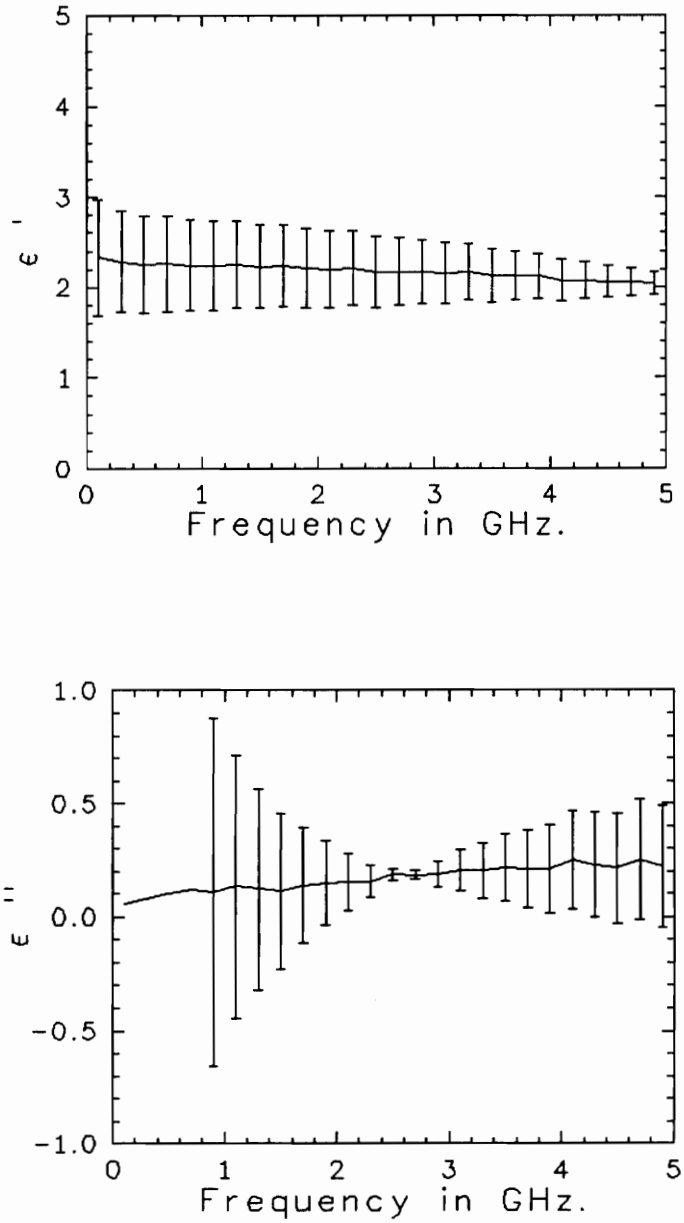

Figure 3.18: Permittivity of Dry Sand Using the S_{21} Equation -- Experimental Error

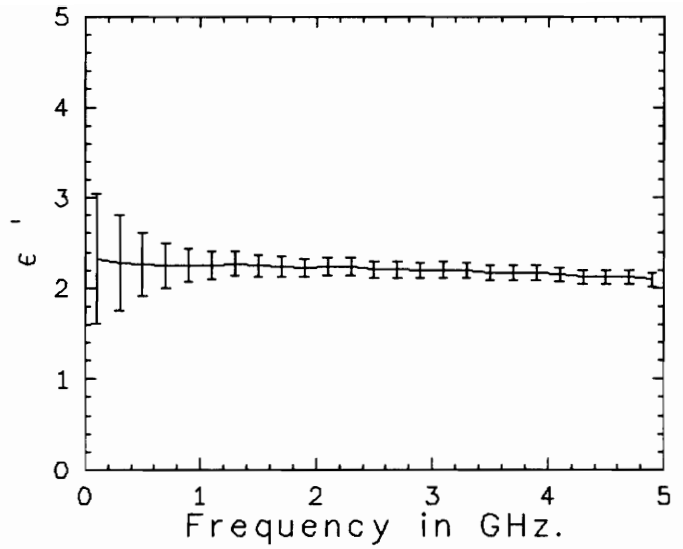

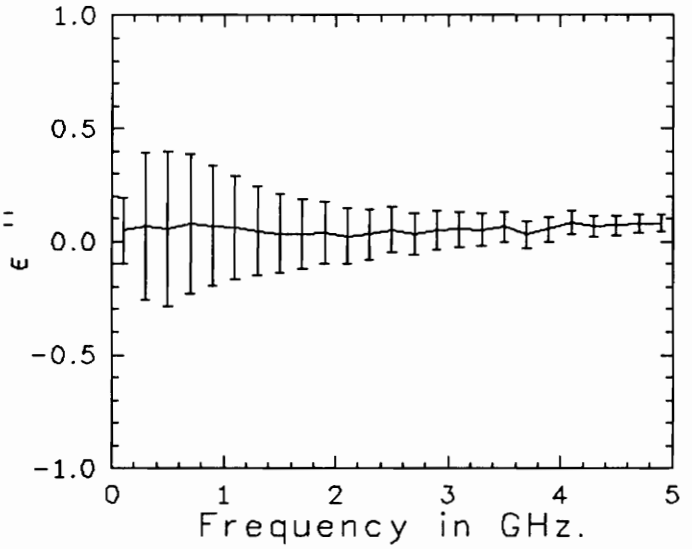

Figure 3.19: Permittivity of Dry Sand Using the Baker-Jarvis Equation -- Experimental Error

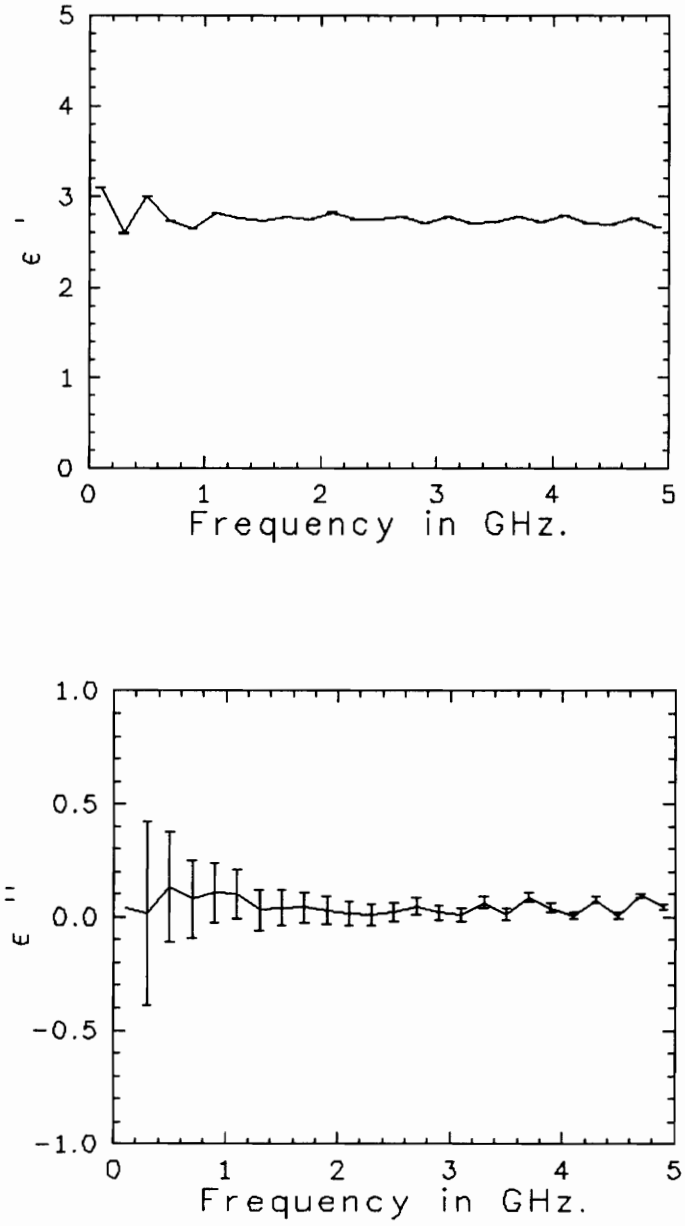

Figure 3.20: Permittivity of Dry Sand Using Cole's Equation -- Experimental Error

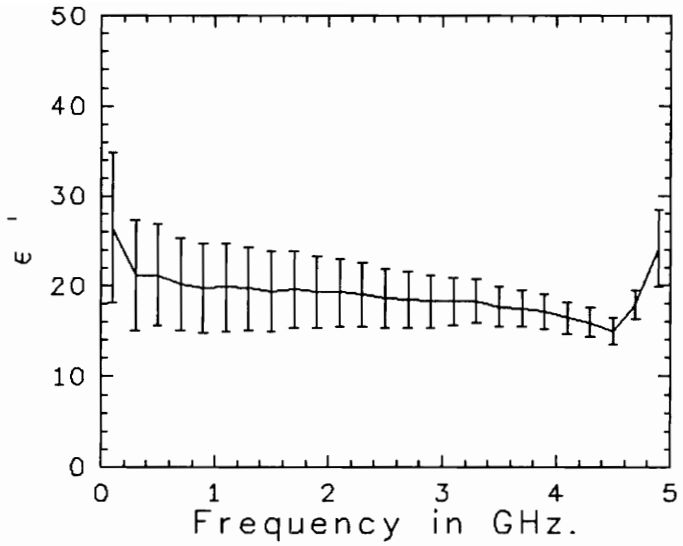

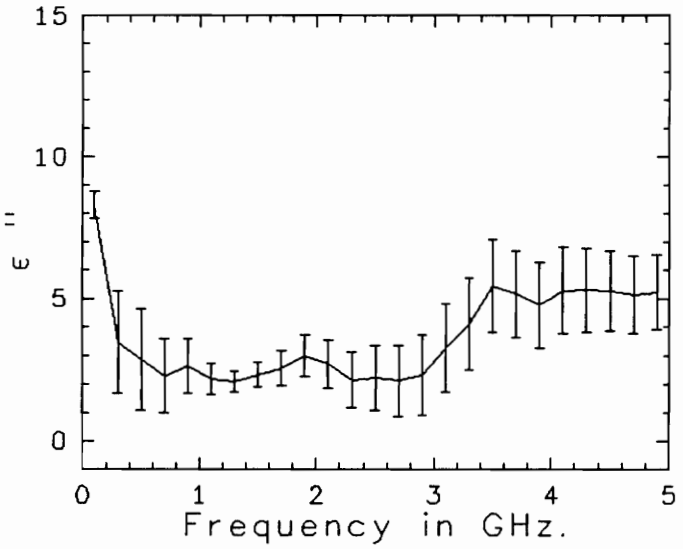

Figure 3.21: Permittivity of Wet Sand Using the S_{11} Equation -- Experimental Error

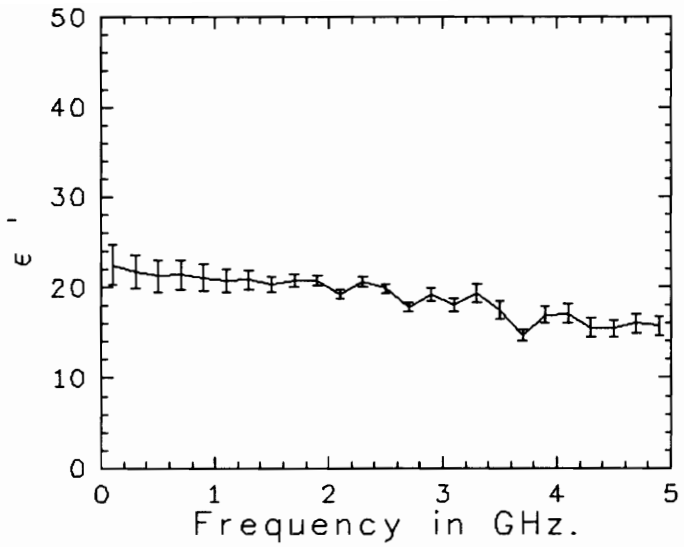

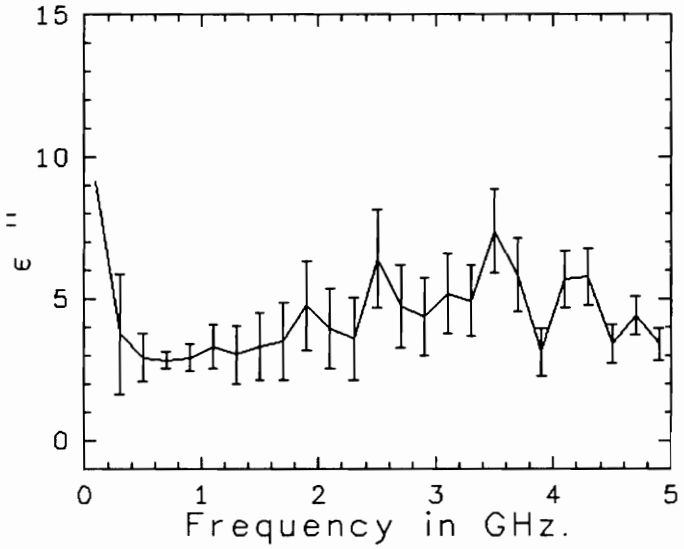

Figure 3.22: Permittivity of Wet Sand Using the S_{21} Equation -- Experimental Error

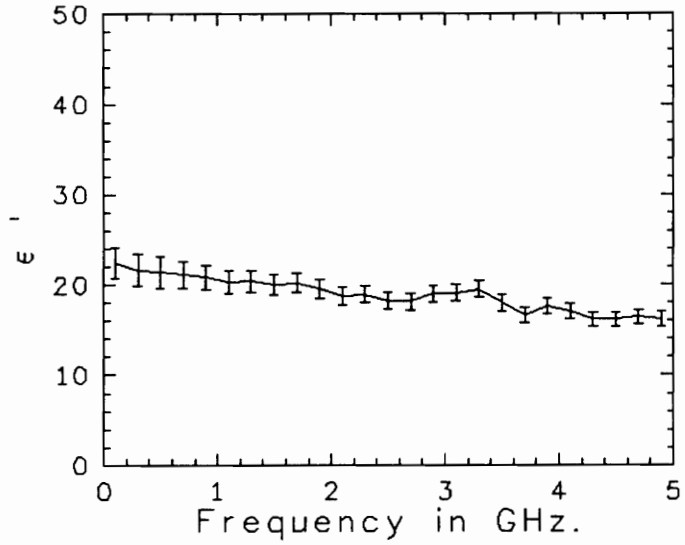

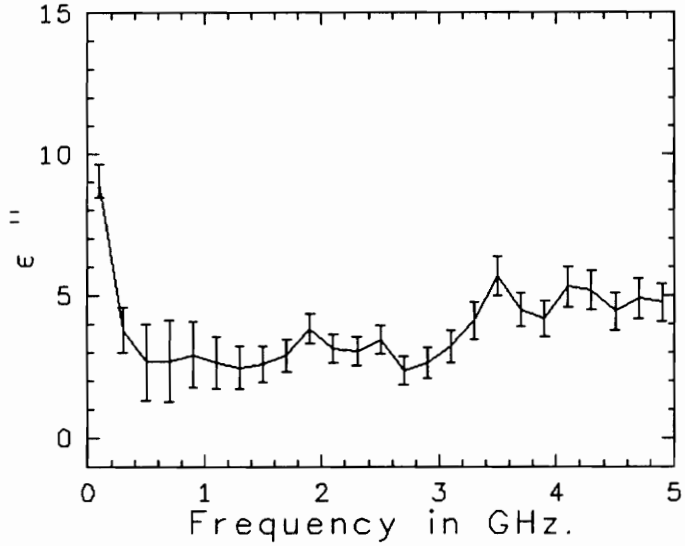

Figure 3.23: Permittivity of Wet Sand Using the Baker-Jarvis Equation -- Experimental Error

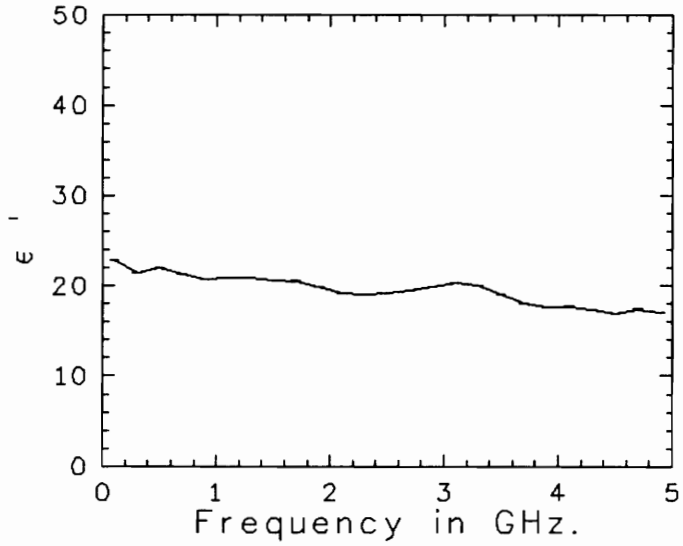

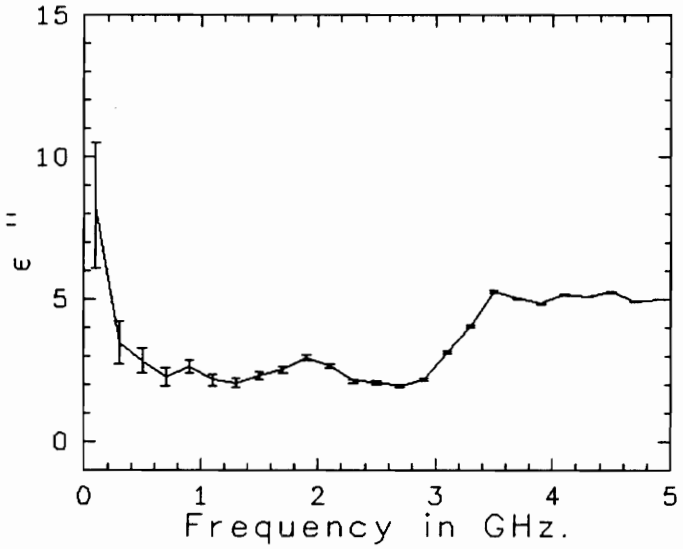

Figure 3.24: Permittivity of Wet Sand Using Cole's Equation -- Experimental Error

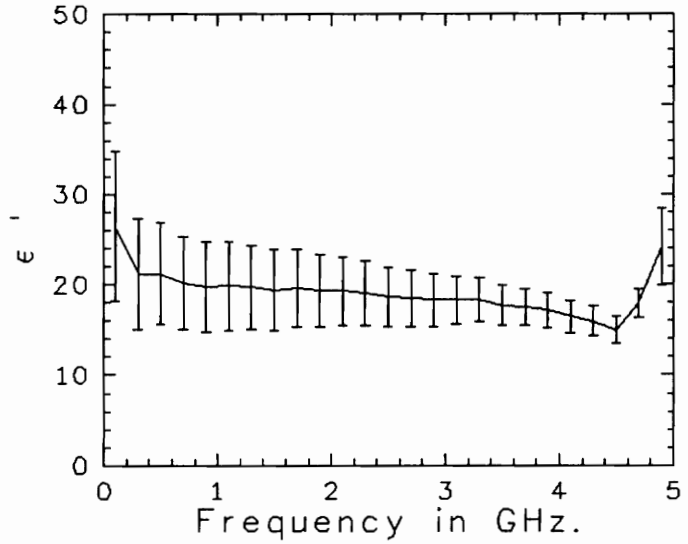

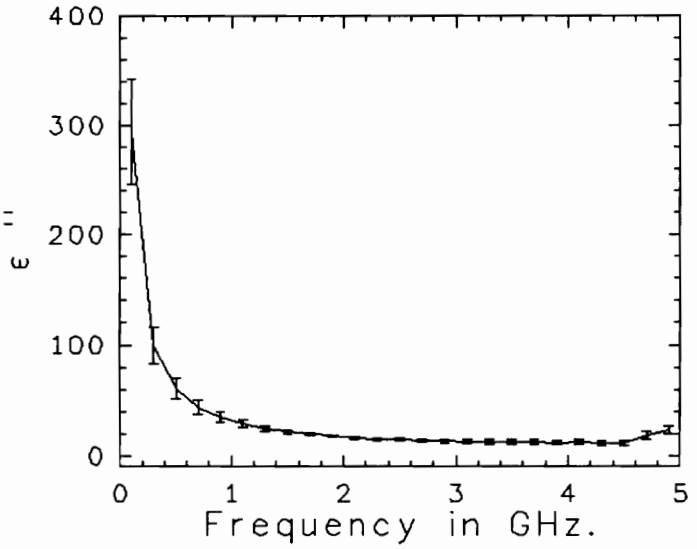

Figure 3.25: Permittivity of Saltwater Sand Using the S_{11} Equation -- Experimental Error

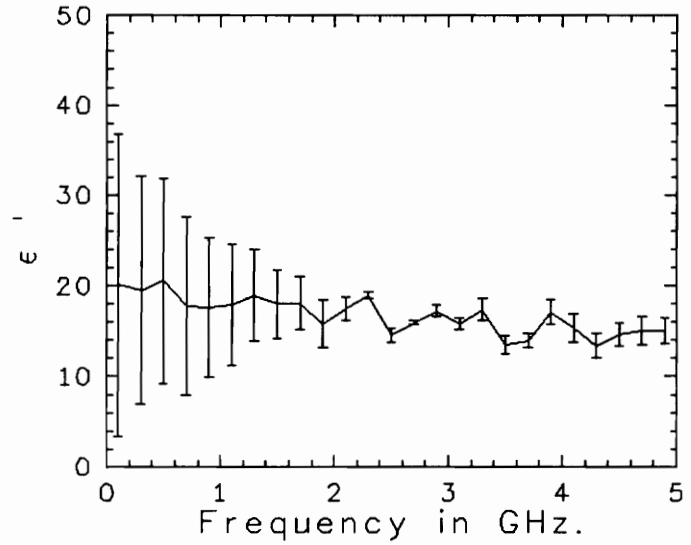

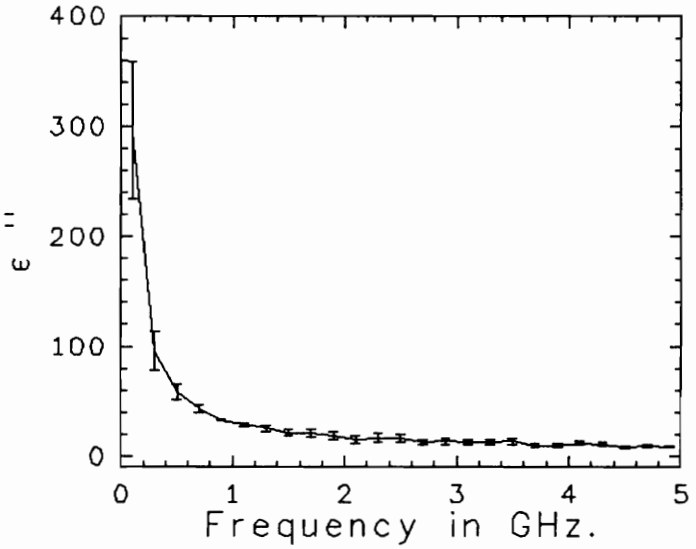

Figure 3.26: Permittivity of Saltwater Sand Using the S_{21} Equation -- Experimental Error

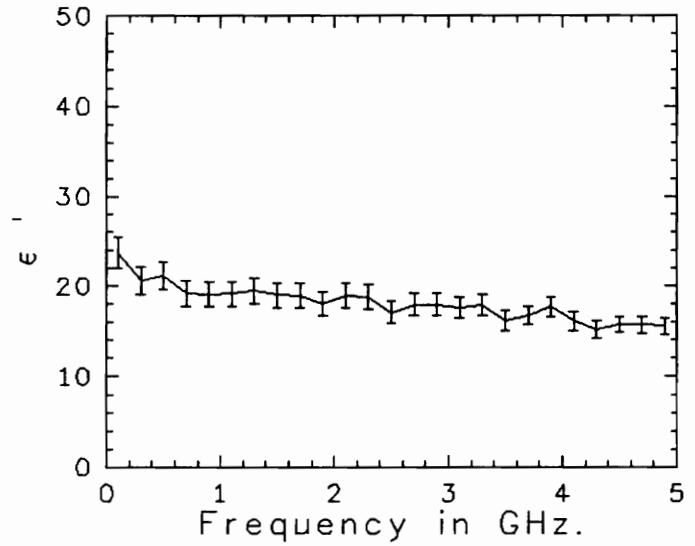

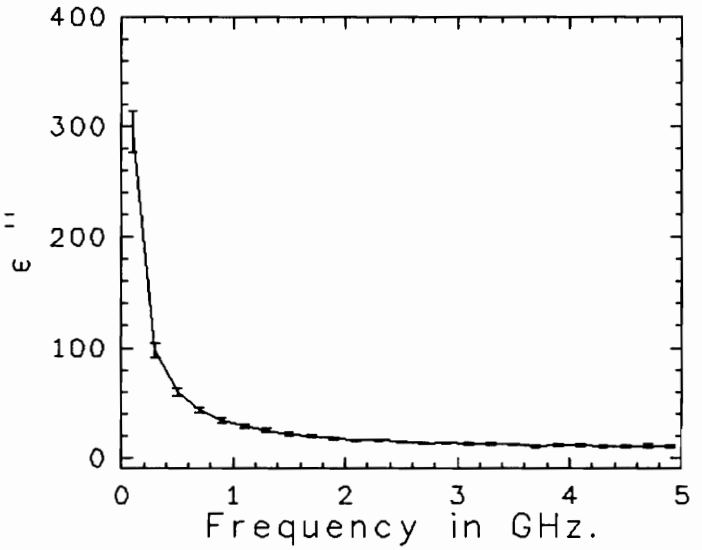

Figure 3.27: Permittivity of Saltwater Sand Using the Baker-Jarvis Equation -- Experimental Error

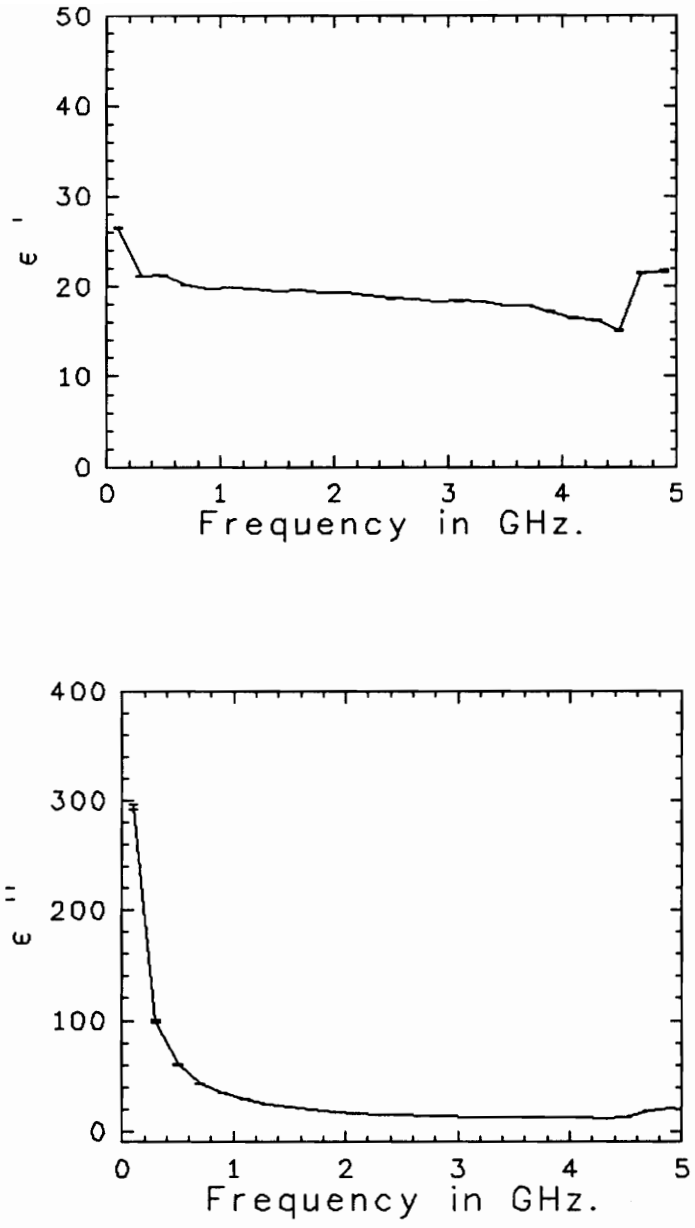

Figure 3.28: Permittivity of Saltwater Sand Using Cole's Equation -- Experimental Error

It is clear from these results that the impedance dependent algorithms are far less sensitive to measurement error than any of the other schemes. However, they make use of only half the available information (reflection data) and therefore are not as smooth versus frequency as the Baker-Jarvis equation results. Also, comparison of these graphs with those presented in figures 3.4 through 3.16 indicates that errors due to repeatability constraints far outweigh those caused by measurement inaccuracies. These repeatability problems could be reduced by sieving the sand to produce a uniform particle size and packing schemes designed to reduce density gradations appearing in the samples, but since the intent of this series of measurements is to provide comparison data for later simulated in situ measurements, and not to provide exact values for the material permittivity, laboratory preparation of the above nature did not seem to be indicated and was not attempted.

The problem of multimoding in the sample holder caused some initial concern. The cutoff frequency for the TE_{11} mode in 14 mm air line is 9.93 GHz and this is inversely proportional to the square root of the sample permittivity. This leads to the conclusion that the wet samples, with permittivities of about 20, could support TE_{11} mode propagation at 2.2 GHz. Although circumferential variations due to grain size and packing variation seem to be likely in

these samples, the characteristic jump in calculated permittivity and loss commonly seen during high order mode propagation [37] were not experienced in these measurements. It is possible that the losses due to ionic conduction may account for this, but other mechanisms may also be involved.

The next chapter discusses measurements made with an open-circuited coaxial sample holder. The above results seem to indicate that repeatability is a major concern and that more variability with frequency may be expected in a pure reflection measurement. These results also serve as basis information for comparison to later measurements, and in this regard it is anticipated that the Baker-Jarvis and impedance based data will be most useful.

CHAPTER IV

THE OPEN CIRCUITED COAXIAL SAMPLE HOLDER

This chapter concerns investigations into the behavior of the shielded open circuit terminated coaxial sample holder. Unlike the previous chapter, all measurements made with this sample holder are reflection measurements, and the sample holder is not terminated in a matched load. The particular sample holder used also differs from the earlier system in length. Earlier samples were about 0.5 cm in length, and those used in the open circuit coaxial holder are much longer - close to 10 cm. This was in keeping with the progression of these investigations toward the twin lead ground probe, which is 30 cm in length, but the longer propagation distance led to some interesting difficulties which will be discussed in the error analysis.

As in the previous chapter, the experimental setup will be described first, followed by a description of the mathematical algorithms used to derive the permittivity information from the measured data. Experimental results and an error analysis applied to those results conclude the chapter.

EXPERIMENTAL SETUP

The sample holder used was one of a group fabricated by Bussey for his measurements [38]. It is comprised of a length of 14 mm coaxial line which is 15.34 cm long from the proximal connector plane to the end of the outer conductor. The base of the sample holder is a GR-900 connector which is constructed in the following way. The center conductor proceeds from the base of the connector through an 7.2 mm air space and into a teflon bead which is 7.4 mm in thickness. Within the bead the center conductor is undercut so as to maintain a 50 ohm impedance within the teflon dielectric i.e. the bead is compensated. The center conductor extends from the bead for a length of 9.15 cm and the end of the center conductor is hemispherical. The outer conductor extends past the end of the inner conductor for a distance of 4.83 cm where it is cut perpendicular to the center conductor. The entire sample holder is silver plated to reduce conductor resistivity. A diagram of this device is shown in figure 4.1.

The sample holder was connected to the sampling oscilloscope through a coaxial network consisting of an SMA to GR-900 adapter, three 30 cm coaxial air lines, a GR-900 elbow adapter, and two more 30 cm coaxial air lines (figure

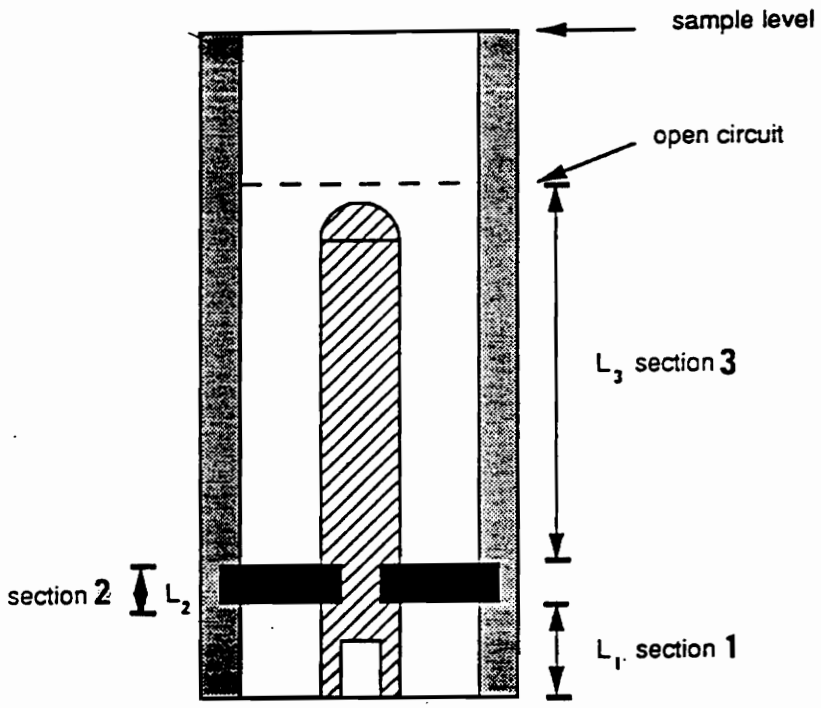

Figure 4.1: The Open Circuited Coaxial Sample Holder

4.2). The SMA to GR-900 adapter was necessary to mate the coaxial air lines to the SMA connectors on the oscilloscope, and the elbow was used to allow a vertical orientation for the sample holder. The coaxial air lines serve two purposes - they provide a clean 50 ohm reference for the acquired waveform and they guard against possible corruption of the acquired waveform if the scope is not well back matched. That is, a signal reflected from the sample could be re-reflected by a poorly matched sampling head and then be reflected from the sample once again to produce a corrupted waveform. This is very unlikely in the case of the HP-54120 oscilloscope which seems to be very close to 50 ohms in input impedance, but in any case such a signal would have to traverse a path 3 m longer than the desired waveform and so would arrive at the sampling head a minimum of 10 ns later than it, well outside of the 5 ns sampling window.

The internal step generator of the oscilloscope was once again used as the excitation waveform in an attempt to reduce the corrupting effects of jitter by taking advantage of this oscilloscope's excellent internal trigger circuitry. For each sample three measurements were made. First, the sample holder was measured empty. This provided a waveform which could be used as a calibration standard in later calculations since the permittivity of air is known. The second acquired waveform was taken with a precisely machined brass shorting

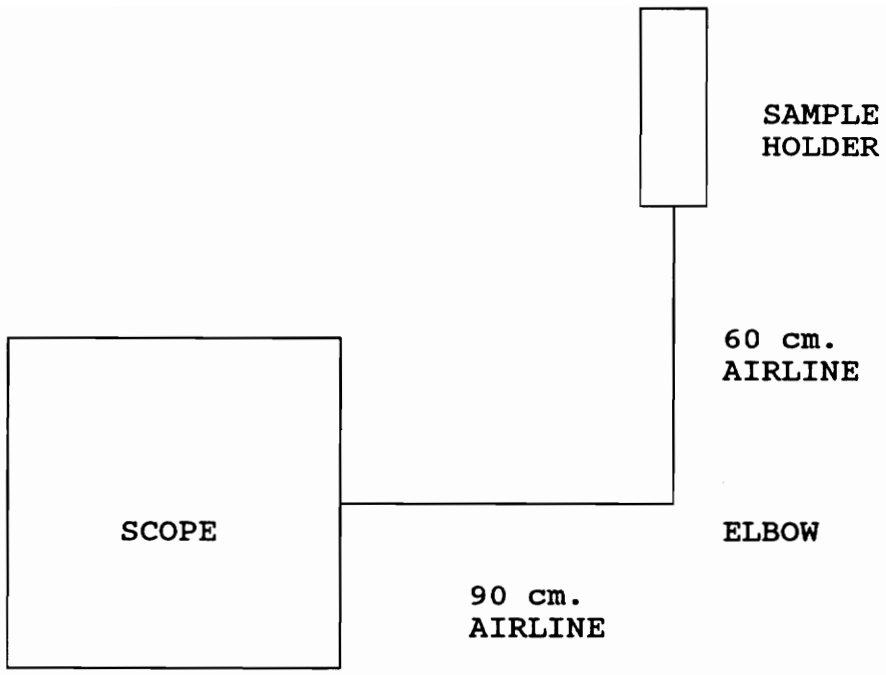

Figure 4.2: Experimental Layout for the Open Circuited Coaxial Sample Holder

bar inserted into the sampling holder. This bar was turned on a lathe to produce a tight fit in the sample holder, and a coaxial hole was drilled in the center to fit the inner conductor. The intention was to produce an inverted replica of the excitation waveform seen by the sample. This waveform differed from the oscilloscope's step generator output because of the effects of passage through the GR-900 connector and the teflon bead. The third waveform was acquired with the sample holder filled with the sample. The holder was always completely filled (i.e. the sample extended well past the end of the center conductor) so that any fringing fields would stay within the sample. During the course of these acquisitions the sample holder was also replaced with a precision GR-900 short circuit on several occasions, and these waveforms were also acquired.

Each acquired waveform was taken with a resolution of 1024 points over a time window of 5 ns, and each was averaged 2048 times using the internal routines of the oscilloscope. This procedure is exactly equivalent to that used for the earlier coaxial sample holder measurements.

In the same fashion as the previous chapter, S_1 of the sample holder/sample combination may be evaluated as minus the quotient of the Fourier transform of the waveform acquired using the sample filled line divided by the Fourier

transform of the waveform acquired using the line with the shorting bar inserted. This yields

$$\frac{\mathcal{F}(V_A(t-t_0-2t_a-2t_b))}{\mathcal{F}(V_S(t-t_0-2t_a-2t_b))} = \frac{\mathcal{F}(V_I(t-t_0-2t_a-2t_b) \otimes s_1(t))}{\mathcal{F}(-V_I(t-t_0-2t_a-2t_b))} = S_1(\omega) \tag{4.1}$$

where t_0 is once again the time required for the step excitation to traverse the round trip distance between the sampling head and the sample holder, t_a is the time required to traverse the one-way distance through the air dielectric portion of the GR-900 connector, and t_b is the one-way transit time through the teflon bead. The effect of this action is to deconvolve the excitation waveform from the reflected waveform in the frequency domain. Note that the plane of the short circuit provided by the shorting bar is at the same point along the coaxial line as the proximal plane of the sample so no phase adjustment is needed.

The Fourier transform of the excitation waveform may be derived in two other ways from the acquired information. Under the assumption that the air dielectric and teflon filled portions of the sample holder contribute only phase delay effects and using the time delay property of the Fourier transform, a comparison of the waveform acquired using the precision short circuit ($v_S(t_0)$) with the waveform acquired using the shorting bar yields

$$\mathcal{F}(V_I(t-t_0-2t_a-2t_b)) = e^{-\left(\frac{j\omega}{c}\right)\left(2l_a\sqrt{\epsilon_{R_{air}}}+2l_b\sqrt{\epsilon_{R_{teflon}}}\right)} \cdot \mathcal{F}(V_I(t-t_0)) \quad \textbf{(4.2)}$$

where l_a and l_b are the lengths of the air dielectric portion of the line and the teflon bead respectively. In the same fashion, the waveform acquired from the air filled sample holder represents a phase delayed version of the excitation waveform present at the proximal plane of the sample so that

$$\mathcal{F}(V_I(t-t_0-2t_a-2t_b)) = e^{+\left(\frac{j\omega}{c}\right)\left(2l\sqrt{\epsilon_{R_{air}}}\right)} \cdot \mathcal{F}(V_I(t-t_0-2t_a-2t_b-2t_{cc})) \quad \textbf{(4.3)}$$

where l and t_{cc} represent the length and one way transit time of the center conductor.

The electrical length of the center conductor is subject to some ambiguity due to the fringing fields present at the abrupt open circuit termination. The problem was discussed in a paper by Somlo [57] who determined that this effect could be modeled as a capacitive termination which could in turn be expressed as an extension of the physical line. Bussey gives an equation which quantifies the amount of extension needed for different frequencies and permittivities [38]

$$d' = (b-a)\,(0.6034+0.9464x^2+18.18x^{5.127}) \quad x<0.3$$

where $x = \dfrac{f\,b\,\sqrt{\epsilon_R'}}{c}$ **(4.4)**

and a = inner conductor radius
b = outer conductor inside radius

but does not carry his results past x=0.3, corresponding to a frequency of about 1.2 GHz for the wet samples (ϵ_R'=25). Since this investigation covers frequencies well past this point, another equation was derived to fit Somlo's data for the region 0.3 < x < 0.38274.

$$d' = (b-a)\,(2.1876E\text{-}9e^{49.6759x} + 0.5942e^{0.6399x}) \quad 0.3< x <0.3827$$

(4.5)

This upper bound represents the onset of TE_{11} propagation, and Somlo points out that a virtual short circuit is produced at the end of the inner conductor for frequencies above this value, leading to a line extension of $\lambda/4$.

The calibrated short circuit does not suffer from this ambiguity however, and was used instead of the shorting bar to determine the reference excitation waveform for the wet samples. The shorting bar in those cases was found to produce a much larger experimental spread between successive series of acquisitions and it is assumed that slight eccentricities are present in either the inner or outer surfaces of the bar. These apparently produce phase errors

in the measurement which are magnified due to the relatively large values of permittivity in the measured samples. No such difficulty was noticeable in the dry sand acquisitions and for these the shorting bar produced acceptable results.

MATHEMATICAL ALGORITHMS

Three different methods were used to derive permittivity information from the open circuit coaxial sample holder data. Two of these relied upon S parameter information and the third was based upon impedance measurements.

The first equation used was derived using the bounce diagram for the open circuit holder (figure 4.3). This gives an equation which represents the total reflection from the sample.

$$\begin{aligned} S_1(\omega) &= \rho+(1-\rho^2)\tau^2+(1-\rho^2)(-\rho)\tau^4+(1-\rho^2)(-\rho)^2\tau^6+\ldots \\ &= \rho+(1-\rho^2)\tau^2\ [1+(-\rho\tau^2)+(-\rho\tau^2)^2+(-\rho\tau^2)^3\ldots] \\ &= \frac{\rho+\tau^2}{1+\rho\tau^2} \end{aligned} \qquad (4.6)$$

Once again, the l used in calculating $\tau(\omega)$ incorporated the Somlo/Bussey length extension to account for the capacitive fringing field.

The second equation used comes from an unpublished paper [Appendix C] which investigates the error sensitivities of the open circuit coaxial holder for both the compensated and

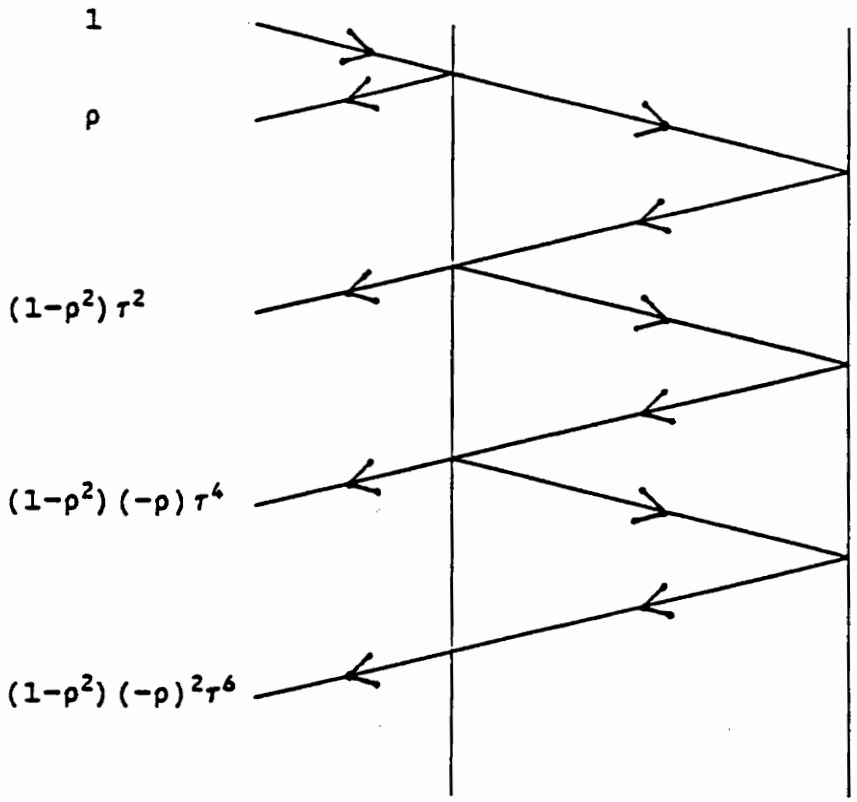

Figure 4.3: Bounce Diagram for the Open Circuited Coaxial Cell

uncompensated cases where measurements are being made using the HP-8510 ANA. For the compensated bead case the equation derived is

$$S_1(\omega) = \frac{\frac{1}{\sqrt{\epsilon_R}} - \tanh(\gamma l)}{\frac{1}{\sqrt{\epsilon_R}} + \tanh(\gamma l)} \qquad (4.7)$$

$$\text{where} \quad \gamma = j\omega \frac{\sqrt{\epsilon_R}}{c}.$$

The last method used was derived by Cole in the same paper [7,8] which furnished one of the algorithms used in the previous chapter. This algorithm relies on admittance measurements to derive permittivity information and was attractive because the original work was done in the time domain and also because the error analysis from the last chapter seemed to indicate the impedance derived values show much lower sensitivity to experimental errors. The equation used is

$$\epsilon_R = \left(-\frac{1}{j\omega l \frac{\sqrt{\epsilon_R}}{c}} \right) \left(\frac{V-R}{V+R} \right) \qquad (4.8)$$

where V and R represent the incident and reflected wavefronts of the sample.

All three of these equations were used with some trepidation in the case of the wet sand samples as all three model the frequency domain steady-state case of total reflection. At 30 cm/ns a wavefront could normally make over 7 round trips through the air filled sample holder within the 5 ns acquisition window. This number is inversely proportional to the square root of the real part of ϵ_R and falls to just over 4 in the case of the sample holder filled with dry sand. This still appears to be adequate to recover most of the reflection information as is illustrated in figure 4.4. In this figure the reflected waveform from the dry sand is plotted along with the reflected waveform from the air filled sample holder. Note that the dry sand waveform shows very little variation due to its last reflection and that it closely approaches the same final value as the air waveform.

The situation is noticeably different in the case of the sand and water sample plotted in figure 4.5. Only two reflections have occurred, the first from the proximal face of the sample and the second from the open circuit at the end of the sample holder. The reflected waveform does not approach the air filled sample holder final value and does not even reach the same amplitude it was injected at. The initial drop in reflection amplitude is characteristic of a high dielectric constant in the line, and the fact that the

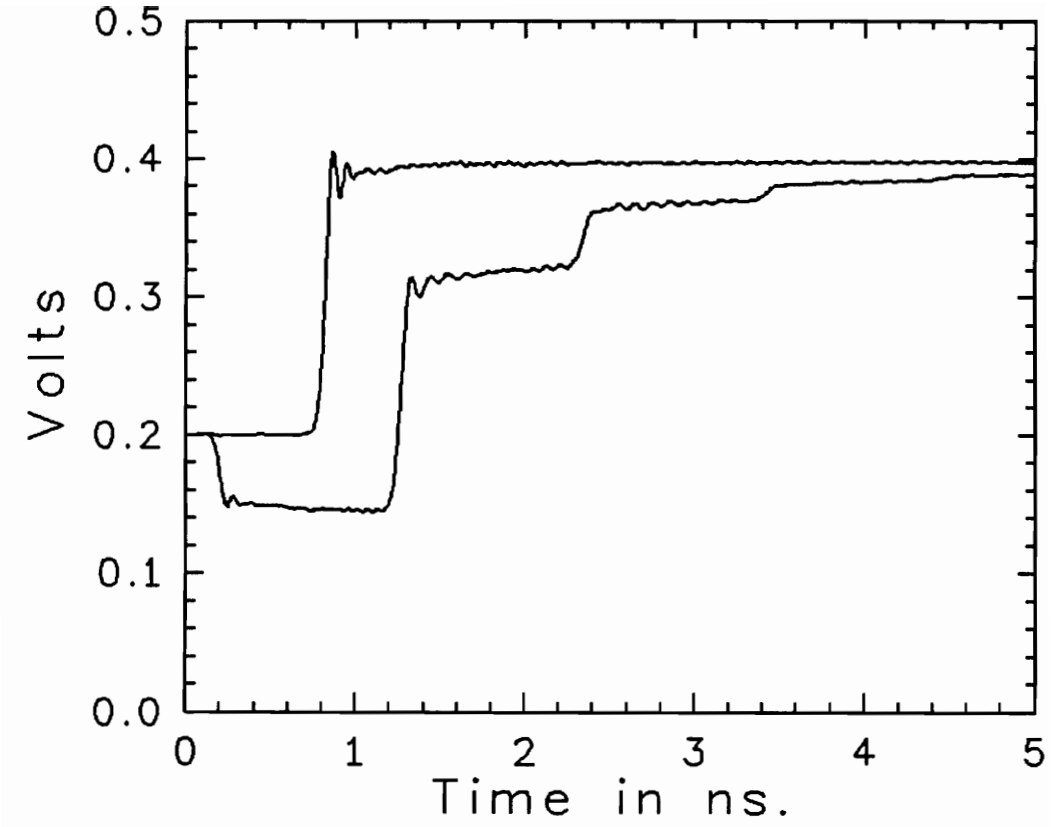

Figure 4.4: Time Domain Response of Air and Dry Sand

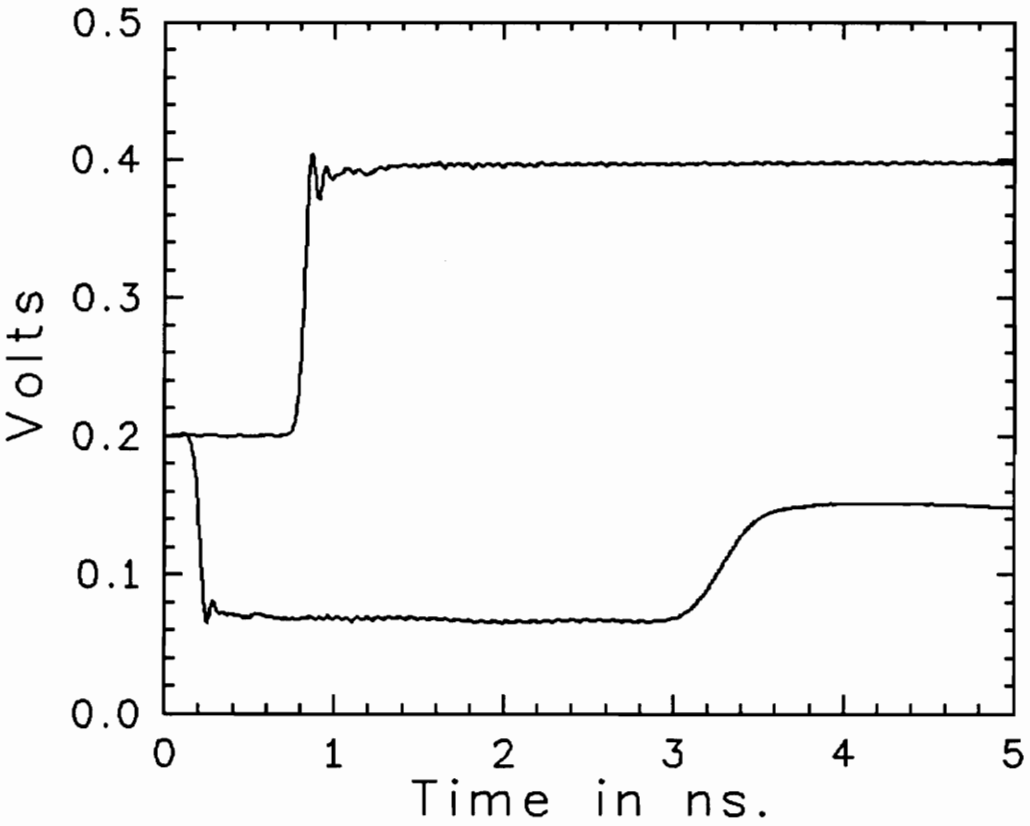

Figure 4.5: Time Domain Response of Air and Wet Sand

wavefront returned from the open circuit is at less than its initial amplitude shows that a significant loss is occurring in the medium. This is even more evident in figure 4.6, where the reflection response of the sand and saltwater sample is plotted. Here, the proximal face reflection drops almost to zero immediately (a near short circuit indication) and no effect from the open circuit reflection is visible in the waveform.

In order to test the conjecture that the reflection information acquired did not include the total response, the first two terms of equation 4.6 (representing the first proximal face reflection and the open circuit reflection) were applied to the data and solved. The results were within 2% for the sand and water case and within machine error bounds for the sand and saltwater case leading to the observation that the effect of losses combined with the relatively long samples allows these measurements to be adequately modeled as total reflections.

EXPERIMENTAL RESULTS

The same three material compositions were studied in this series of measurements as in the last chapter. These were dry sand, sand saturated with water, and sand saturated with a solution of 1 N. saltwater. The length of the sample

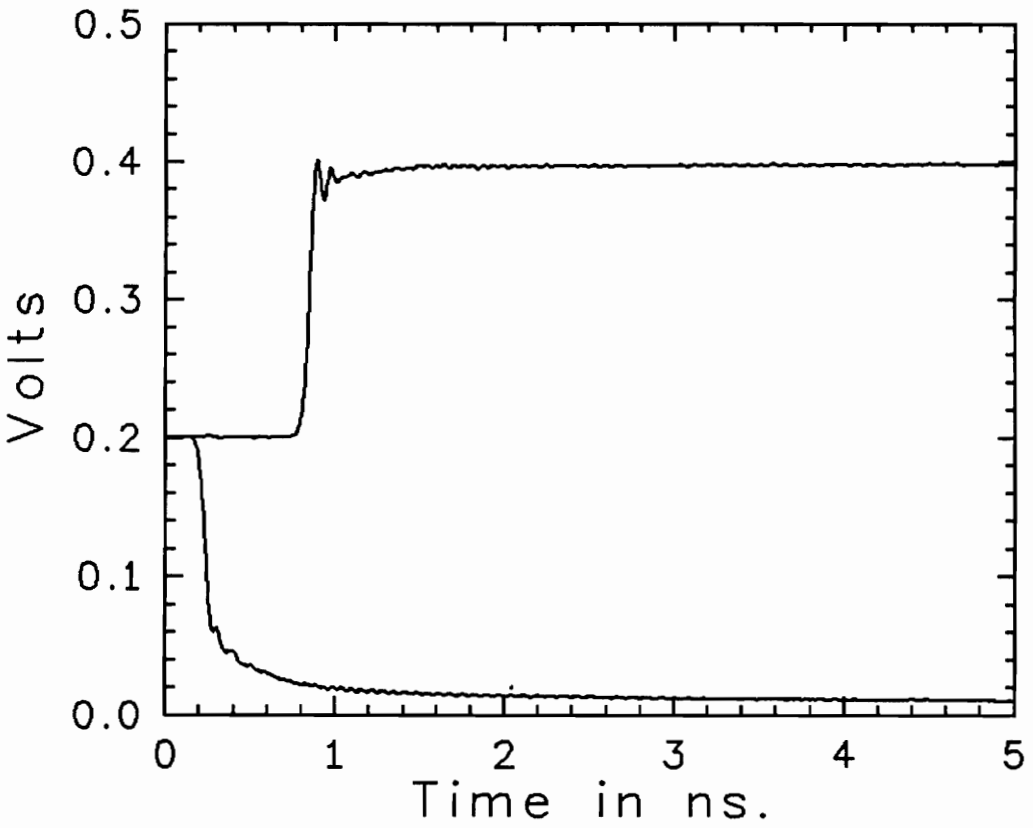

Figure 4.6: Time Domain Response of Air and Saltwater Sand

holder increased the possibility of voids in the sample, so a vibrating table was used to help assure even distribution during the filling process and the wet samples were introduced in small quantities and slightly packed during introduction. Additional amounts of liquid were also added to the wet samples as necessary during packing to maintain the sand in a thoroughly saturated state. Once again, five sets of acquisitions were taken for each material and the graphs indicate the average permittivities and the maximum and minimum excursions from those values.

The results of the dry sand measurements are presented in figures 4.7 through 4.9. The ϵ' results are very nearly the same as those measured using the match terminated coaxial sample holder and the S_{11} and modified Cole algorithms, but two differences are immediately apparent. The low frequency instability is gone, which adds credence to the possibility that it was caused by a residual effect of the teflon washers, and the experimental spread is somewhat smaller between different acquisitions. The open circuit coaxial sample holder also seems to indicate a slightly higher value for ϵ'' at low frequencies than was measured using the match terminated sample holder. The tighter experimental spread may indicate a strong sensitivity to length in the match terminated holder calculations, since these samples were all of slightly different lengths but the length of the center

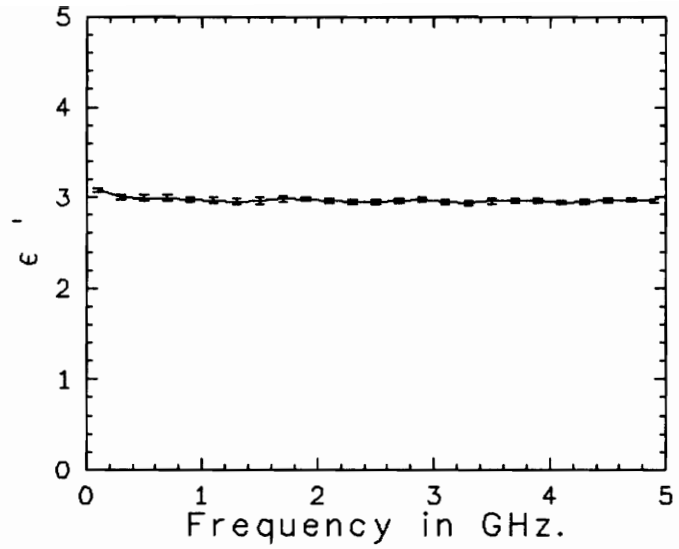

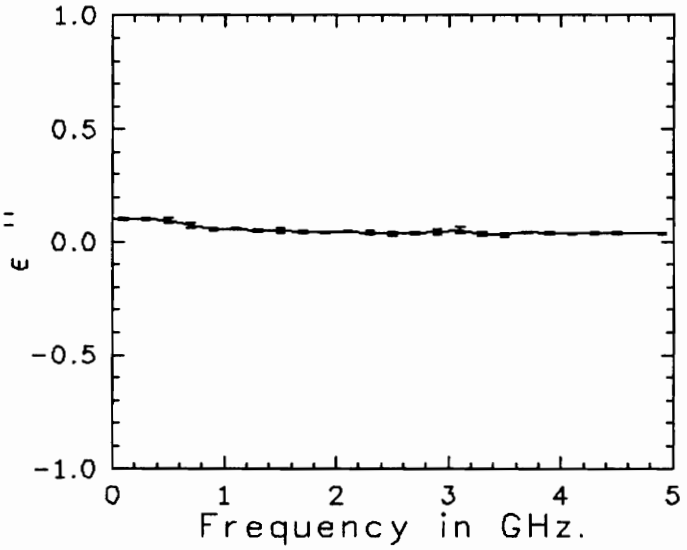

Figure 4.7: Permittivity of Dry Sand Using the S_1 Equation Experimental Spread

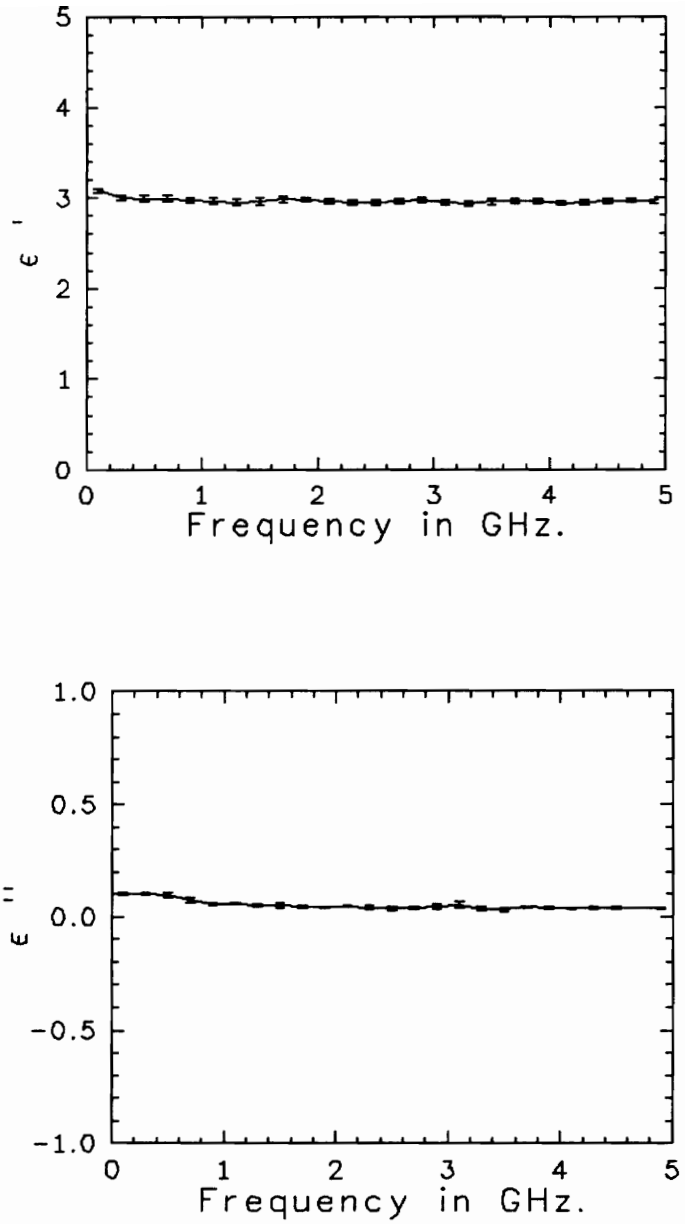

Figure 4.8: Permittivity of Dry Sand Using the Baker-Jarvis Equation -- Experimental Spread

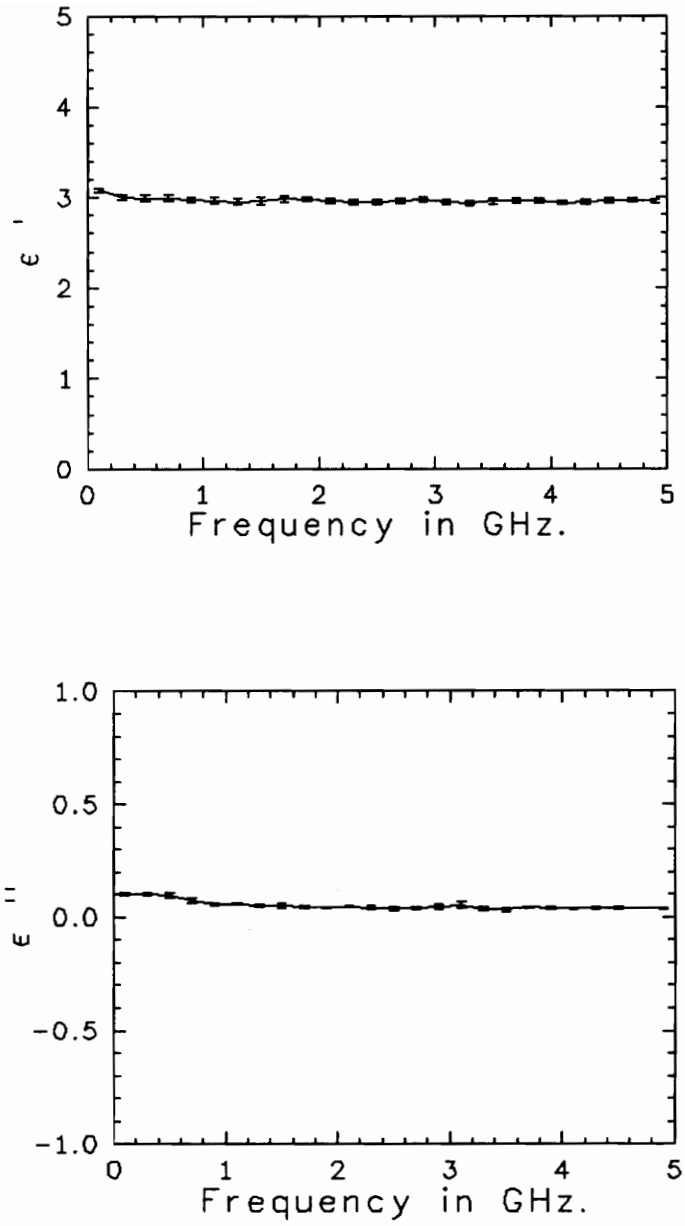

Figure 4.9: Permittivity of Dry Sand Using Cole's Equation Experimental Spread

conductor in the open circuit coaxial holder remains fixed for each acquisition. The low frequency increase in ϵ'' remains unexplained but may be due to a slight amount of moisture in the sand which could lead to an ionic conduction component noticeable at low frequencies.

The graphs in figures 4.10 through 4.12 show the results of the sand and water mixture measurements. A much lower value for both ϵ_R' and ϵ_R'' is derived at the first measurement frequency than at the others and this is probably erroneous.

An oscillation is also evident in the ϵ_R'' results at frequencies lower than 2 GHz and in the ϵ_R' results at frequencies above 2 GHz. At first this was thought to be evidence of a length error somewhere in the experimental calculations, but the fact that it appeared in both quantities and disappeared in one at about the same frequency that it appeared in the other seemed to indicate that this was not the case. The possibility of a length error in the calculations was eliminated by measuring air, and the result from one of these measurements is given in figure 4.13. Another strange factor was the frequency of oscillation, about 600 MHz, which seemed to indicate a physically large resonant network or perhaps some kind of measurement error. This topic will be discussed further in the error analysis portion of this chapter, but at this point it appears that

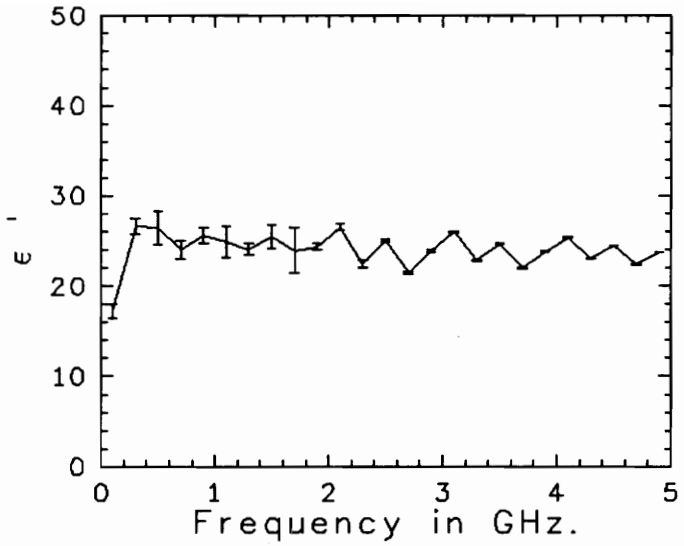

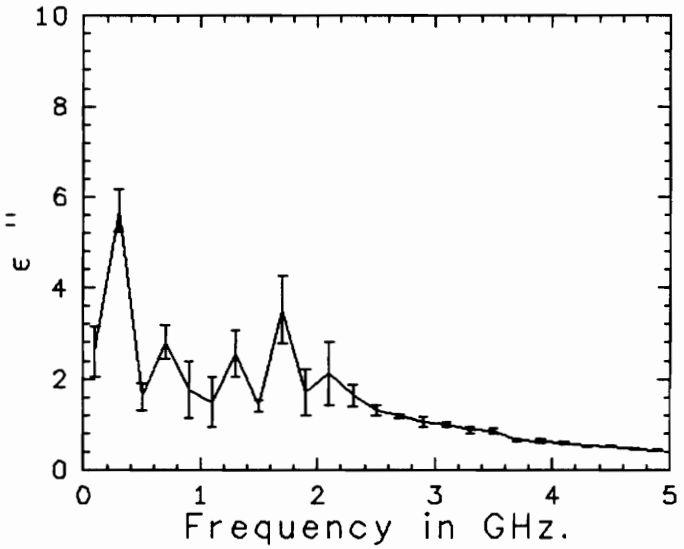

Figure 4.10: Permittivity of Wet Sand Using the S_1 Equation -- Experimental Spread

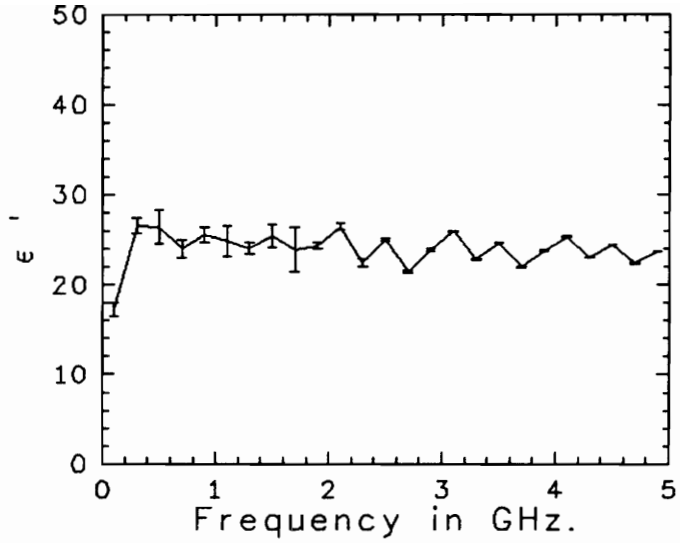

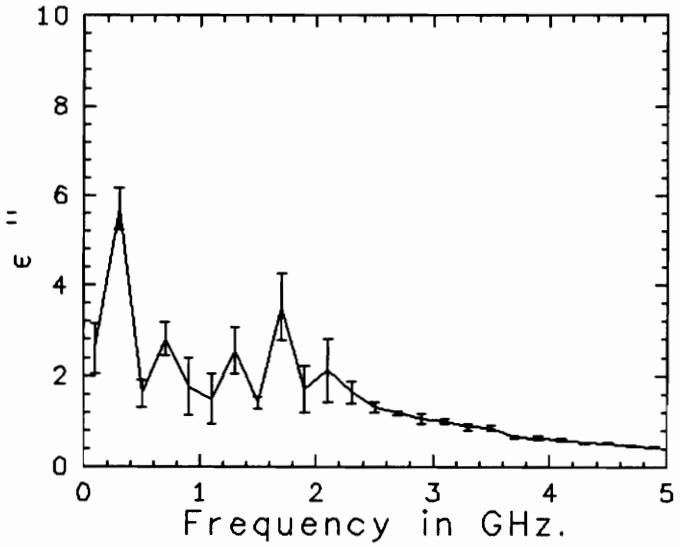

Figure 4.11: Permittivity of Wet Sand Using the Baker-Jarvis Equation -- Experimental Spread

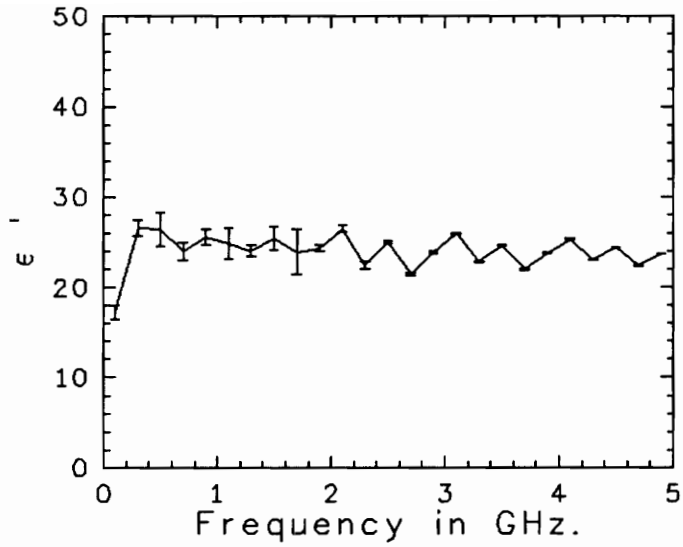

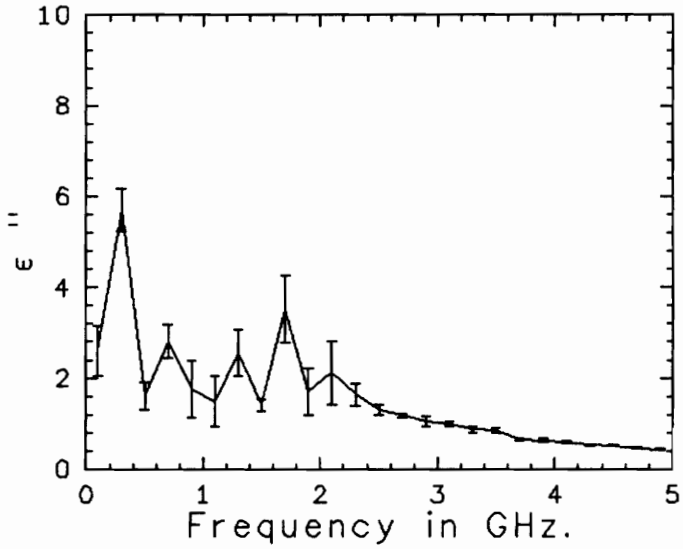

Figure 4.12: Permittivity of Wet Sand Using Cole's Equation -- Experimental Spread

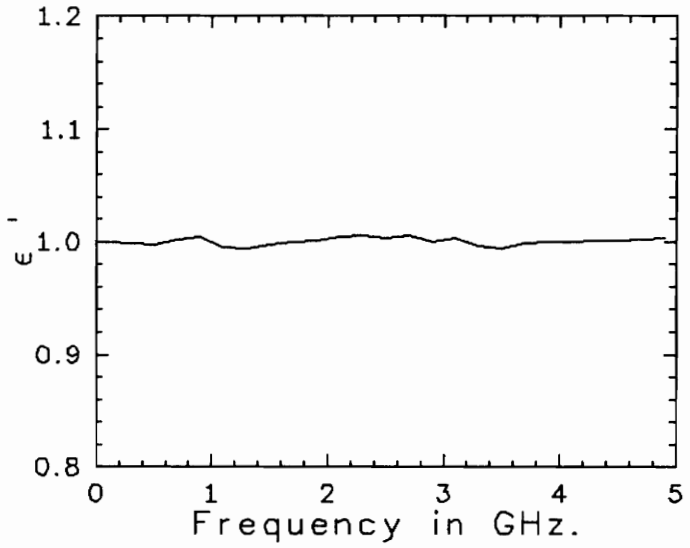

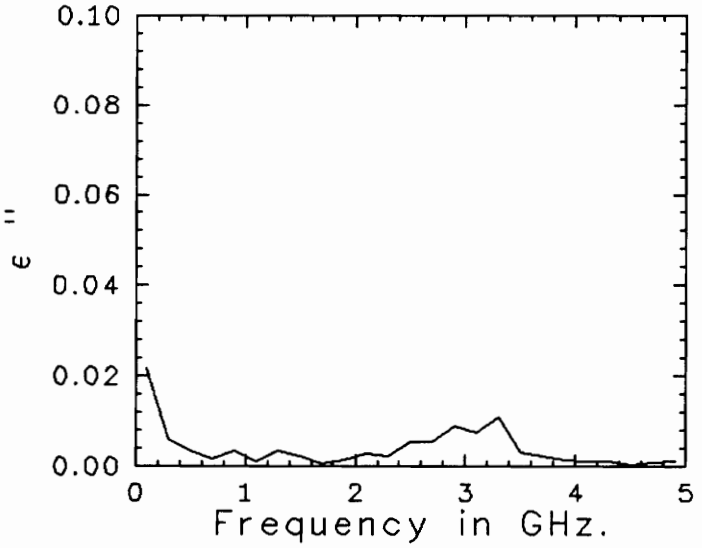

Figure 4.13: Permittivity of Air Using the S_1 Equation

the effect is due to a combination of factors including losses in the sample and limitations of instrument sensitivity, as well as possible resonance effects.

Permittivities derived from the sand and saltwater measurements are graphed in figures 4.14 through 4.16. An oscillation of similar amplitude and frequency to that of the sand and water measurements is again present in ϵ_R' but this time it extends over the entire measurement bandwidth. The permittivity calculated for the lowest frequency is inordinately high and is assumed to be in error. Finally, the characteristic 1/f shape which indicates ionic conduction is clearly present in the ϵ_R'' curves.

The wet sample curves in this series of measurements indicate a slightly higher value of permittivity than those of the match terminated coaxial sample holder experiments. Although the choice of 100% moisture saturation was made to try to prevent differences in the level of moisture between the various different sample samples, it is likely that some moisture was lost in the match terminated sample holder experiments due to the pressure needed to for the teflon washer/sample combination into the sample holder in those measurements, as well as the water repellant properties of the teflon itself. This could easily account for the small differences in the measured values.

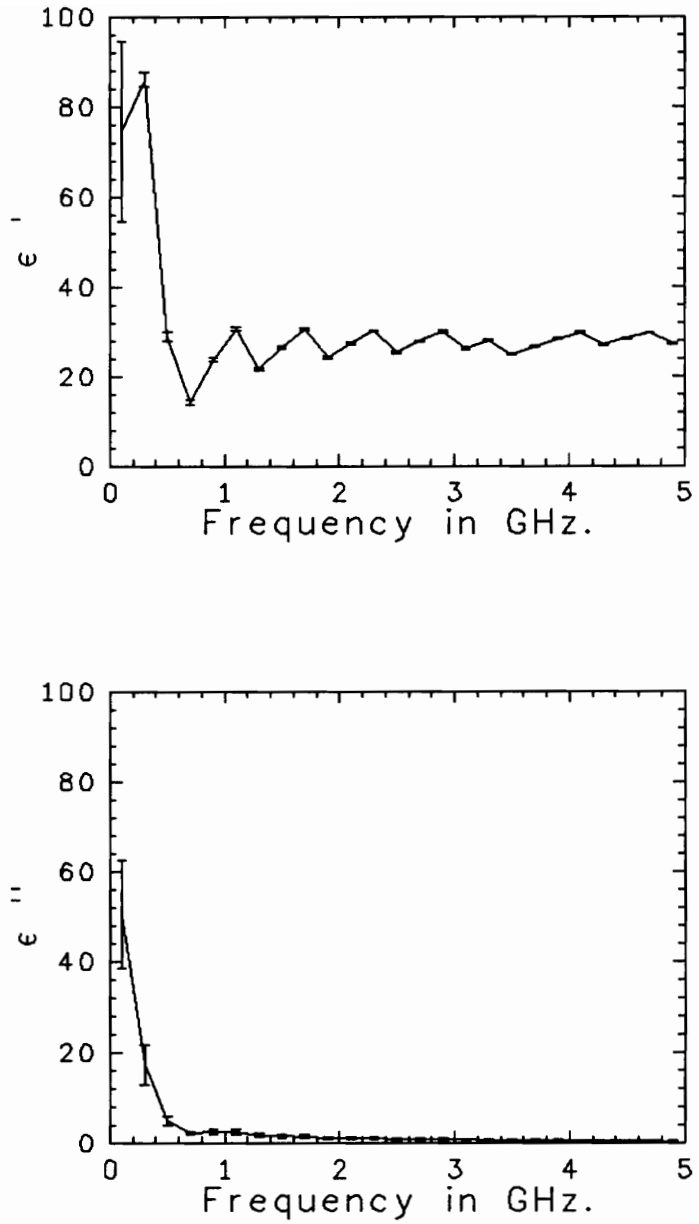

Figure 4.14: Permittivity of Saltwater Sand Using the S_1 Equation -- Experimental Spread

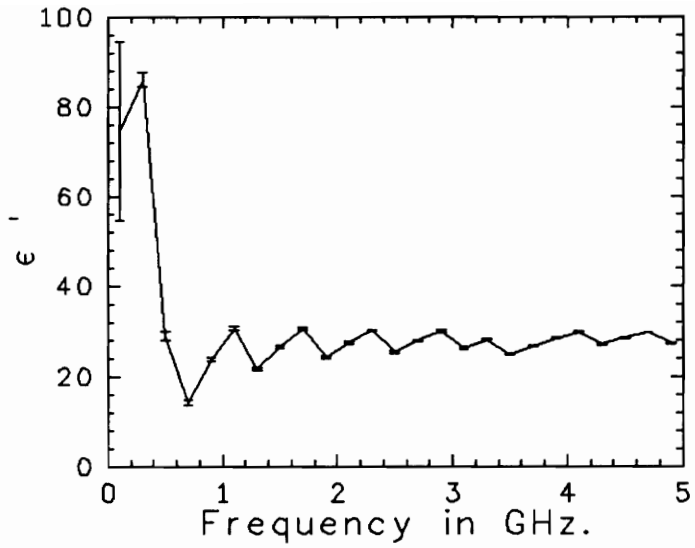

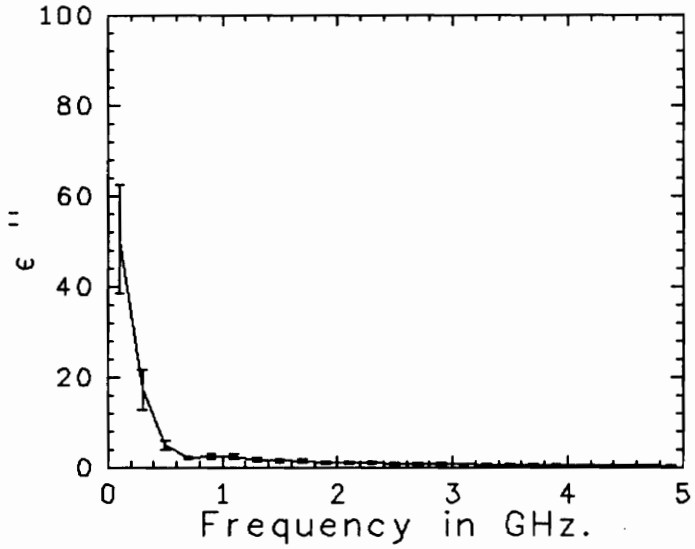

Figure 4.15: Permittivity of Saltwater Sand Using the Baker-Jarvis Equation -- Experimental Spread

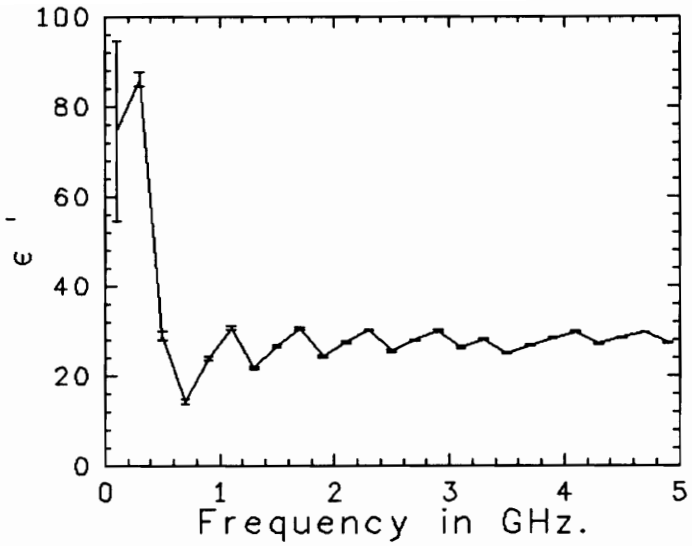

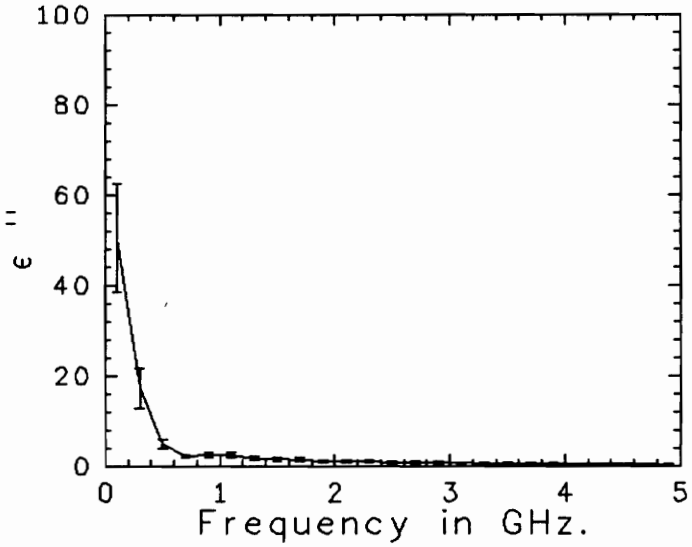

Figure 4.16: Permittivity of Saltwater Sand Using Cole's Equation -- Experimental Spread

ERROR ANALYSIS

The results of the last chapter seemed to indicate that repeatability might be a major error factor in this series of measurements, but this was not the case. The error bounds in figures 4.6 through 4.16 show that variation between measurement runs was very small and, in fact, all three solution techniques gave substantially the same answers for any given measurement. This lack of variation is probably due to the fixed lengths associated with this sample holder, as well as the fact that the teflon bead is fixed in place and compensated so that it contributes only phase effects. The much larger quantities of samples used probably also helps reduce measurement variations.

The length of the sample holder contributed to some potential difficulties in the use of an iterative root finder to solve the necessary equations. All of the methods used incorporate multivalued functions of ϵ^*_R. These functions repeat when the real part of the quantity $\frac{(\omega l\sqrt{\epsilon_R})}{c}$ changes by π. For small values of ϵ_R or l or small bandwidth measurements this does not cause a problem. However, in the case of the wet sample measurements studied here, where l is close to 10, this repetition causes roots of these equations to occur at about 6 unit intervals at 2.5 GHz and closer than 4 unit intervals at 4.1 GHz. This situation is illustrated

in figures 4.17 and 4.18 which show the zero level contours of the real part of the $S_1(\omega)$ equation overlaid with the zero level contours of the imaginary part of the same equation for 2.5 GHz and 4.1 GHz respectively. The close proximity of possible roots at the higher frequencies causes the root finder (Muller's Method) to be very sensitive to the initial guess given.

At first, an initial guess for ϵ_R of 25 - j*1 was tried at all frequencies, but this produced values of ϵ_R' on the order of 40 for the higher frequencies. Setting the initial guess at any given frequency to the solution at the previous frequency, with a low frequency guess of 25 - j*1 produced the same results. Finally, a contour diagram similar to those of figures 4.17 and 4.18 was produced at each frequency of interest, and the initial guess for that frequency was set to the contour intersection which was closest to the previous solution, with a view towards producing a solution whose real part was decreasing with frequency. The rationale for this last constraint involves the fact that the major portion of the dielectric behavior of the wet samples occurs due to the water which has an $\epsilon_R(\omega)$ which monotonically decreases with frequency below the relaxation frequency (about 20 GHz). This scheme may be termed the 'Guided Root Method' and was described to point out that the oscillation was not an artifact of the root finding algorithm.

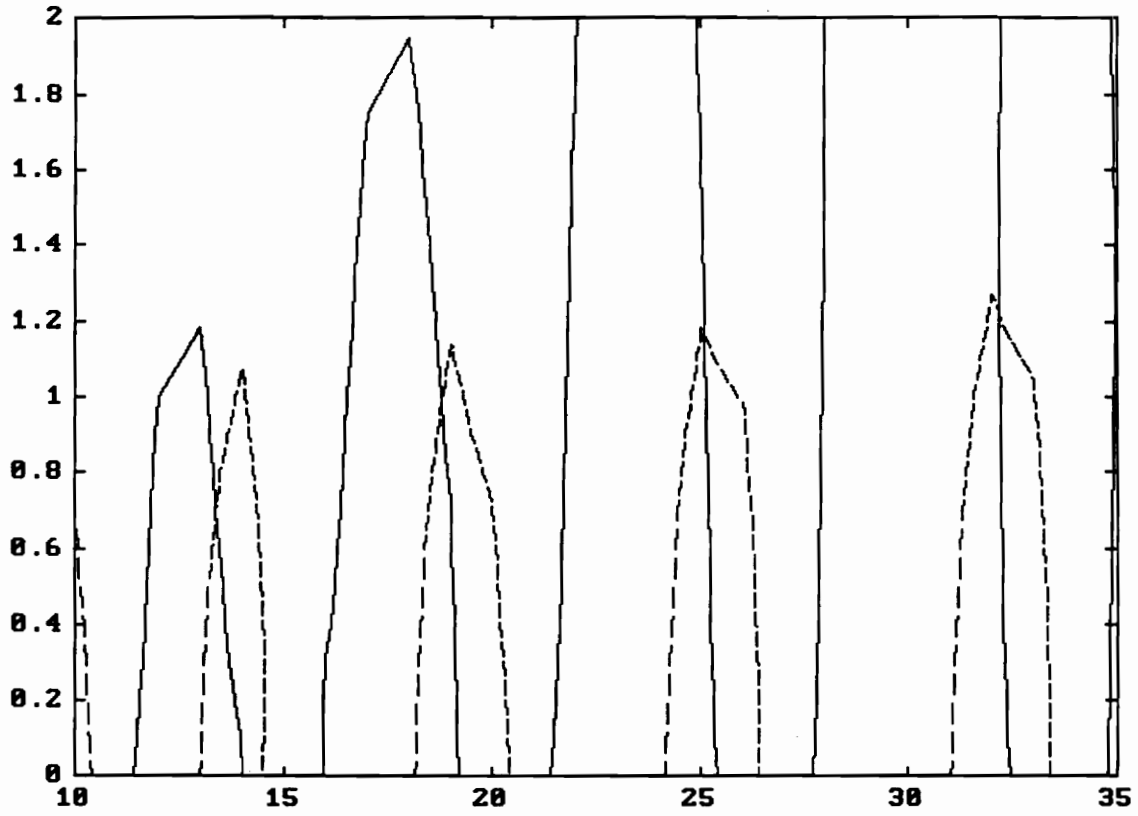

Figure 4.17: Zero Level Contours for S_1 Equation at 2.5 GHz.

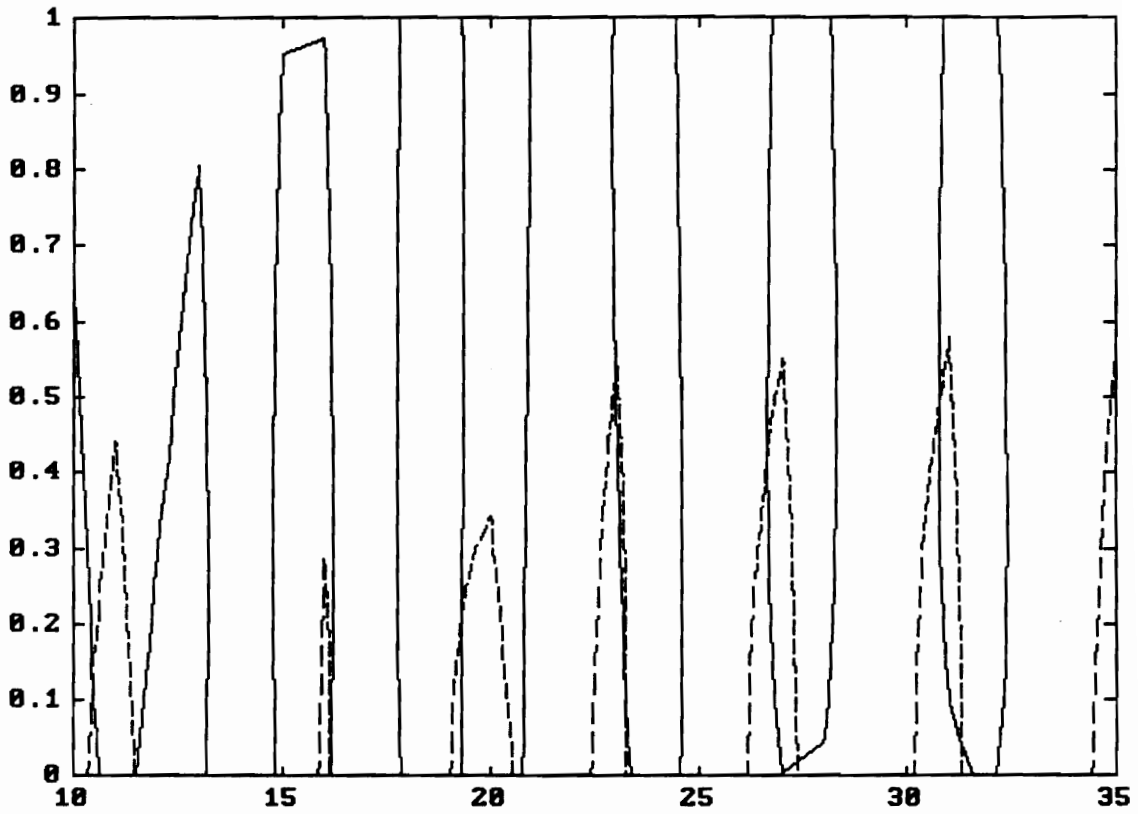

Figure 4.18: Zero Level Contours for S_1 Equation at 4.1 GHz.

Another problem associated with the combination of the length of the samples and the relatively high values of ϵ_R' being measured is the loss of sensitivity at frequencies where the sample length represents on odd multiple of $\lambda/4$ in the sample. At these frequencies the reflected waveforms are 180° out of phase with the incident signal and a minima of $S_1(\omega)$ results. For the wet samples with ϵ_R' about 25 and a sample holder length of 9.15 cm + Somlo extension of about 5 mm, these bands of heightened uncertainty occur initially at 155 Mhz and at 310 MHz intervals thereafter. The attenuation associated with these samples should reduce this effect, but data points near these frequencies (1.7 GHz and 4.5 GHz are both within 5 MHz of one of these harmonics) may be more prone to error.

A differential error analysis was performed, similar to the one used with the match terminated coaxial sample holder data. The relevant equations for the open circuit coaxial sample holder are:

$$\frac{\partial S_1}{\partial \epsilon_R} = \frac{1}{1 + \rho\tau^2}\left[\tau^2 S_1\left(\left(\frac{1}{2}\right)\left(\frac{1+\rho}{\epsilon_R+\sqrt{\epsilon_R}}\right)+\frac{\gamma\, l\, \rho}{\epsilon_R}\right) - \left(\left(\frac{1}{2}\right)\left(\frac{1+\rho}{\epsilon_R+\sqrt{\epsilon_R}}\right)+\frac{\gamma\, l\, \tau}{\epsilon_R}\right.\right. \tag{4.9}$$

$$\frac{\partial S_1}{\partial l} = \frac{2\,\gamma\,\tau^2}{1-\rho\tau^2}\,(\rho S_1 - 1) \tag{4.10}$$

$$\frac{\partial \epsilon_R}{\partial S_1} = \left(\frac{\partial S_1}{\partial \epsilon_R} \right)^{-1} \qquad (4.11)$$

$$\frac{\partial \epsilon_R}{\partial l} = - \frac{\frac{\partial S_1}{\partial l}}{\frac{\partial S_1}{\partial \epsilon_R}} \qquad (4.12)$$

for the S_1 bounce diagram derived equation,

$$\frac{\partial BJ}{\partial \epsilon_R} = \frac{1}{2 + 2\sqrt{\epsilon_R}\tanh(\gamma l)} \left[\frac{BJ-1}{\epsilon_R} - \frac{(BJ+1)\gamma l}{\sqrt{\epsilon_R}} \, sech^2(\gamma l) \right] \qquad (4.13)$$

$$\frac{\partial BJ}{\partial l} = - \frac{\gamma \, sech^2(\gamma l)}{\frac{1}{\sqrt{\epsilon_R}} + \tanh(\gamma l)} \, (1 + BJ) \qquad (4.14)$$

$$\frac{\partial \epsilon_R}{\partial S_1} = \left(\frac{\partial BJ}{\partial \epsilon_R} \right)^{-1} \qquad (4.15)$$

$$\frac{\partial \epsilon_R}{\partial l} = -\frac{\frac{\partial BJ}{\partial l}}{\frac{\partial BJ}{\partial \epsilon_R}}$$

where

$$BJ = \frac{\frac{1}{\sqrt{\epsilon_R}} - \tanh(\gamma l)}{\frac{1}{\sqrt{\epsilon_R}} + \tanh(\gamma l)} \qquad (4.16)$$

for the Baker-Jarvis equation, and

$$\frac{\partial Cole}{\partial \epsilon_R} = -\left(\frac{1}{2} + \frac{\gamma l}{\sinh(2\gamma l)}\right) \qquad (4.17)$$

$$\frac{\partial Cole}{\partial l} = -\frac{2\ \gamma\ \epsilon_R}{\sinh(2\gamma l)} \qquad (4.18)$$

$$\frac{\partial Cole}{\partial Y} = -\frac{\frac{\sqrt{\epsilon_R}}{\tanh(\gamma l)}}{\frac{\partial Cole}{\partial \epsilon_R}} \qquad (4.19)$$

$$\frac{\partial \epsilon_R}{\partial l} = -\frac{\frac{\partial Cole}{\partial l}}{\frac{\partial Cole}{\partial \epsilon_R}} \qquad (4.20)$$

where

$$Cole = \left(\frac{V-R}{V+R}\right)\sqrt{\epsilon_R}\coth(\gamma l)$$

for the Cole equation.

The results of applying these equations to the experimentally derived permittivity data are shown by the error bars in figures 4.19 through 4.27 where, as in the previous chapter, admittances and scattering parameters are assumed to be accurate to 2% and lengths to 1%.

These graphs indicate that algorithmic inaccuracies should be very small for these data under the assumed error parameters of the instrumentation. A slightly greater error bound is seen for the lowest frequency values of ϵ_R' than for higher frequencies, and fairly large inaccuracies could exist in the small values which characterize ϵ_R'' for the dry sand.

A number of factors were investigated as possible causes for the oscillations seen in the wet sample results. Initially an error in either the inner conductor length or the teflon bead length was suspected, but calculations with a theoretical model using fresh water permittivity values calculated from an equation in [58] with a refractive mixing rule [55]

$$\sqrt{\epsilon_m^*} = f_1\sqrt{\epsilon_1^*} + (1-f_1)\sqrt{\epsilon_2^*} \qquad (4.21)$$

where f_1 = volume fraction of component 1
$(1-f_1)$ = volume fraction of component 2

indicated that length errors in these components did not produce oscillatory results.

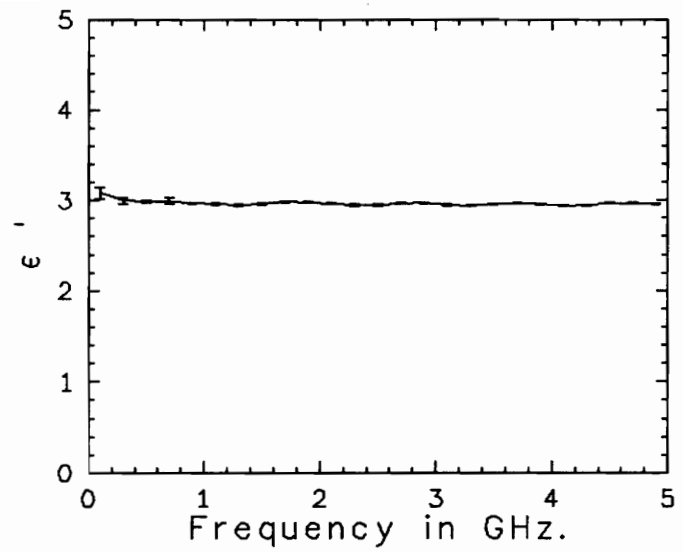

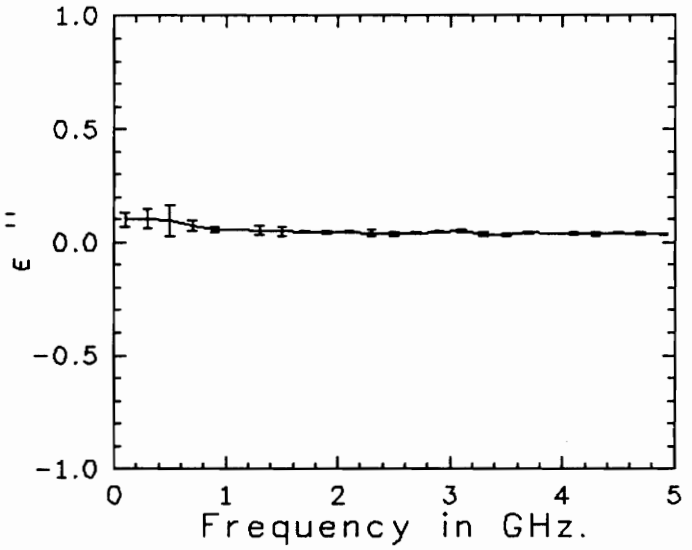

Figure 4.19: Permittivity of Dry Sand Using the S_1 Equation -- Experimental Error

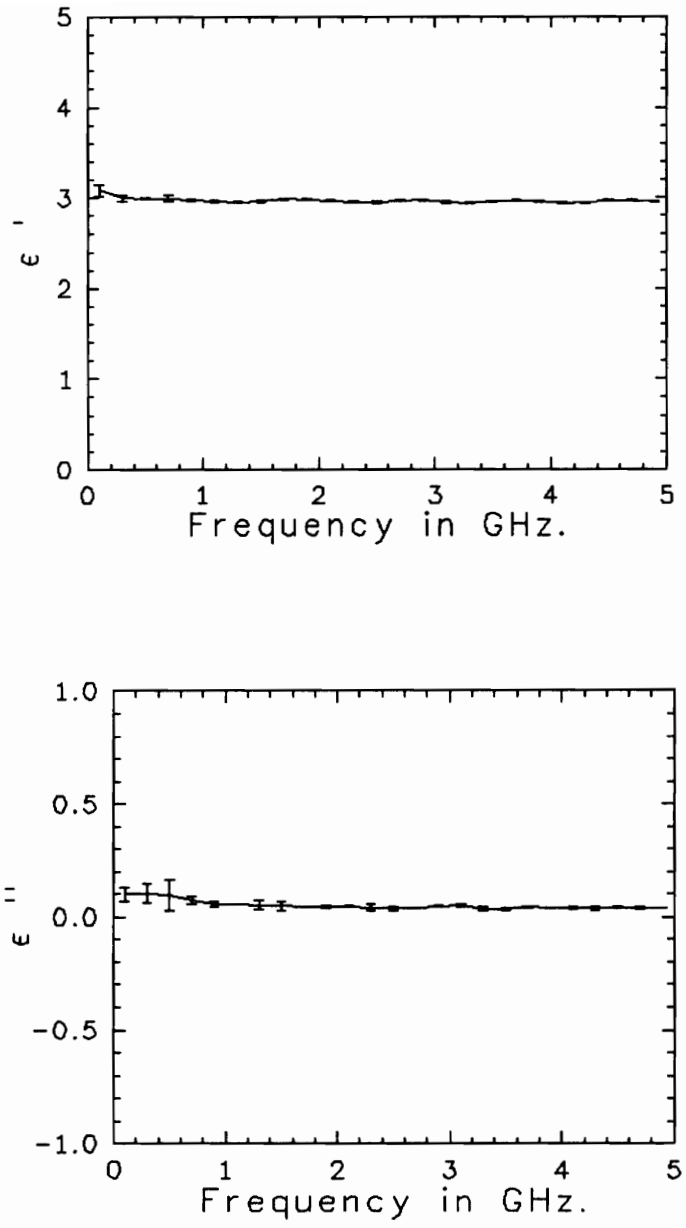

Figure 4.20: Permittivity of Dry Sand Using the Baker-Jarvis Equation -- Experimental Error

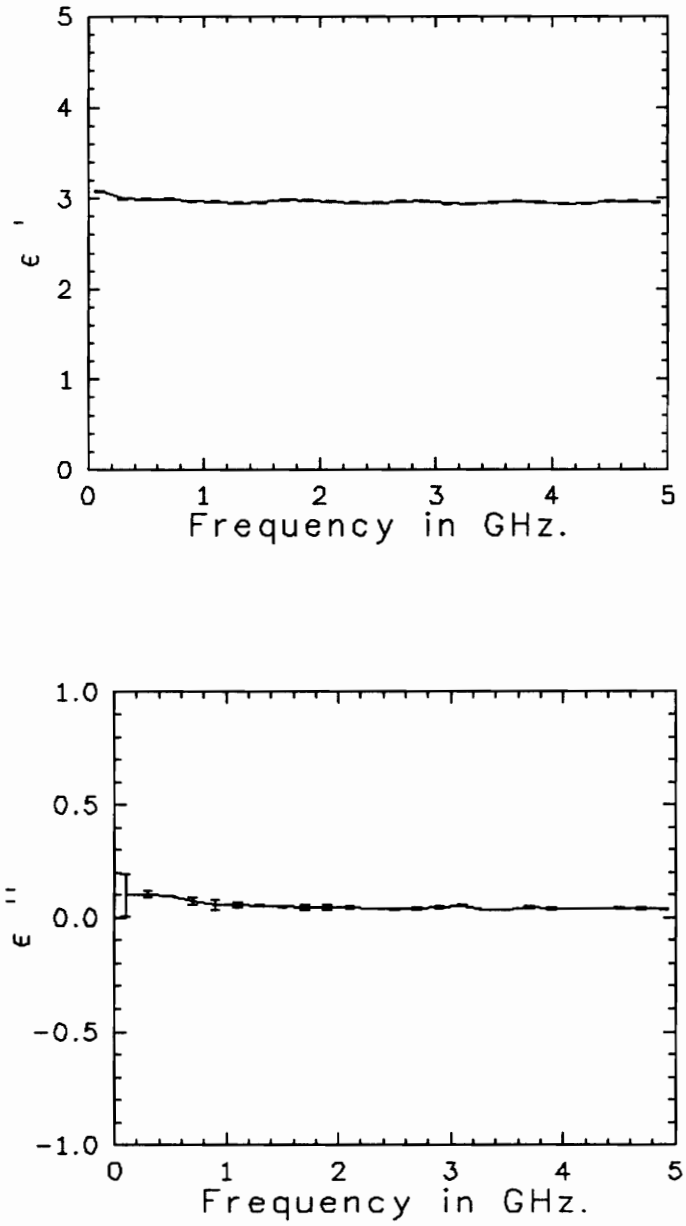

Figure 4.21: Permittivity of Dry Sand Using Cole's Equation -- Experimental Error

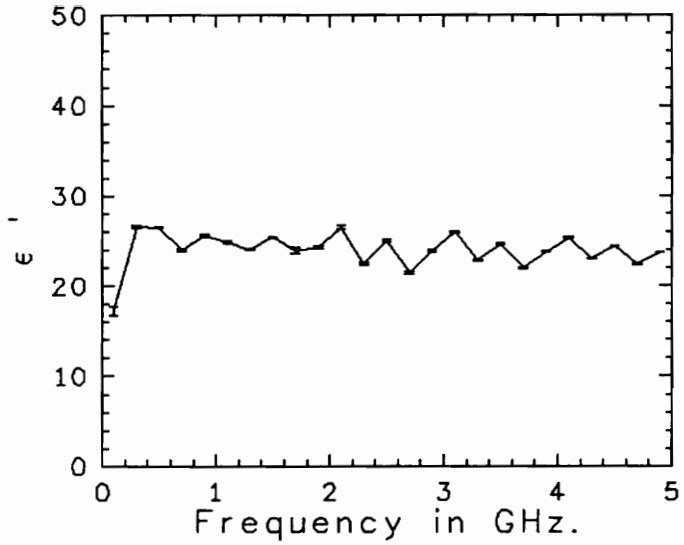

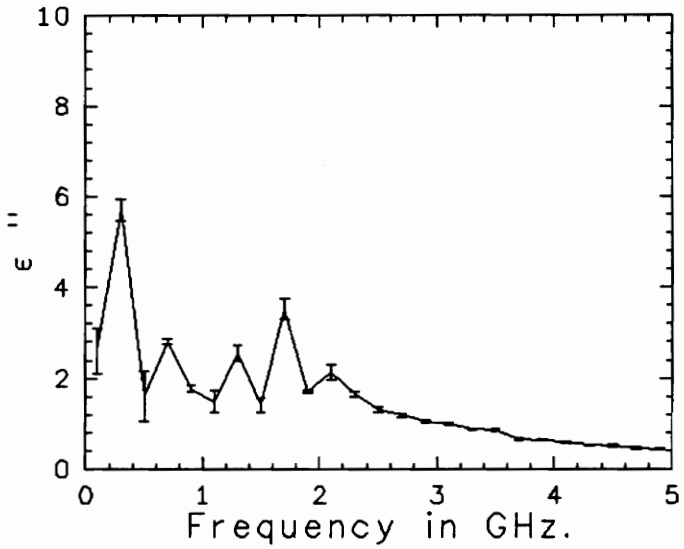

Figure 4.22: Permittivity of Wet Sand Using the S_1 Equation -- Experimental Error

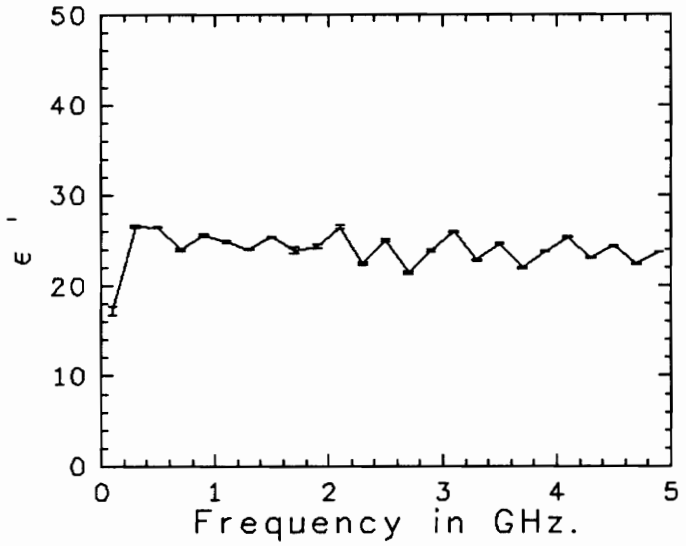

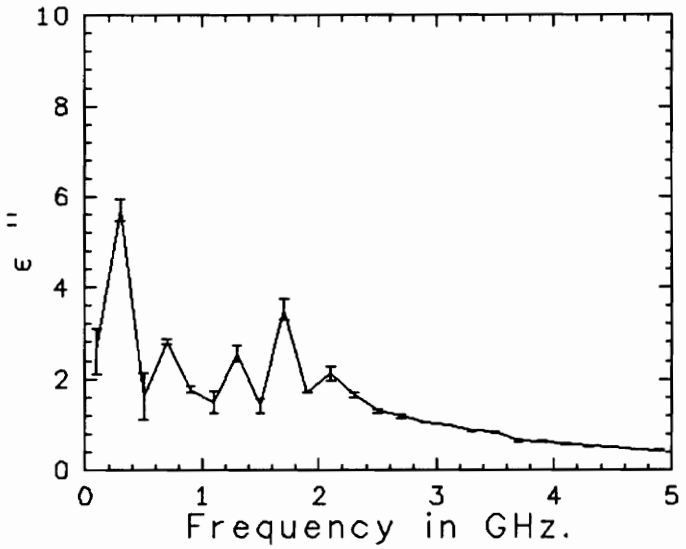

Figure 4.23: Permittivity of Wet Sand Using the Baker-Jarvis Equation -- Experimental Error

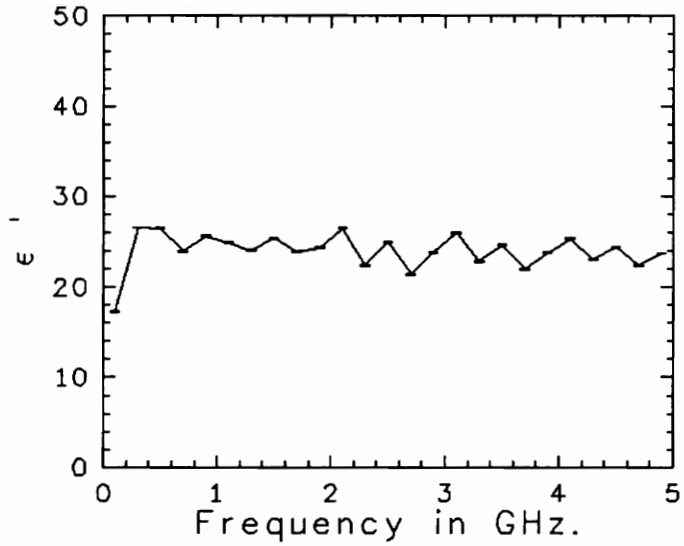

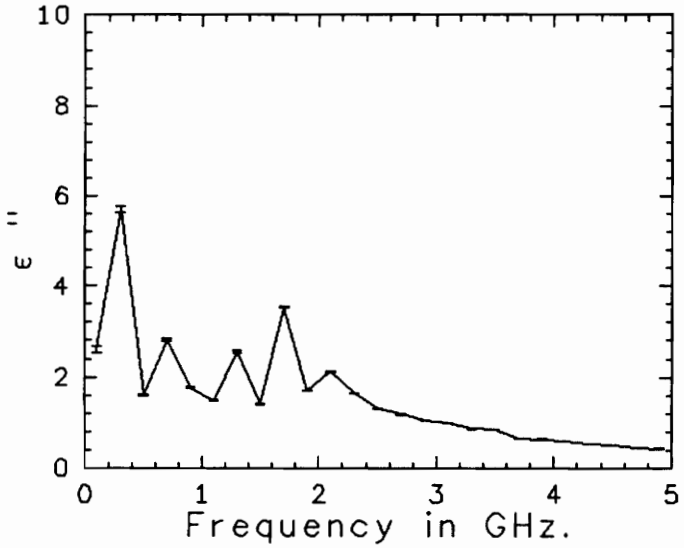

Figure 4.24: Permittivity of Wet Sand Using Cole's Equation -- Experimental Error

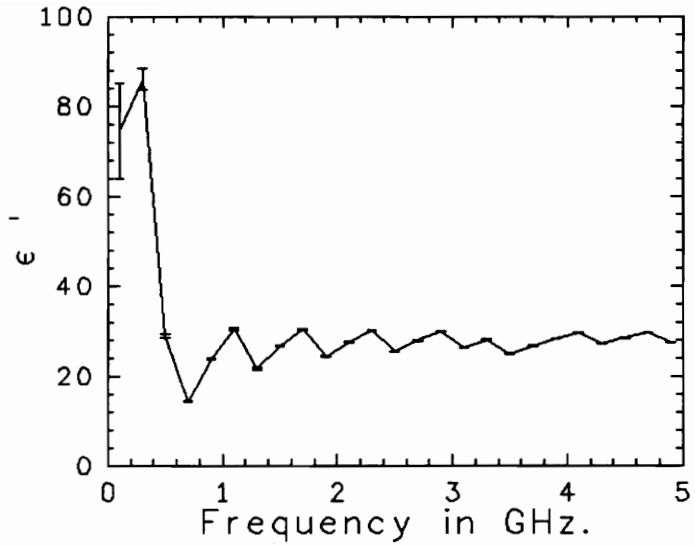

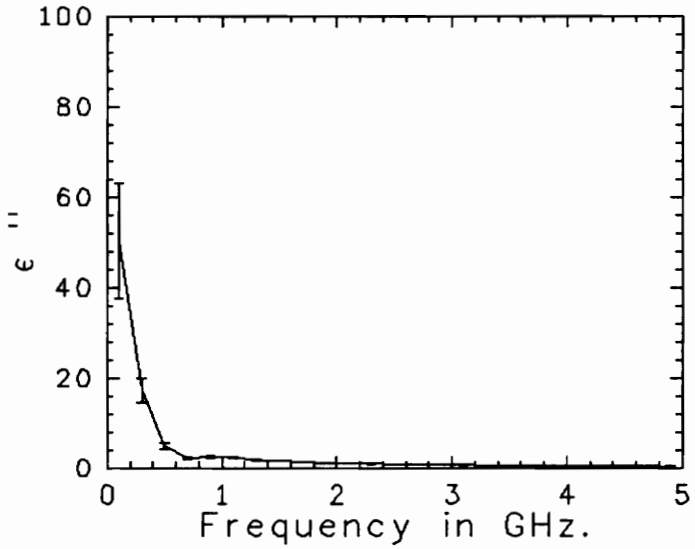

Figure 4.25: Permittivity of Saltwater Sand Using the S_1 Equation -- Experimental Error

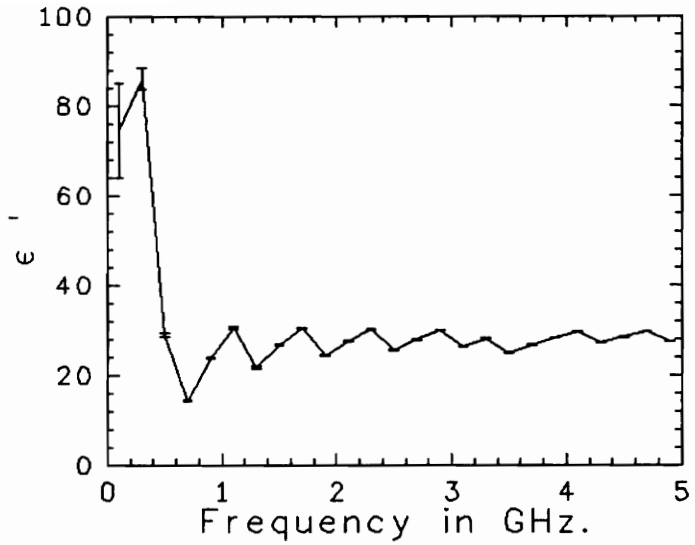

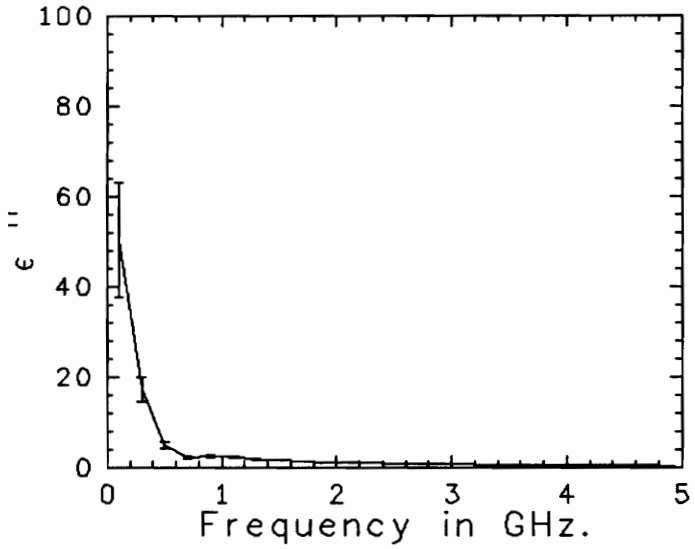

Figure 4.26: Permittivity of Saltwater Sand Using the Baker-Jarvis Equation -- Experimental Error

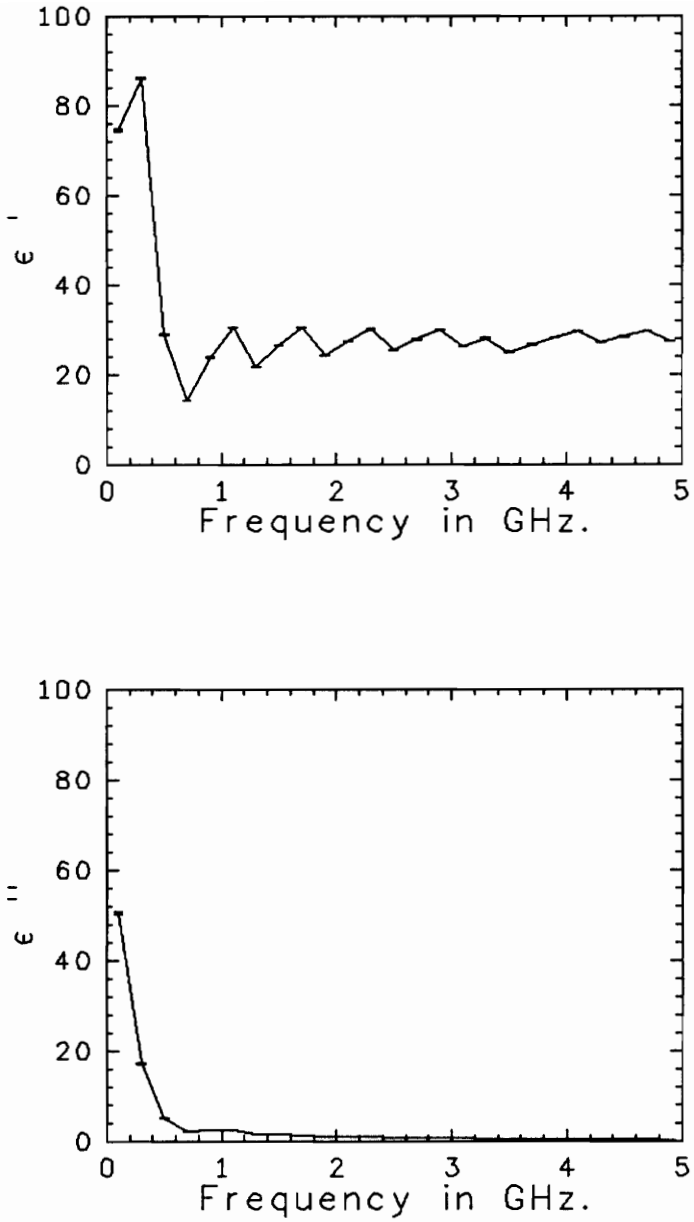

Figure 4.27: Permittivity of Saltwater Sand Using Cole's Equation -- Experimental Error

It seemed possible that very minor errors in the bead compensation could produce an oscillating waveform in the sample holder which could have a greater effect on the signal of interest for samples with high dielectric contrast to the teflon. This was tested using [59]

$$S_{1_{Measured}} = \frac{S_{11_{Teflon}} - S_{1_{True}} \det S_{Teflon}}{1 - S_{1_{True}} S_{22_{Teflon}}} \qquad (4.22)$$

where the S parameters of the teflon filled section of line were calculated using equations 3.11 and 3.12 but the intrinsic impedance of that portion of line was perturbed from 50 ohms to represent incorrect compensation. The final results were found to be very insensitive to compensation errors so this idea was discarded.

A number of calculations were made [Appendix D] to examine the possibility of some sort of high order mode resonance or possibly some sort of hetrodyning effect between two such resonances, but none of these indicated any likelihood of low frequency oscillation.

Because of the oscillatory nature of this error, it is believed to be related to phase measurement difficulties caused by the very small power content of the excitation signal

$$\frac{200 \text{ millivolts}^2}{50 \text{ ohms}} = 800 \text{ microwatts} \qquad (4.23)$$

coupled with the loss inherent in the wet samples over the length of the sample holder. A simulation was run in which a postulated permittivity of 25 + j2 was used in equation 4.6 to produce synthetic S_1 values. To these were added a sinusoidal perturbation with a strength equal to 10% of the magnitude of the original values. The resulting numbers were fed to the same root finding algorithm which was used in the original experiments, and the numerical root finder was given a starting guess of 25 + j2. The resulting permittivity solutions oscillated about the correct value by about 4% and the oscillation was at exactly the same frequency and phase as that of the perturbation. This seems to imply that some sort of oscillatory signal is corrupting the acquisition of the waveforms used to derive the S parameters, but this signal must not be common to both the sample and the reference reflection waveforms and therefore is probably generated inside the sampling scope in some fashion when the high permittivity/ high loss acquisitions are being made. In any case, the permittivity value about which the oscillation occurs appears to be correct by comparison to the results derived in the previous chapter.

The next chapter discusses work done with the twin lead balun driven ground probe. Length problems may become even more intractable with this device as it is 30 cm in length, but the ability to measure using two different length lines (15 cm probes are available) may partially alleviate this problem.

CHAPTER V

THE BALUN-DRIVEN TWIN LEAD GROUND PROBE

In this chapter experiments conducted using the balun-driven twin lead ground probe will be discussed. This device shares several characteristics with the open circuited coaxial sample holder examined in the last chapter in that it is a one port device (reflection measurements only) and it is physically long (15 and 30 cm probes), with all of the difficulties that implies. It also shares a trait with the coaxial sample holder system discussed in Chapter III in that an uncharacterized network precedes the transmission line structure and must be dealt with in the measurements.

The next section describes the experimental setup. This is followed by a description of mathematical algorithms, experimental results, and an error analysis of those results.

EXPERIMENTAL SETUP

The balun-driven twin lead ground probe is a device manufactured by the Soilmoisture Equipment Corp. to facilitate the measurement of ground water content. The probe head comes with three interchangeable pairs of stainless steel probes of lengths 15 cm., 30 cm., and 45 cm.

and is attached to the sampling oscilloscope with a 2 m. shielded cable which has a BNC connector on the scope end and an SMA connector on the head end. The probes themselves are 8 mm. in diameter and actually 1.5 cm. longer than the lengths given above. The excess length fits inside the head and is attached there through a clamping arrangement which is facilitated by a groove or detent milled into the head side of the probe. The twin probes are 52 mm. apart when clamped into the head and the end of the probe which enters the ground is hemispherical.

The ground probe head, which is a passive device, contains a balun transformer and its associated components. This transformer, ANZAC type TP-103, is an RF pulse transformer which is designed to match a 50 ohm unbalanced network to a 200 ohm balanced network. It is specified to be flat within 1 dB from 500 kHz. to 1GHz. A picture of the entire ground probe is given in figure 5.1.

Experiments were performed replacing the 2 m. length of shielded cable with a 1 m. piece of Gore precision 50 ohm flexible coaxial cable to ascertain if the shielded cable produced any noticeable degradation of the signal reaching the ground probe. As none was found, the 2 m. shielded cable was used in all acquisitions to more fully simulate actual conditions of field use.

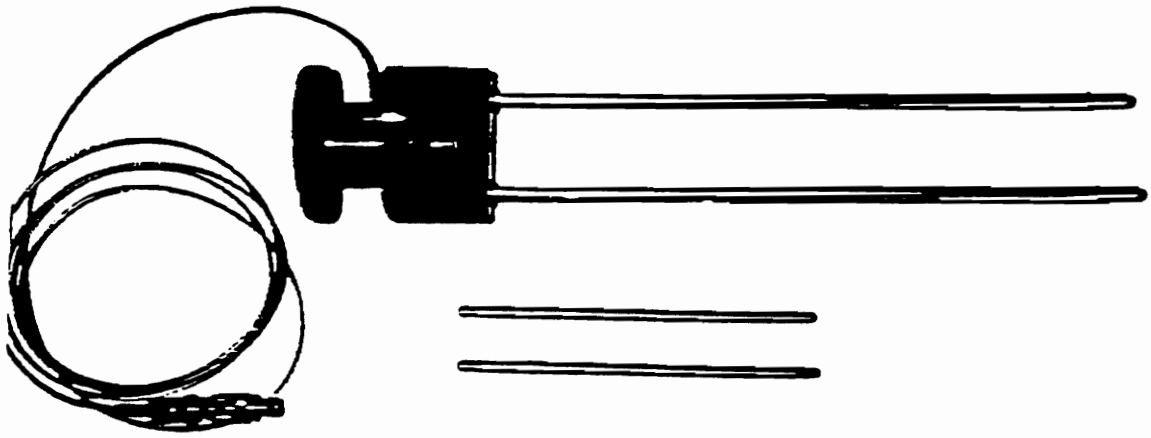

Figure 5.1: The Balun Driven Twin Lead Ground Probe

The 200 mv. step from the internal generator of the sampling scope was used as the excitation waveform, and four acquisitions were made for each sample measurement. The samples, which were contained in a plastic sample cell 28 cm. in diameter and 33 cm. deep, were measured with the 15 cm. probe and again with the 30 cm. probe. A reference waveform was obtained by measuring the ground probe head with a brass shorting bar (7 cm. x 2.5 cm. x 5 mm.) clamped into it. A pair of brass probes one meter in working length which were threaded on the end to allow them to be attached to the brass shorting bar were also measured to evaluate the waveform with a known termination. One measurement of the head with no probes attached (an 'open' termination) was also made during the course of this investigation.

In order to ascertain the impedance seen by the probe looking back towards the scope, a non-inductive resistor was attached to the ground probe head with copper tape and varied experimentally until no reflection was measured. This indicated a probe head impedance seen by the probe of 216 ohms. This differs slightly from the 200 ohms predicted by the balun transformer specifications, and the measured value is the one used in all calculations.

The transmission line formed by the twin probes had a calculated impedance of 307 ohms using

$$Z_{0_{air}} = 120 \cosh^{-1}\left(\frac{s}{d}\right) = 120 \cosh^{-1}\left(\frac{52}{8}\right) = 307\ \Omega \quad \textbf{(5.1)}$$

but was measured by the above procedure at 335 ohms. Once again, the measured value was used in all subsequent calculations.

All waveforms were acquired over a time window of 5 ns. with 1024 samples and all waveforms were ensemble averaged 2048 times by internal routines in the oscilloscope.

MATHEMATICAL ALGORITHMS

The mathematical manipulation of the ground probe measurements presented two different tasks. The first problem to be solved involved deembedding the effects of the balun transformer to produce useable S_1 information. The inversion of this information into permittivity values was the second task. The deembedding problem will be presented first.

The time domain waveforms shown in figure 5.2 clearly indicate the strong effect the balun transformer has on the ground probe measurement. The upper waveform shows the ground probe return with no probes attached, and the lower waveform is the signal seen with the 15 cm. probes immersed in dry sand. The inductive 'bump' of the balun transformer

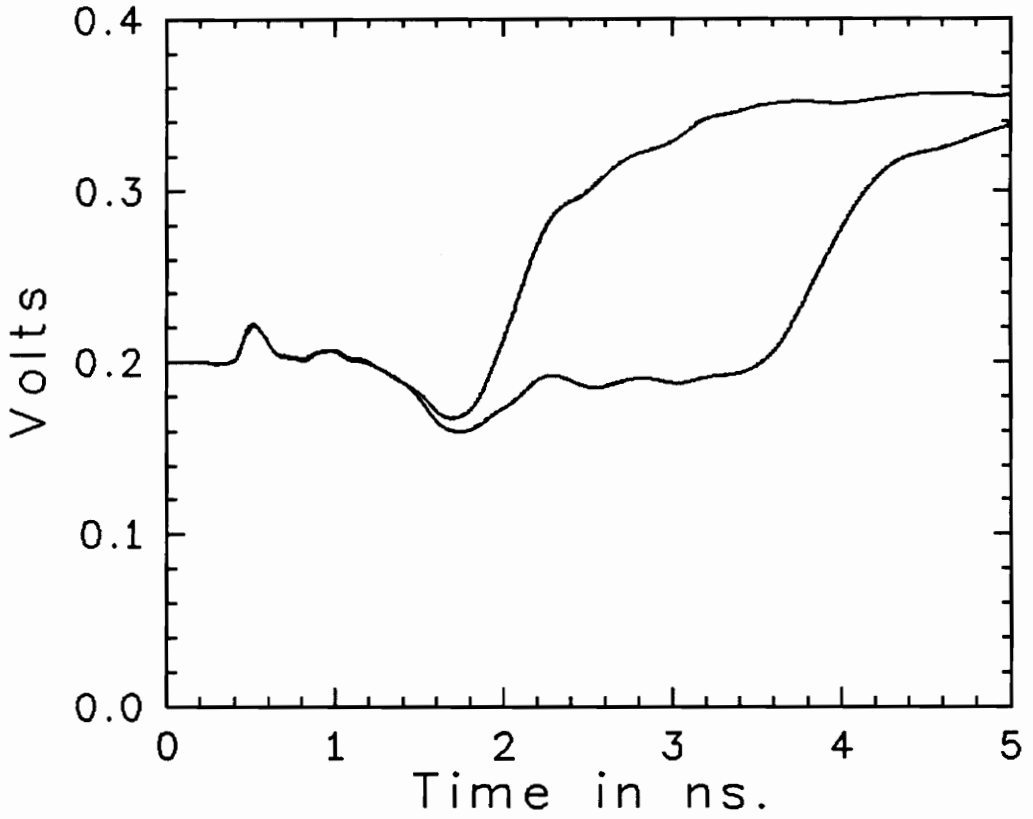

Figure 5.2: Time Domain Response of Open and Dry Sand

is clearly visible in the initial portion of the waveforms, and a downward sloping portion of the waveform occurs subsequent in time to the inductive effect. This portion may represent a transmission line structure inside the head which has a decreasing characteristic impedance with length. This could be accomplished with striplines whose separation is gradually increasing, a distinct possibility since the balun transformer leads are spaced at 5.1 mm. apart but the probes to which they connect are 52 mm. apart. In any case, these effects must be removed or reduced in order to obtain a useable S_1 waveform. Two different schemes were used to accomplish this task.

The first deembedding method is also one of the simplest and was used in some of the earliest time domain dielectric characterization work to remove errors due to imperfect transmission lines and connectors in the transmission path. This is the method used by Nicholson and Ross [12] in which the reference waveform is simply measured after the effects have occurred and the frequency domain deconvolution which occurs in the division of the Fourier transform of the desired waveform by that of the reference waveform is assumed to remove these effects. The lack of precision terminations for the ground probe configuration made this scheme, as well as the next deembedding scheme, difficult to implement, but the shorting bar was used to provide at least an approximate

short circuit termination, and the waveform measured with no probes attached to the head was assumed to approximate an open circuit termination (albeit one with possible radiation losses). This worked surprisingly well, and the results of using this deembedding method with these two different terminations is plotted in the experimental results portion of this chapter.

The other scheme which was used to some benefit may be derived from examination of the ground probe signal flow graph, figure 5.3. This indicates that the signal seen at the sampling oscilloscope is

$$V_R = V_I\left(1+\frac{\rho_1(1+\rho_g)+\rho_L B}{(1-\rho_g\rho_1)(1-\rho_L\rho_b)}\right)$$
$$B = (1+\rho_g)(\tau_1\tau_2-\rho_1\rho_2) \qquad (5.2)$$
$$\rho_b = \rho_2+\left(\frac{\rho_g\tau_1\tau_2}{1-\rho_g\rho_1}\right)$$

where ρ_1 represents the reflection coefficient of the sample, ρ_g is the reflection coefficient looking towards the oscilloscope from the scope side of the sampling head, and ρ_b is the composite reflection coefficient seen by the ground probes looking back towards the ground probe head and oscilloscope.

This expression may be evaluated for 'samples' consisting of a short circuit (ρ_L=-1),

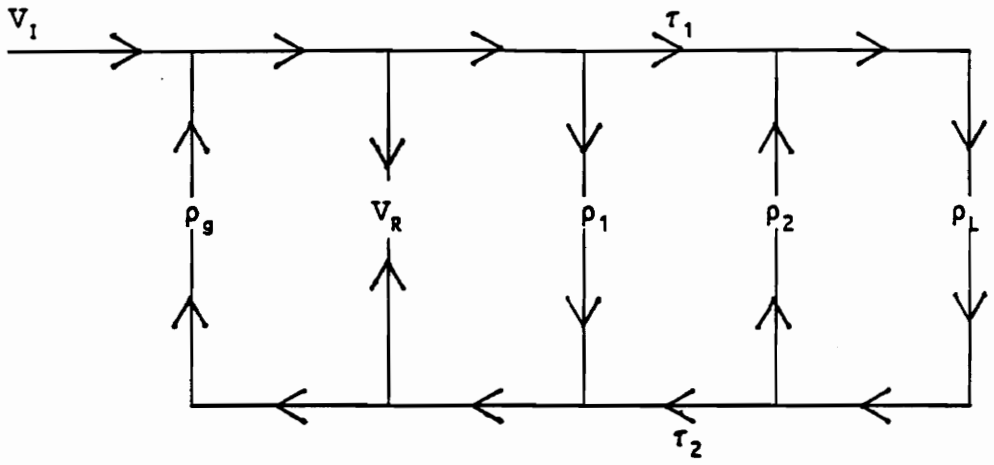

Figure 5.3: Ground Probe Signal Flow Graph

$$V_{R_{short}} = V_I \left(1+\frac{\rho_1(1+\rho_g)-B}{(1-\rho_g\rho_1)(1+\rho_b)}\right) \qquad (5.3)$$

a known reflection coefficient k,

$$V_{R_k} = V_I \left(1+\frac{\rho_1(1+\rho_g)+kB}{(1-\rho_g\rho_1)(1-k\rho_b)}\right) \qquad (5.4)$$

and an open circuit (ρ_L=1).

$$V_{R_{open}} = V_I \left(1+\frac{\rho_1(1+\rho_g)+B}{(1-\rho_g\rho_1)(1-\rho_b)}\right) \qquad (5.5)$$

If the short circuit termination is used to produce the main reference waveform, then combination of these equations leads to

$$\frac{V_R-V_{R_k}}{V_{R_{short}}-V_{R_k}} = \frac{k-\rho_L}{k+1}\,\frac{1+\rho_b}{1-\rho_L\rho_b} \qquad (5.6)$$

$$\frac{V_{R_{open}}-V_{R_k}}{V_{R_{short}}-V_{R_k}} = \frac{k-1}{k+1}\,\frac{1+\rho_b}{1-\rho_b} \qquad (5.7)$$

where the second expression is solved for ρ_b which is then used in the first expression to evaluate ρ_L which is

equivalent to S_1. Another pair of expressions results from using the open circuit derived waveform as the main reference waveform.

$$\frac{V_R - V_{R_k}}{V_{R_{open}} - V_{R_k}} = \frac{\rho_L - k}{1-k} \frac{1-\rho_b}{1-\rho_L\rho_b} \qquad (5.8)$$

$$\frac{V_{R_{short}} - V_{R_k}}{V_{R_{open}} - V_{R_k}} = \frac{k+1}{k-1} \frac{1-\rho_b}{1+\rho_b} \qquad (5.9)$$

These expressions are treated in the same way as equations 5.6 and 5.7 to solve for S_1.

The inversion of the S_1 information into permittivity is the next problem which must be solved. This is aggravated by the length of the ground probes in combination with the finite time window available for measurement. Inspection of figure 5.2 shows that, even for dry sand (ϵ_R = 3) and the 15 cm. probe leads, the excitation signal has only enough time for two complete transits of the probe length before the end of the time window. The situation is even worse in the case of the wet samples (ϵ_R = 25) where the signal only has time for one round trip to the end of the probe and back.

This leads to the conjecture that the measurements made with the ground probe do not present a good approximation to total reflection measurements from which may be inferred that

steady state frequency domain equations will not adequately model the system under test. This indeed turns out to be true, as all attempts to apply the Baker-Jarvis and Cole equations (equations 4.7 and 4.8) met with failure. Utilization of the *entire* bounce diagram derived equation (4.6) were similarly unsuccessful, but use of only the first two terms of that equation,

$$S_1(\omega) = \rho + (1-\rho^2)\tau^2 + \ldots \qquad \textbf{(5.10)}$$

worked adequately with the 15 cm. probe measurements.

Observation of the fact that $\tau_{15}^2 = e^{-j\frac{(2\cdot15)\ \omega\sqrt{\epsilon_R}}{c}} = \tau_{30}$ initially lead to the hope that some combination of the two measurements with different length probes such as

$$\rho^3 - (S_{30}+1)\rho^2 + (2\ S_{15}-1)\rho + (S_{30}-S_{15}^2) = 0 \qquad \textbf{(5.11)}$$

or

$$S_{30} - (S_{15}-\rho)\tau_{15}^2 - \rho = 0 \qquad \textbf{(5.12)}$$

could be used, but these did not produce useful results, probably because they are predicated on the assumption that the signal entirely traverses the probe length in both directions at least once, and this does not hold true for the wet samples and the 30 cm. probe. In any case, only equation

5.10 was used to derive permittivity results for the ground probe measurements, and these results were derived entirely from measurements made with the 15 cm. ground probes.

EXPERIMENTAL RESULTS

Once again, the three materials measured were dry sand, sand saturated with water, and sand saturated with 1 N. saltwater. The sample 'cells' (plastic buckets) were filled with the samples only once, so that the same samples are used for all five measurements of a given material. The cells were covered with a plastic sheet between measurements to reduce water loss to a minimum, but no liquid was added to the cells during the measurement period (about two weeks). The appearance of small amounts of standing liquid on the top surface of the wet samples seemed to indicate that no significant moisture loss was occurring.

The ground probe was removed and reinserted for each measurement, and on insertion the probe was pushed in until the ground probe head rested on the sample. This was to ensure contact along the entire length of the probe. As in the previous chapters, five sets of acquisitions were taken for each material and the results plotted below indicate average values for permittivity among those five measurements and the maximum and minimum excursions from those values.

The graphs plotted in figures 5.4 through 5.7 show the results of the dry sand measurements. Note that sample to sample variation was quite wide in the higher frequencies for the ϵ_R' values derived from the signal flow graph deembedded results but is not so prevalent in those results derived using frequency domain division. This is probably due to variation in the balun back matching reflection coefficient, ρ_b, which is calculated separately for each sample, and may indicate that a more detailed model for the balun network is needed for samples with low permittivities.

The 600 MHz. oscillation seen in the wet samples in the last chapter is present here in the dry samples. This lends more credence to the idea that the oscillation is a product of the time domain sampling system and not of the sample holder being used. Also, some of the ϵ_R'' values are negative, which implies that energy was lost in the reference waveform at some frequencies, probably due to the uncalibrated nature of the terminations used.

The results of the wet sand measurements are presented in figures 5.8 through 5.11. Variation between samples is much less noticeable here, but all graphs show the same low values for ϵ_R' that were experienced in the open circuit sample holder measurements. This effect is unexplained, but apparently real since it occurs consistently throughout the measurements. A disturbance is seen in these graphs and the

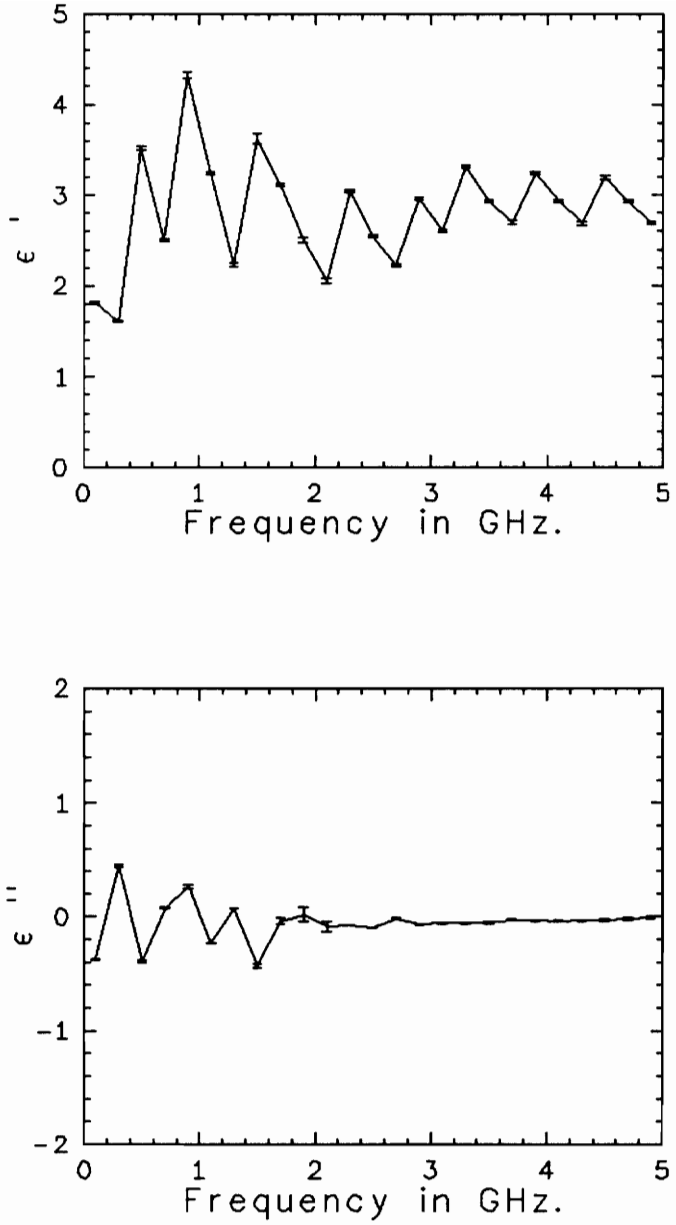

Figure 5.4: Permittivity of Dry Sand Using the Open Deconvolution - Experimental Spread

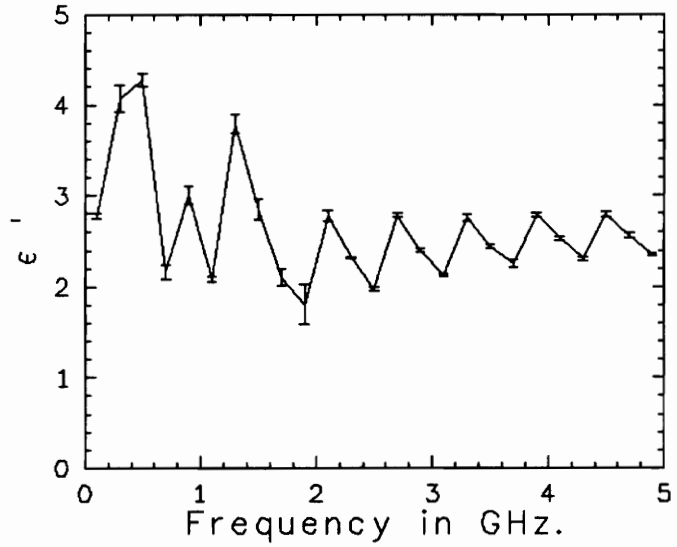

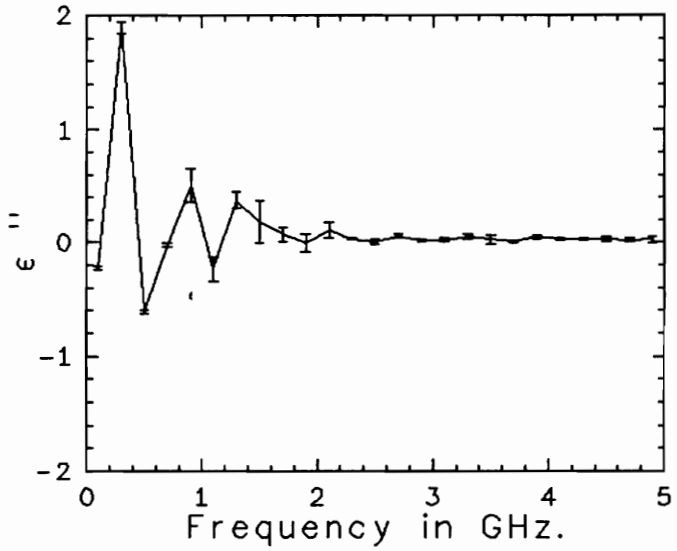

Figure 5.5: Permittivity of Dry Sand Using the Short Deconvolution - Experimental Spread

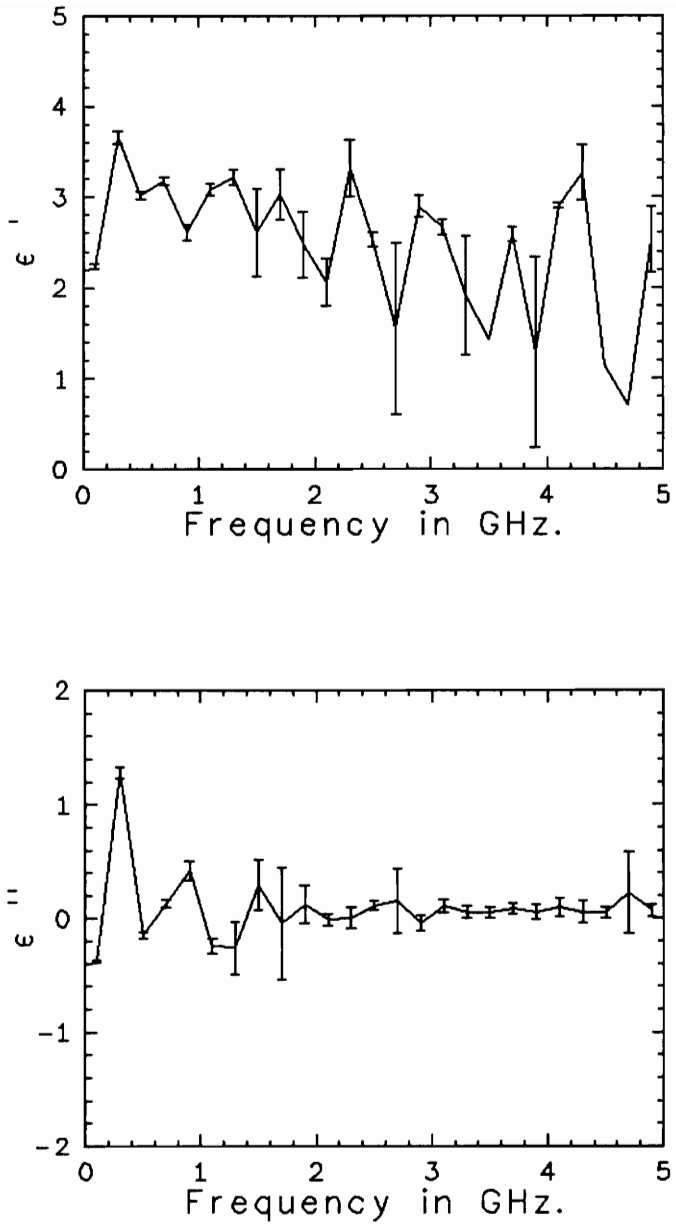

Figure 5.6: Permittivity of Dry Sand Using the Open Deembedding - Experimental Spread

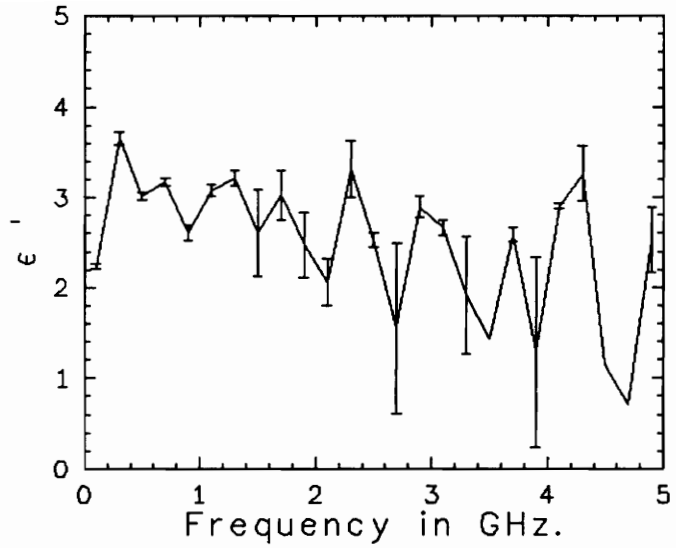

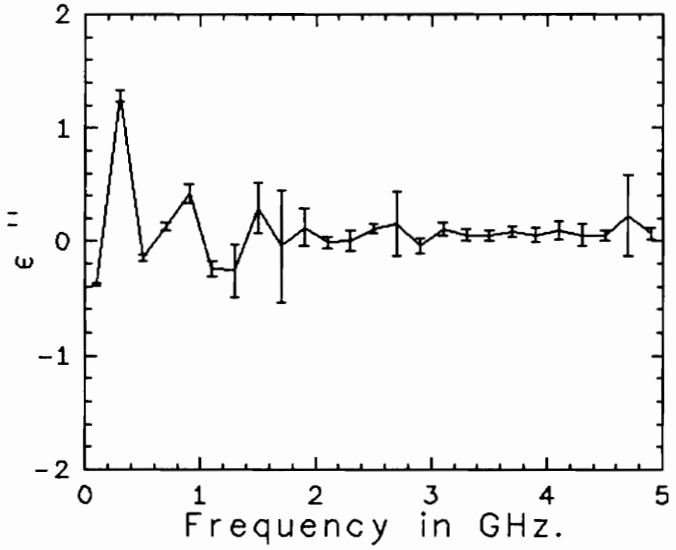

Figure 5.7: Permittivity of Dry Sand Using the Short Deembedding - Experimental Spread

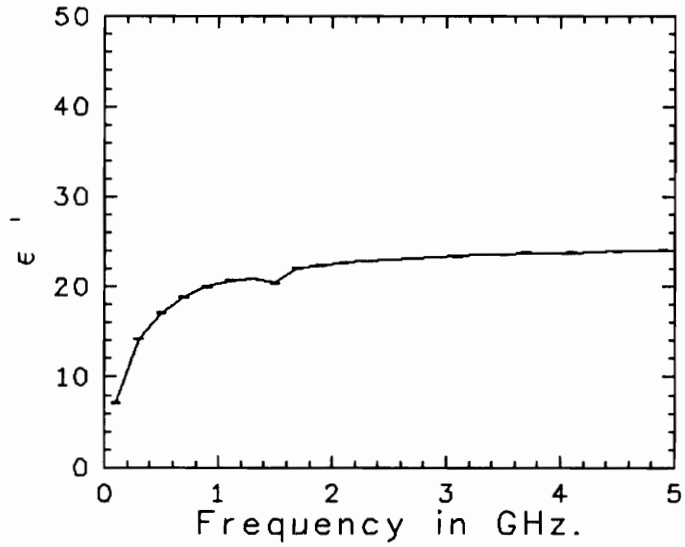

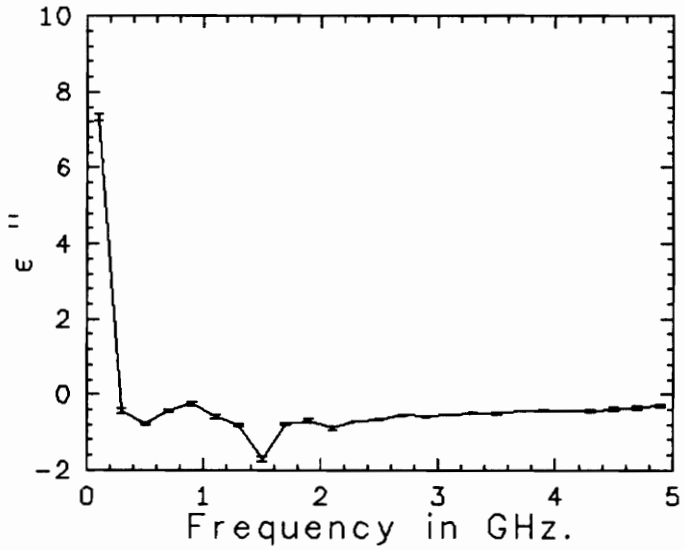

Figure 5.8: Permittivity of Wet Sand Using the Open Deconvolution - Experimental Spread

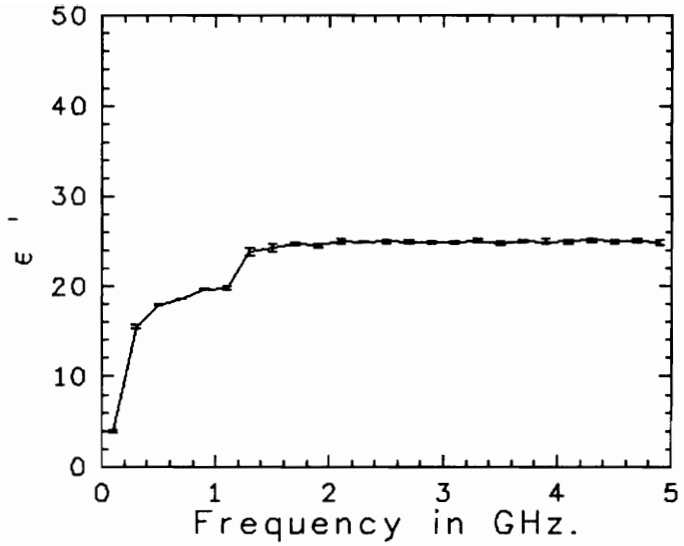

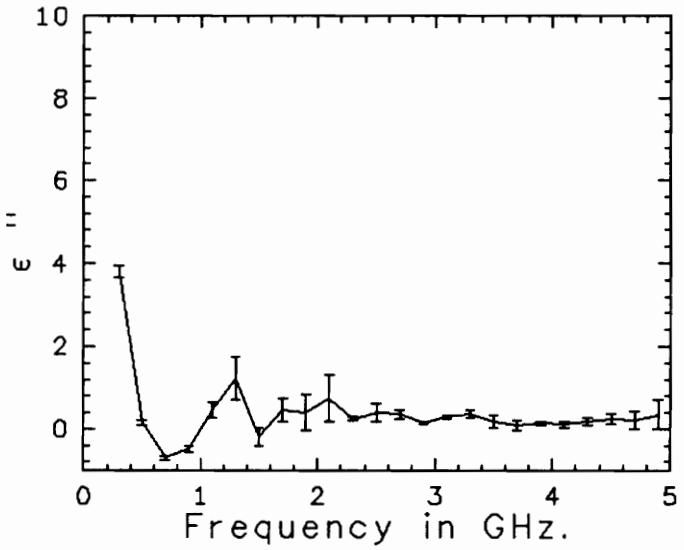

Figure 5.9: Permittivity of Wet Sand Using the Short Deconvolution - Experimental Spread

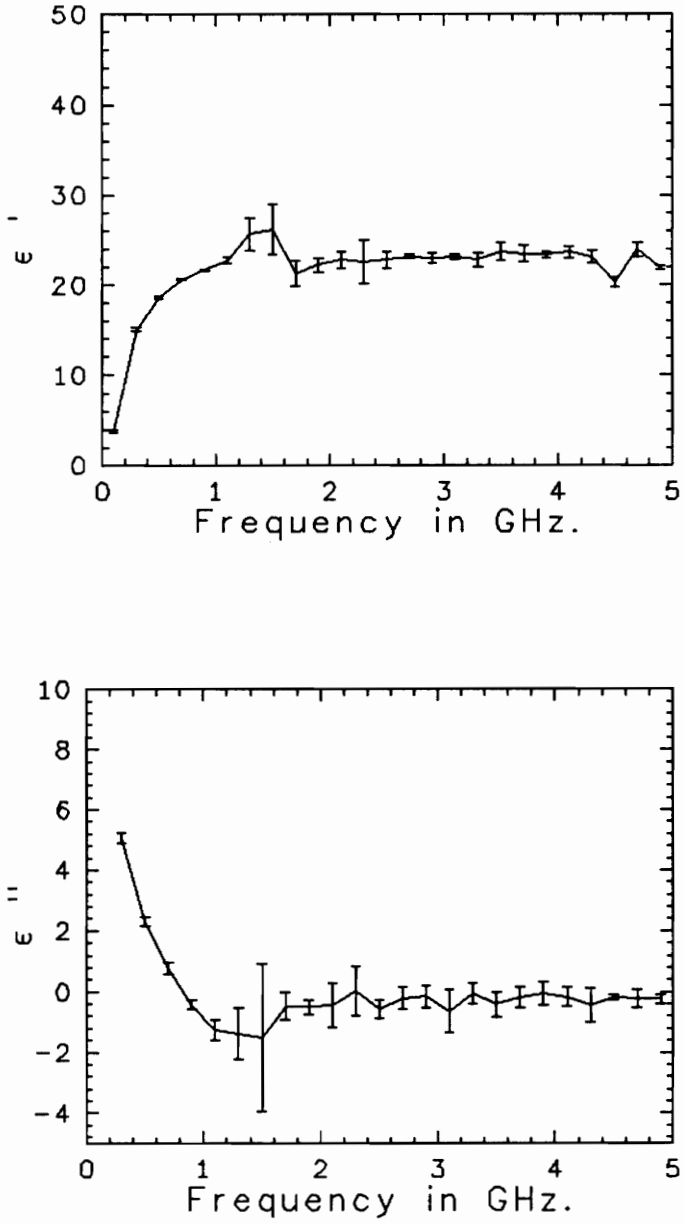

Figure 5.10: Permittivity of Wet Sand Using the Open Deembedding - Experimental Spread

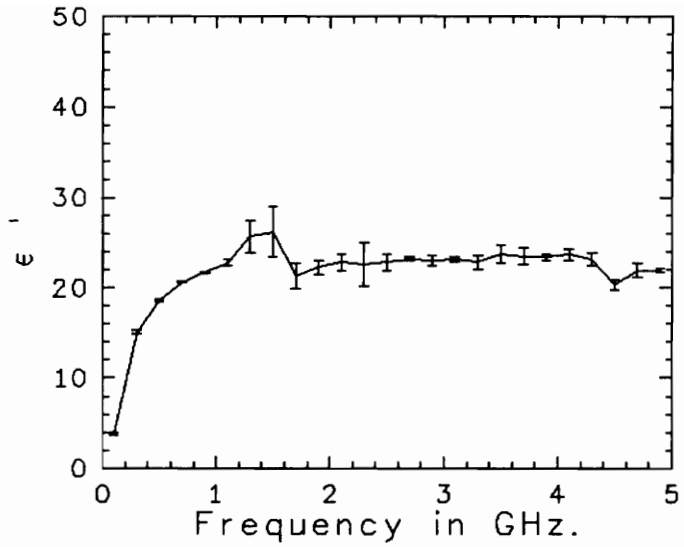

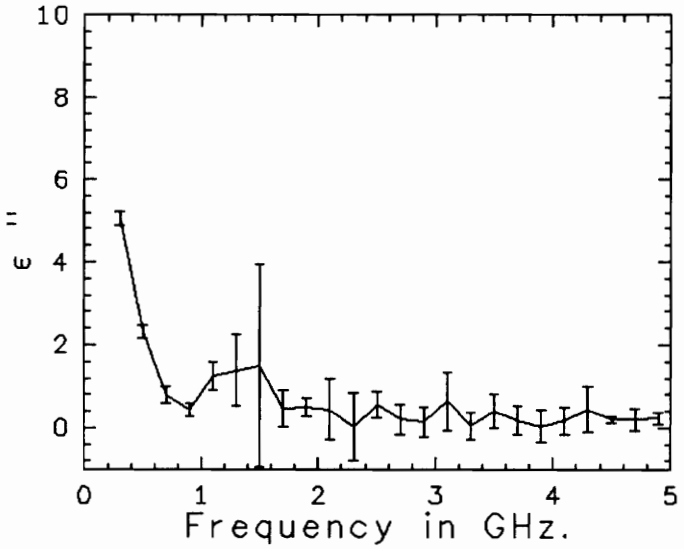

Figure 5.11: Permittivity of Wet Sand Using the Short Deembedding - Experimental Spread

next set at about 1.5 GHz. This is probably a resonance which occurs between the balun transformer and the capacitance of the sample probes. Negative values are again seen for ϵ_R'' at some frequencies.

Saltwater and sand mixture results are given in figures 5.12 through 5.15. The disturbance at 1.5 GHz. seen in the last set of graphs is present here also although the low frequency decline in ϵ_R' values is not as significant.

ERROR ANALYSIS

The ground probe used for these measurements is not fundamentally a microwave quality device, and that fact shows in these experiments. The balun transformer is not rated at frequencies above 1 GHz. and it is clear from the reflection results that no attempt was made to keep internal ground probe head signal paths at a constant impedance. However, it was possible to make useful measurements with this device, even though it suffered from some of the same problems experienced with the open circuit sample holder.

A sort of 'curse of dimensionality' caused difficulties due to length in the open circuit sample holder, and the same effect is even more prevalent in the longer ground probe.

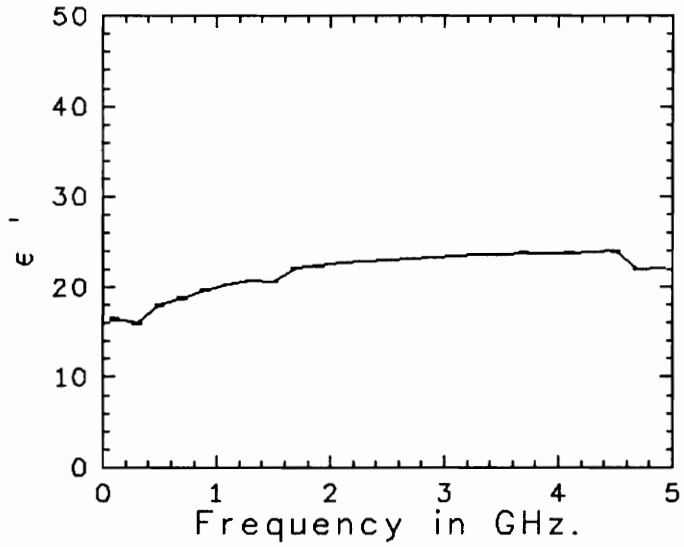

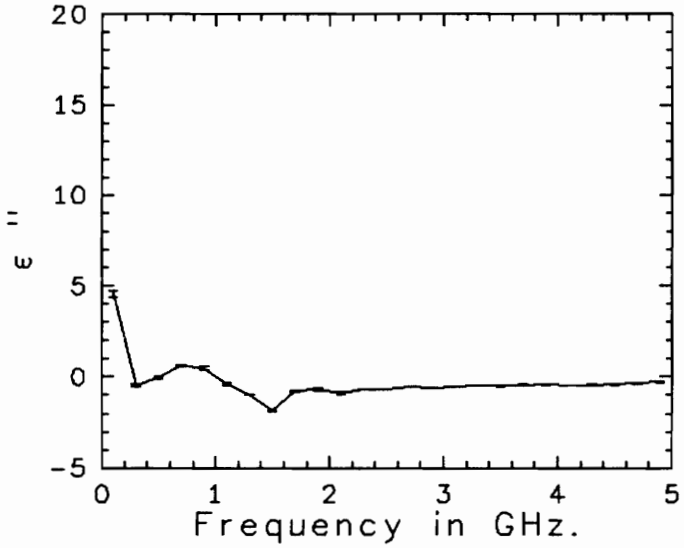

Figure 5.12: Permittivity of Saltwater Sand Using the Open Deconvolution - Experimental Spread

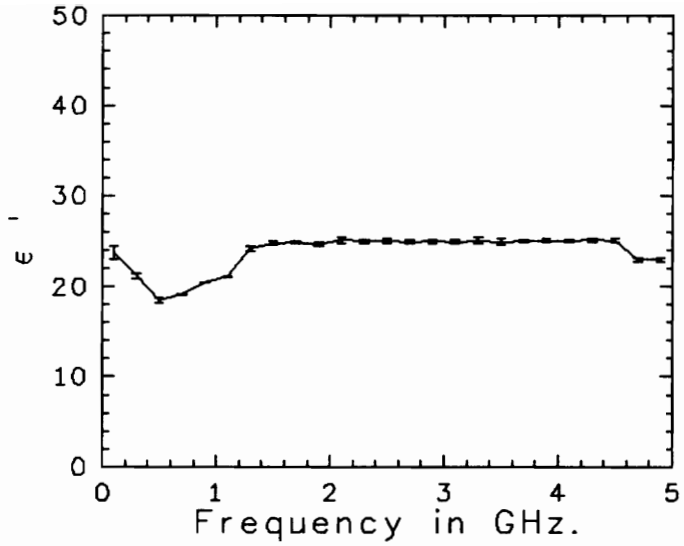

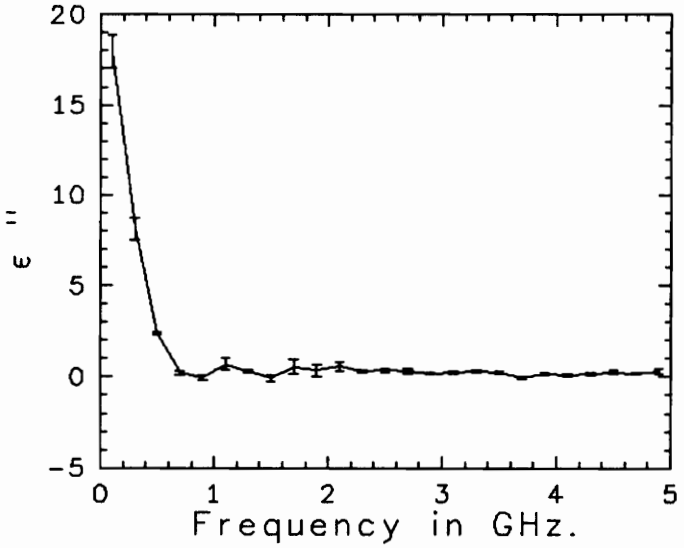

Figure 5.13: Permittivity of Saltwater Sand Using the Short Deconvolution - Experimental Spread

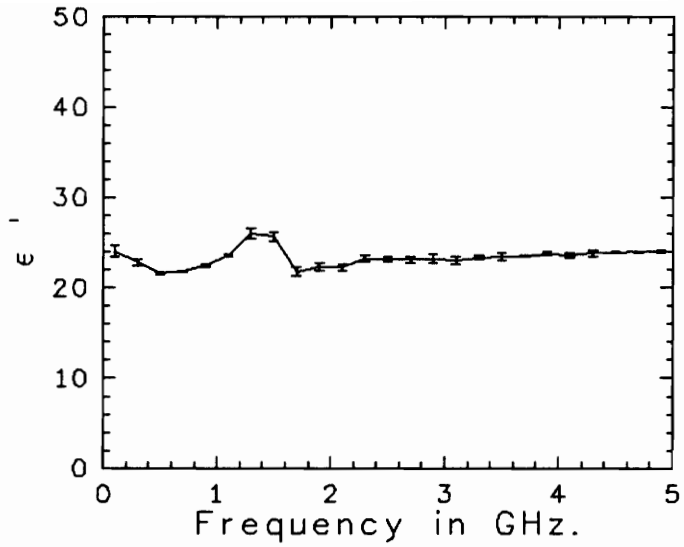

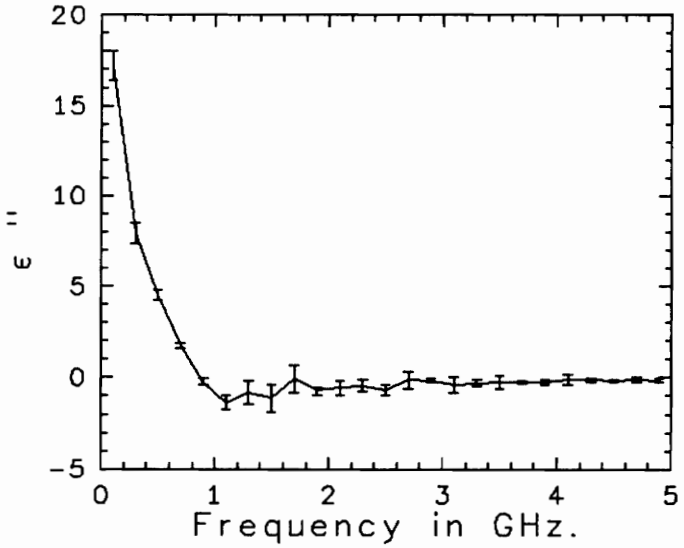

Figure 5.14: Permittivity of Saltwater Sand Using the Open Deembedding - Experimental Spread

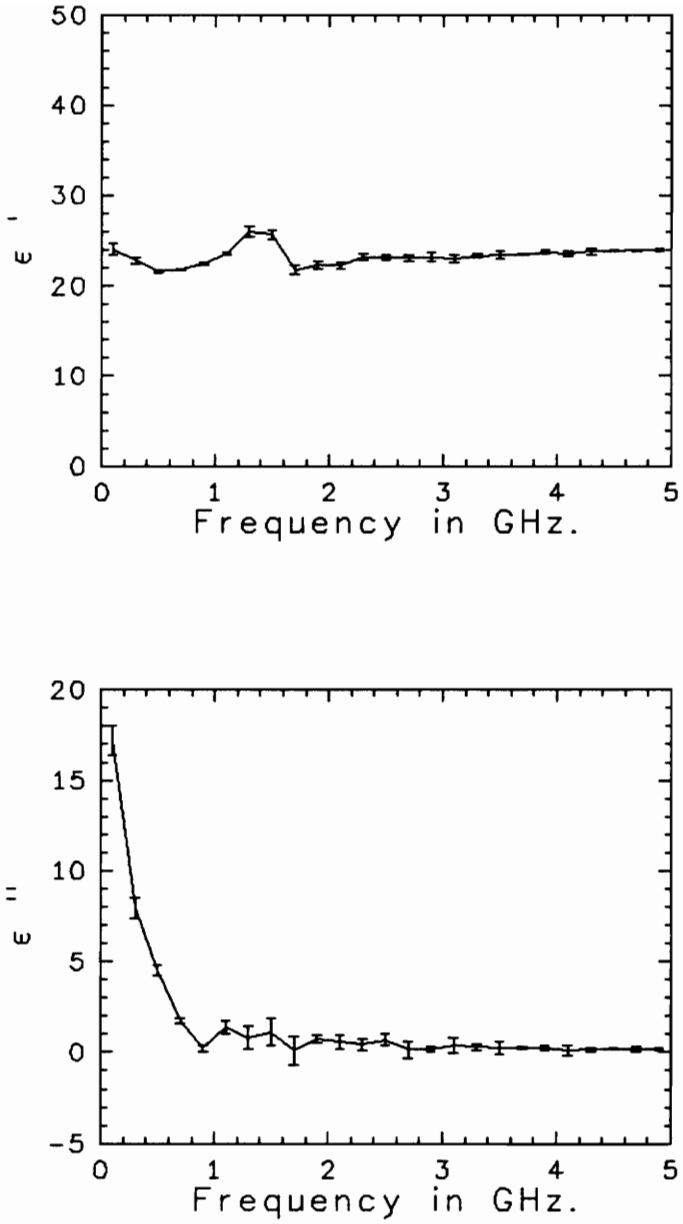

Figure 5.15: Permittivity of Saltwater Sand Using the Short Deembedding - Experimental Spread

Consider that

$$\tau_{15}^{2} = e^{-j(4\pi f 15\frac{\sqrt{\epsilon_R}}{c})} \approx e^{-j2\pi f\sqrt{\epsilon_R}} \quad \text{f in GHz.} \tag{5.13}$$

which shows that τ^2 goes through a complete 360° phase change every time f changes by .2 GHz., the frequency spacing of these experiments. Alternatively, it is clear that at higher frequencies a very small change in epsilon can produce a large change in the phase of τ^2 and therefore in the equation which is being used to match the given S_1 value, if this term predominates.

This is probably the reason why the oscillation seen in the last chapter is not predominant in the wet sample results of this chapter. This also leads to the conclusion that the zero contours of the equation will show very little separation from one another at higher frequencies, which greatly increases the chance that the numerical root finder will converge to the wrong value.

The problem of quarter wave loss of sensitivity is also increased with the long probe length. The 15 cm. probe is a quarter wavelength in air at 500 MHz. and represents an odd multiple at 1 GHz. intervals after that. These figures may be scaled by $\sqrt{\epsilon_R'}$ to show that this sensitivity loss occurs at 100 MHz. and 200 MHz. intervals after that, precisely the

frequencies studied here. Apparently, only the fact that the wet samples are lossy allows useful measurements to be made at all.

The same sensitivity calculations used in the last two chapters were evaluated for the ground probe, again assuming a 2% error in waveform measurement and a 1% error in length measurement. The equations are:

$$\frac{\partial f}{\partial \epsilon_R} = \left(\rho\tau^2 - \frac{1}{2}\right)\left(\frac{1+\rho}{\epsilon_R + \sqrt{\epsilon_R}}\right) - (1-\rho^2)\left(\frac{\gamma l \tau^2}{\epsilon_R}\right) \qquad \textbf{(5.14)}$$

$$\text{where } \gamma = j\frac{\omega\sqrt{\epsilon_R}}{c}$$

$$\frac{\partial f}{\partial l} = (1-\rho^2)(-2\gamma\tau^2) \qquad \textbf{(5.15)}$$

and

$$\frac{\partial \epsilon_R}{\partial S_1} = \frac{1}{\dfrac{\partial f}{\partial \epsilon_R}} \qquad \frac{\partial \epsilon_R}{\partial l} = -\frac{\dfrac{\partial f}{\partial l}}{\dfrac{\partial f}{\partial \epsilon_R}} \qquad \textbf{(5.16)}$$

The results of applying these equations to the measured data are graphed in figures 5.16 through 5.27. The graphs indicate a large possibility for error in the first data point for ϵ_R'' for all techniques and materials under the

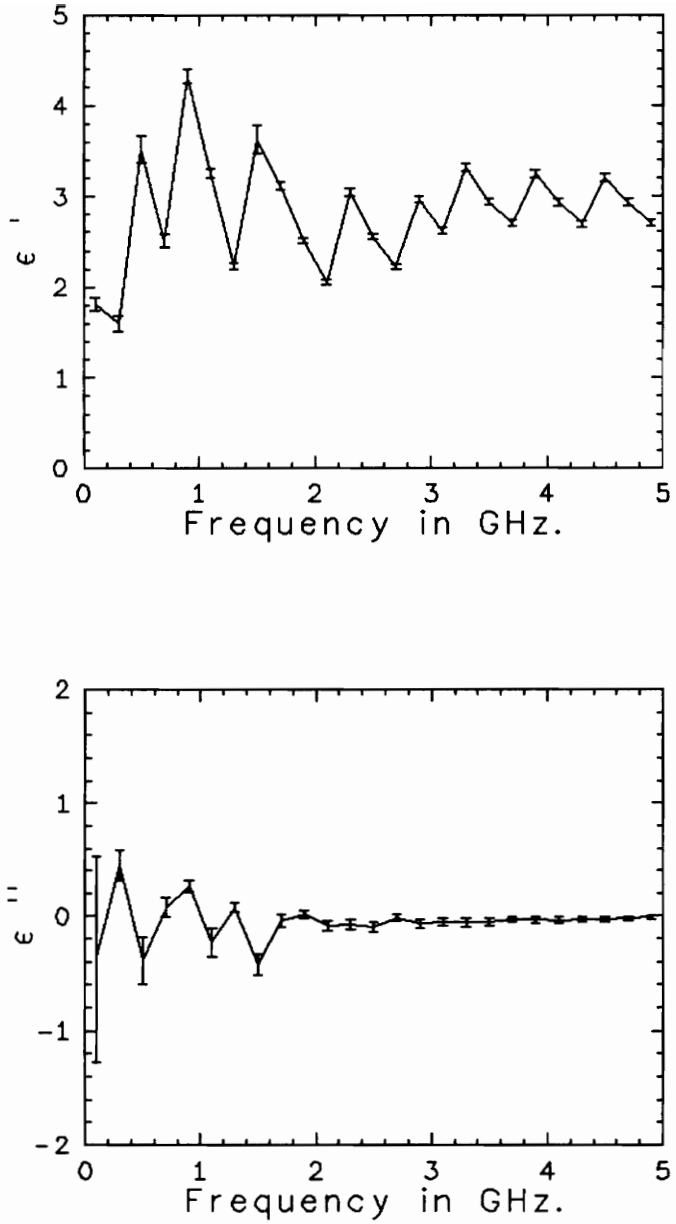

Figure 5.16: Permittivity of Dry Sand Using the Open Deconvolution - Experimental Error

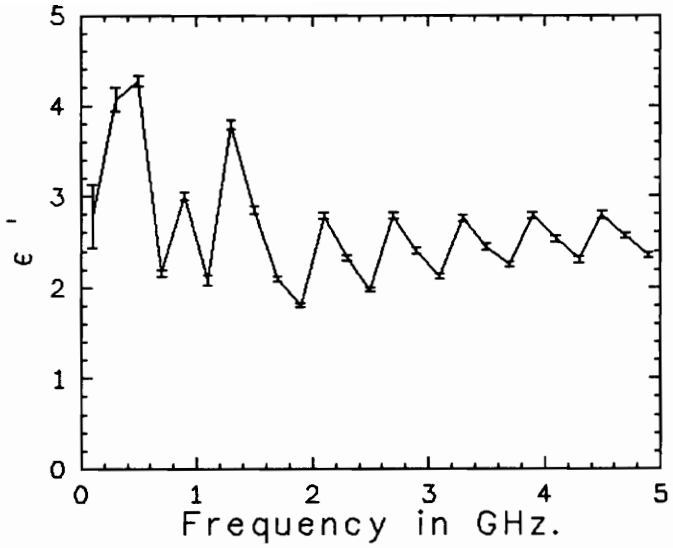

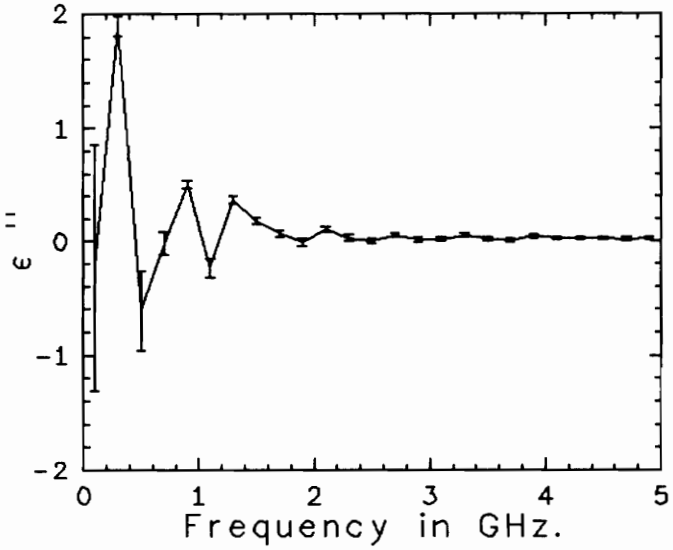

Figure 5.17: Permittivity of Dry Sand Using the Short Deconvolution - Experimental Error

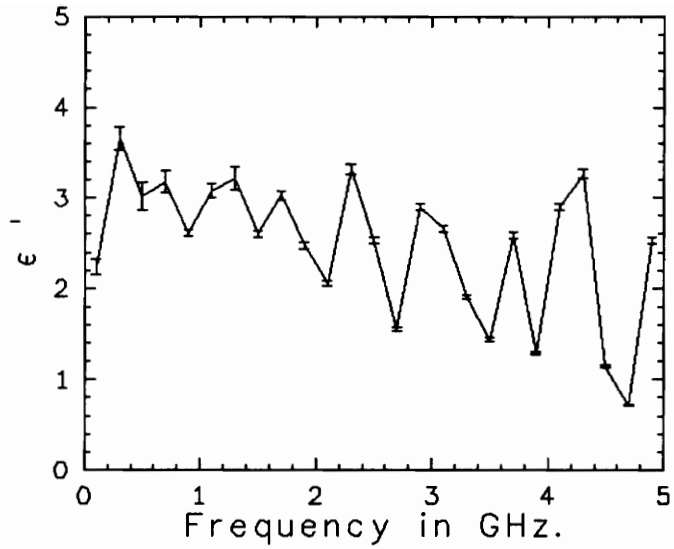

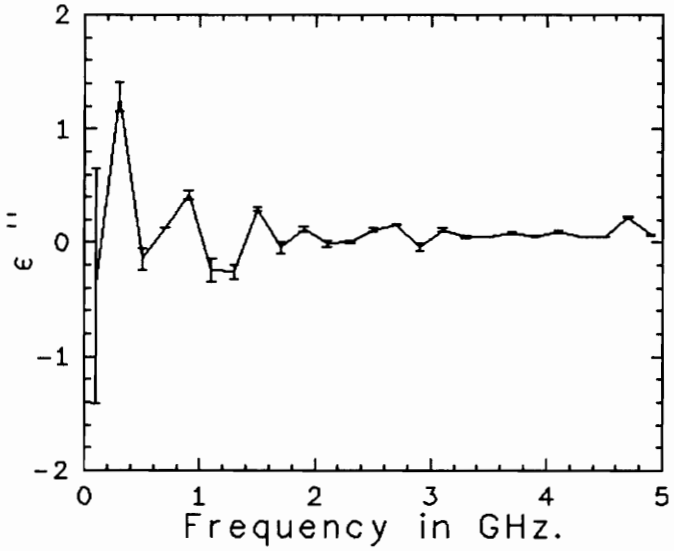

Figure 5.18: Permittivity of Dry Sand Using the Open Deembedding - Experimental Error

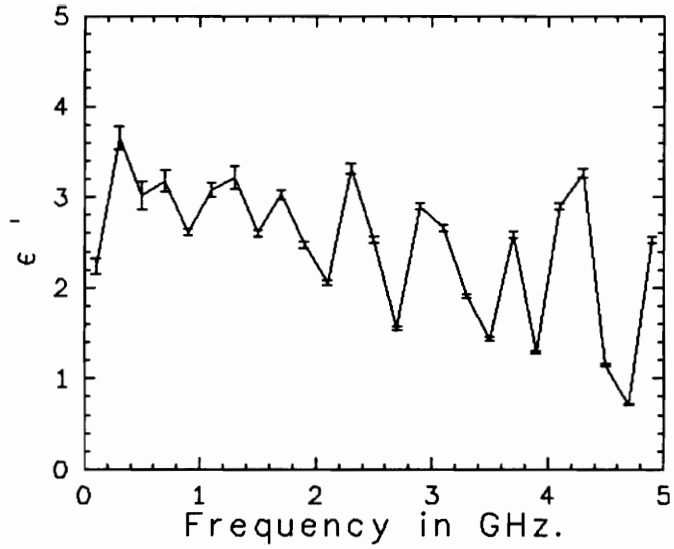

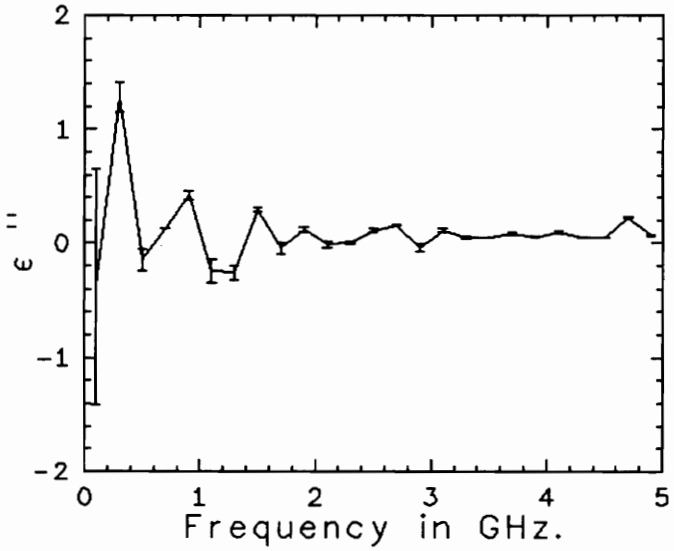

Figure 5.19: Permittivity of Dry Sand Using the Short Deembedding - Experimental Error

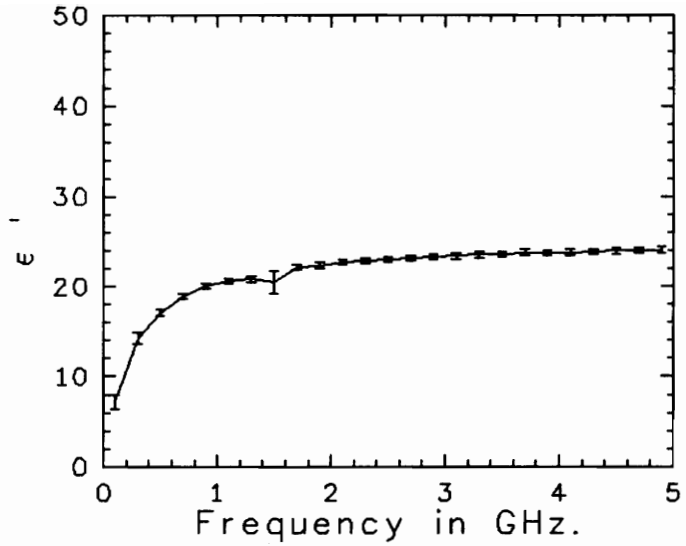

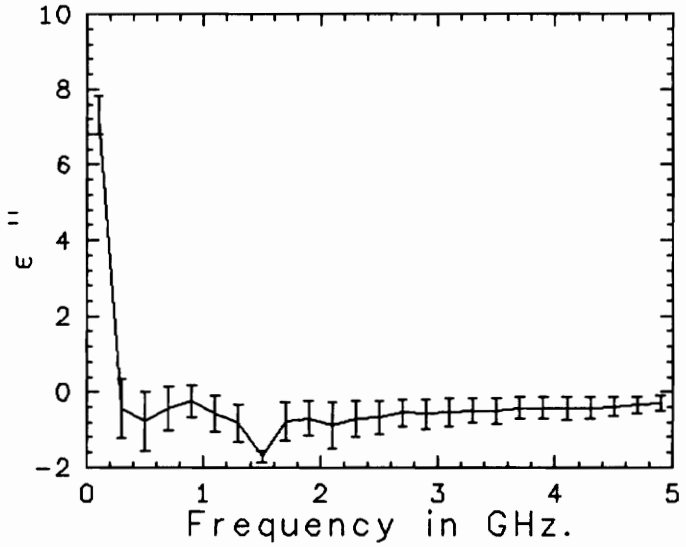

Figure 5.20: Permittivity of Wet Sand Using the Open Deconvolution - Experimental Error

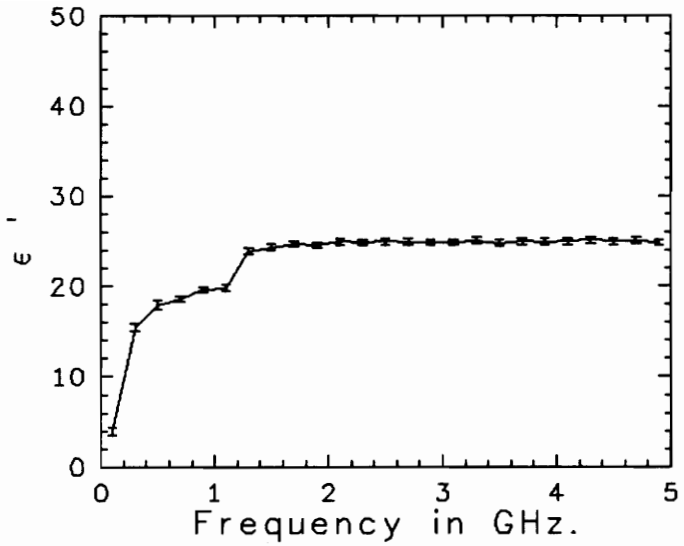

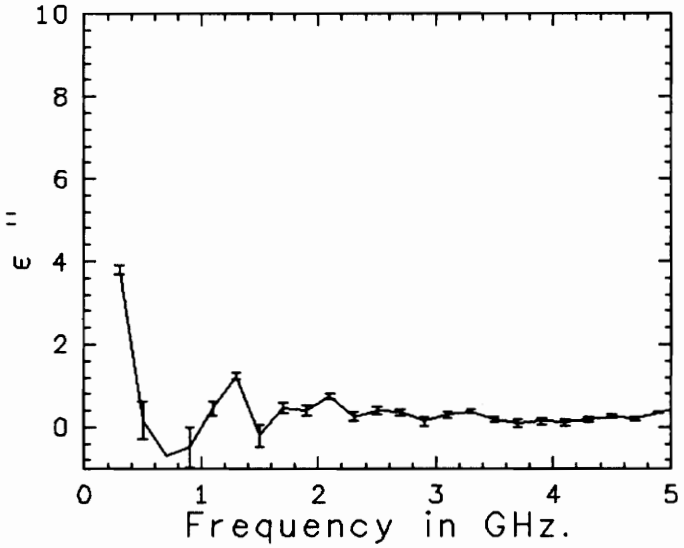

Figure 5.21: Permittivity of Wet Sand Using the Short Deconvolution - Experimental Error

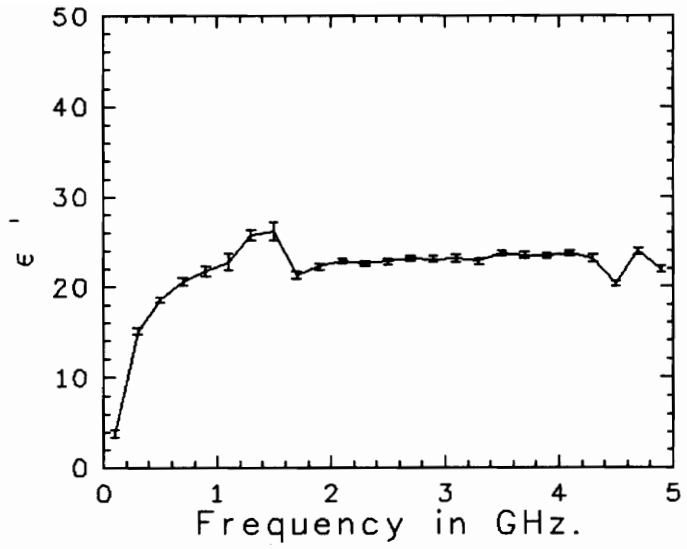

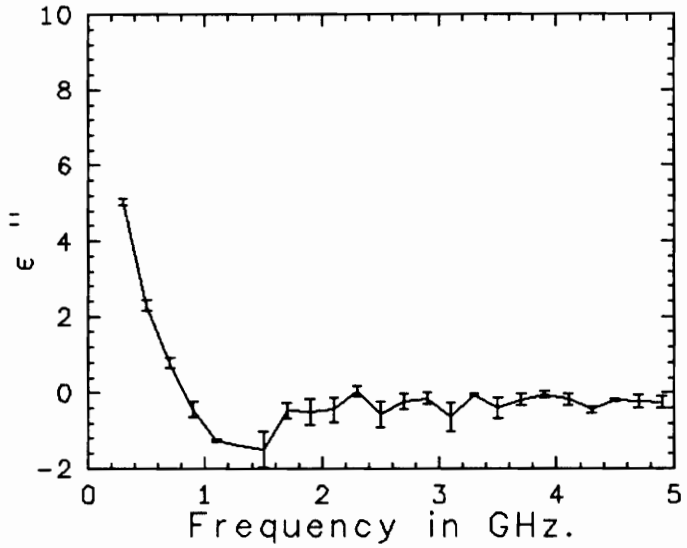

Figure 5.22: Permittivity of Wet Sand Using the Open Deembedding - Experimental Error

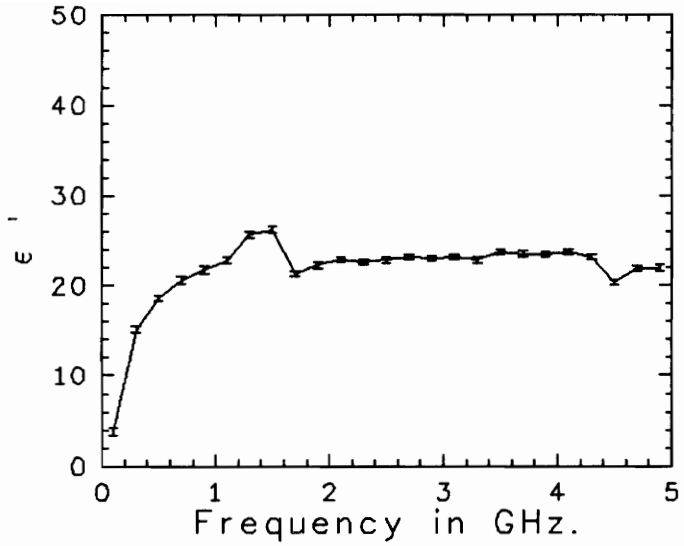

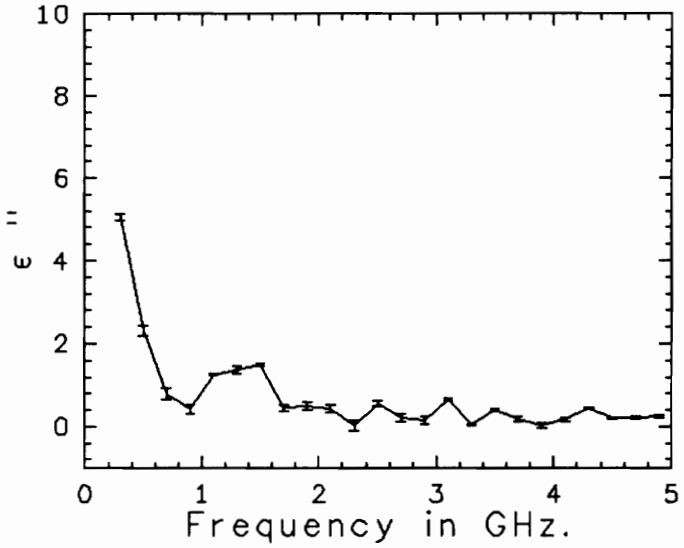

Figure 5.23: Permittivity of Wet Sand Using the Short Deembedding - Experimental Error

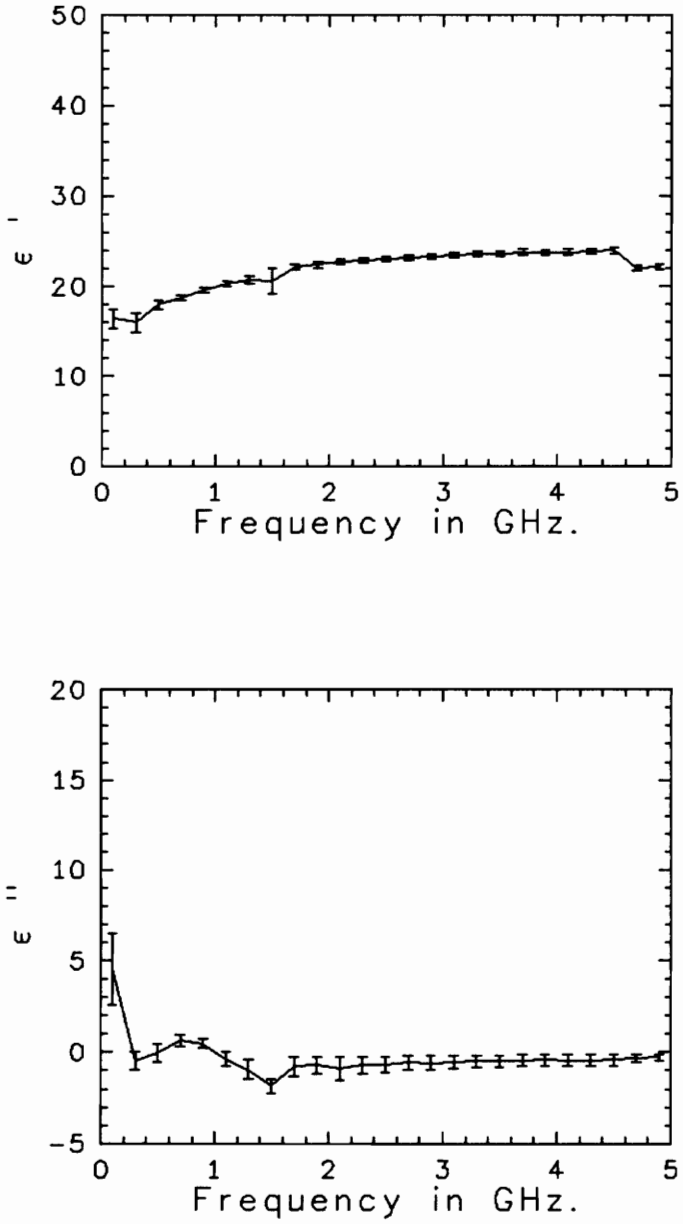

Figure 5.24: Permittivity of Saltwater Sand Using the Open Deconvolution - Experimental Error

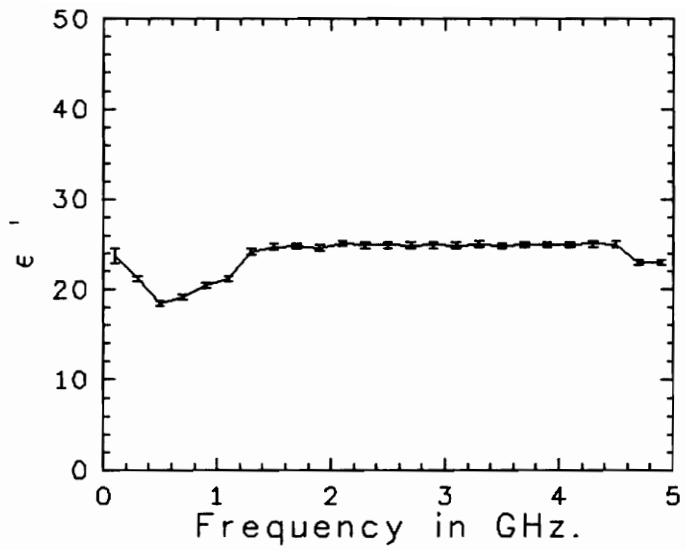

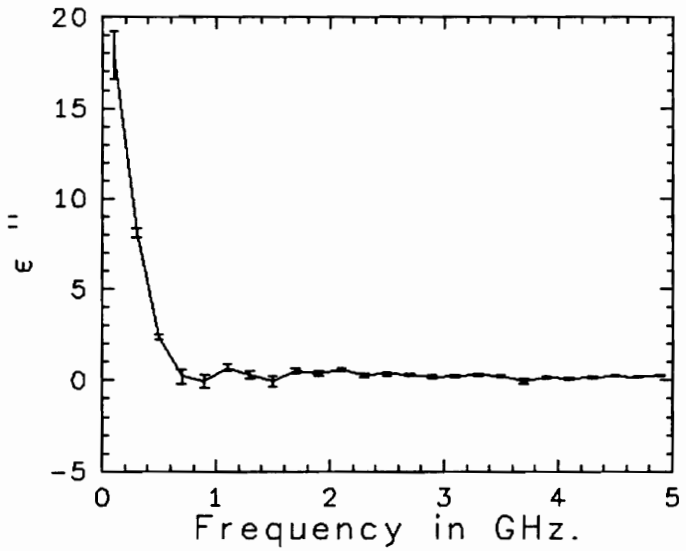

Figure 5.25: Permittivity of Saltwater Sand Using the Short Deconvolution - Experimental Error

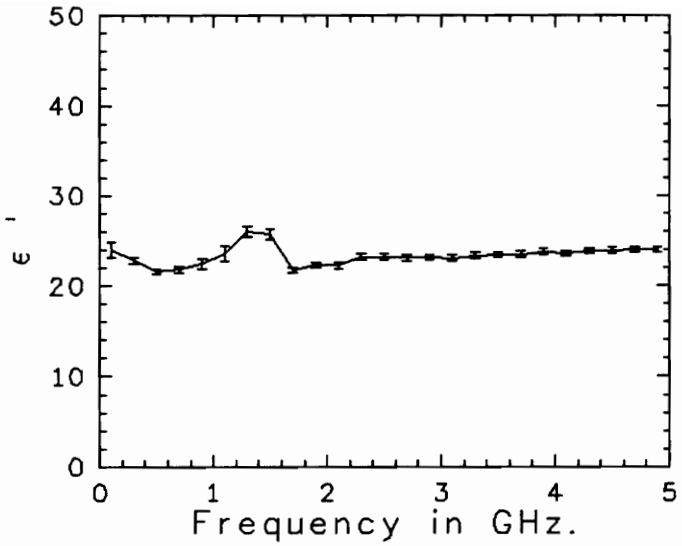

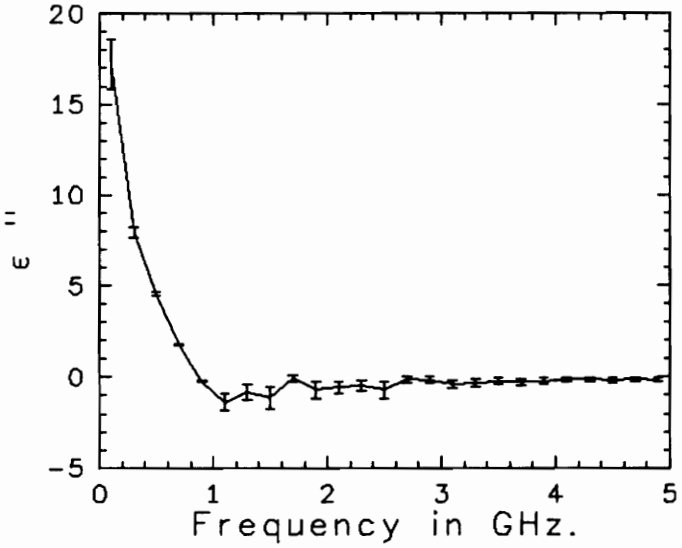

Figure 5.26: Permittivity of Saltwater Sand Using the Open Deembedding - Experimental Error

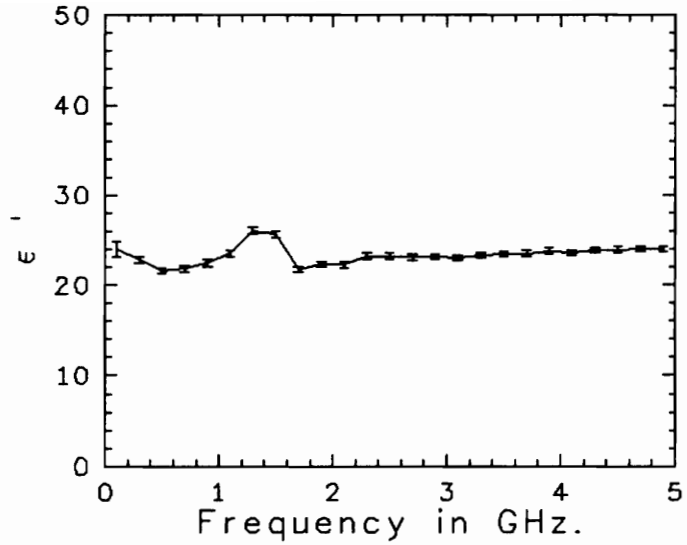

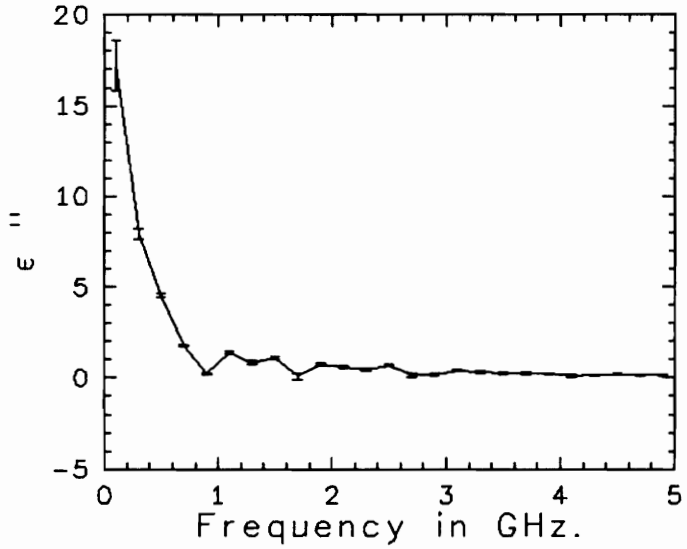

Figure 5.27: Permittivity of Saltwater Sand Using the Short Deembedding - Experimental Error

assumed instrument error bounds, but otherwise show that instrumentation error bounds are low.

The permittivity values derived using the ground probe are similar to those seen with the other two sampling devices. The wet samples are slightly lower in ϵ_R' (about 23 instead of 25) but this may be due to water loss or slight changes in the water/sand ratio with depth.

CHAPTER VI

CONCLUSION

This study was undertaken in order to evaluate the use of a dielectric probe for in-situ dielectric characterization of soils. The method used was to investigate a sample cell with well constrained fields which provided both transmission and reflection information. Measurements made with this device, the match terminated coaxial cell, were evaluated through the use of several different mathematical techniques to assess the limitations of time domain metrology in this type of measurement and to learn the strengths and weaknesses of these different mathematical algorithms. This device also offered an excellent opportunity to study the effects of frequency domain deembedding techniques in a relatively benign environment. Experiments with this device also produced baseline permittivity values for the materials studied.

An open circuited coaxial sample holder was studied next to better understand the limitations imposed by utilization of reflection information only, and to examine the special difficulties engendered by the use of a relatively long sample over this frequency range and with these particular

materials. Several potential measurement difficulties were established in the course of this investigation, and the sensitivity of the numerical root finding scheme to incorrect starting values for large values of the length-frequency-square root of epsilon product was clearly illustrated. This device was also chosen because it had previously been used in national standard quality work by a well known investigator [16].

Both of these initial investigations produced information useful in the evaluation of the balun driven twin lead ground probe. The baseline values produced by the match terminated coaxial sample cell were absolutely necessary to maintain confidence in the results produced by the other two sampling systems and to provide starting values for the iterative mathematical schemes used with them. The experience with the different aspects of frequency domain deembedding were also highly useful as deembedding is one of the two primary tools used to produce useful results from the ground probe.

The experience with the much greater length of the open circuited coaxial sample holder clarified the great importance of attention to the length - frequency - root epsilon product mentioned earlier. The difficulties encountered with long sample holders and large values of permittivity are not well described in the literature and

insight into the effect of this parameter was quite necessary in the evaluation of the ground probe. A possible error factor in the time domain instrumentation leading to oscillation in the permittivity results was also brought to light by these experiments and it is felt that this phenomenon should be further investigated.

SUMMARY

The following objectives have been achieved:

1. A method has been developed for calibrating the balun driven ground probe to achieve accurate permittivity measurements.
2. Data reduction methods for three different sample holders have been evaluated with respect to their utility in the measurement of soil samples.
3. The repeatability of a number of different measurement methods has been examined.
4. The effect of instrumentation error on each of the data reduction methods studied has been characterized.

Further investigation into the cause of the oscillation in the wet sample results should be undertaken. Methods of utilizing the time domain information directly are becoming available and would prove very useful in situations like that

of the ground probe measurements, where the lack of complete reflection information (because of the large value of the aforementioned length - frequency - root epsilon product) causes frequency domain methods to be of limited utility. It would be interesting to undertake some measurements using very short probes to determine if this would improve the characteristics of this measurement system. Finally, experiments using some well characterized materials (various alcohols and esters are often used for this purpose) should be undertaken to more fully understand the limitations of the ground probe and to better calibrate its response.

REFERENCES

[1] H. Fellner-Feldegg, "The measurement of dielectrics in the time domain," J. Phys. Chem., Vol. 73, No. 3, pp. 616-623, March 1969.

[2] H. Fellner-Feldegg and E. F. Barnett, "Reflection of a voltage step from a section of transmission line filled with a polar dielectric," J. Phys. Chem., Vol. 74, No. 9, pp. 1962-1965, April 1970.

[3] R. H. Cole, "Evaluation of dielectric behavior by time domain spectroscopy. I. Dielectric response by real time analysis," J. Phys. Chem., Vol. 79, No. 14, pp. 1459-1469, 1975.

[4] R. Chahine and T. K. Bose, "Comparative studies of various methods in time domain spectroscopy," J. Chem. Phys., Vol. 72 No. 2, pp. 808-815, January 1980.

[5] M. El Kadiri, J. P. Parneix, and A. Chapoton, "General time domain analysis of t.d.s. data: Application to liquid crystals," IEEE Trans. Instrum. Meas., Vol. IM-34, No. 1, pp. 70-74, March 1985.

[6] T. A. C. M. Claasen and M. J. C. van Gemert, "Approximate solutions in multiple reflection time domain spectroscopy," J. Chem. Phys., Vol. 63, No. 1, pp. 68-73, July 1975.

[7] R. H. Cole, "Evaluation of dielectric behavior by time domain spectroscopy. II. Complex permittivity," J. Phys. Chem., Vol. 79, No. 14, pp. 1469-1474, 1975.

[8] R. H. Cole, "Time-domain spectroscopy of dielectric materials," IEEE Trans. Instrum. Meas., Vol. IM-25, No. 4, pp. 371-375, December 1976.

[9] B. P. Kwok, S. O. Nelson, and E. Bahar, "Time-domain measurements for determination of dielectric properties of agricultural materials," IEEE Trans. Instrum. Meas., Vol. IM-28, No. 2, pp 109-112, June 1979.

[10] C. Boned and J. Peyrelasse, "Automatic measurement of complex permittivity (from 2 mhz to 8 ghz) using time domain spectroscopy," J. Phys. E: Sci. Instrum., Vol. 15, pp. 534-538, 1982.

[11] A. M. Nicolson, "Broad-band microwave transmission characteristics from a single measurement of the transient response," IEEE Trans. Instrum. Meas., Vol. IM-17, No. 4, pp. 395-402, December 1968.

[12] A. M. Nicolson and G. F. Ross, "Measurement of the intrinsic properties of materials by time-domain techniques," IEEE Trans. Instrum. Meas., Vol. IM-19, No. 4, pp. 377-382, November 1970.

[13] H. Fellner-Feldegg, "A thin-sample method for the measurement of permeability, permittivity, and conductivity in the frequency and time domain," J. Phys. Chem., Vol. 76, No. 15, pp. 2116-2122, 1972.

[14] W. B. Weir, "Automatic measurement of complex dielectric constant and permeability at microwave frequencies, Proc. IEEE, Vol. 62, No. 1, pp. 33-36, January 1974.

[15] J. Baker-Jarvis, E. J. Vanzura, and W Kissick, "Improved technique for determining complex permittivity with the transmission/reflection method," IEEE Trans. Microwave Theory Tech., Vol. 38, No. 8, pp. 1096-1103, August 1990.

[16] H. Bussey, "Dielectric measurements in a shielded open circuit coaxial line," IEEE Trans. Instrum. Meas., Vol. IM-29, No. 2, pp. 120-124, June 1980.

[17] W. R. Scott, Jr., and G. Smith, "Error corrections for an automated time-domain network analyzer," IEEE Trans. Instrum. Meas., Vol. IM-35, No. 3, pp. 300-303, September 1986.

[18] R. Chahine and T. K. Bose, "Measurement of small dielectric loss by time-domain spectroscopy: Application to water/oil emulsions," IEEE Trans. Instrum. Meas., Vol. IM-32, No. 2, pp. 360-363, June 1983.

[19] T. K. Bose, R. Chahine, M. Merabet, "Computer-based permittivity measurements and analysis of microwave power absorption in conductive dielectrics," IEEE Trans. Ins., Vol. EI-22, No. 1, pp. 41-46, February 1987.

[20] R. H. Cole, J. G. Berberian, S. Mashimo, G. Chryssikos, A. Burns, and E. Tombari, "Time domain reflection methods for dielectric measurements to 10 ghz," J. Appl. Phys., Vol. 66, No. 2, pp. 793-802, July 1989.

[21] R. Nozaki and T. K. Bose, "Broadband complex permittivity measurements by time-domain spectroscopy," IEEE Trans. Instrum. Meas., Vol IM-39, No. 6, 945-951, December 1990.

[22] B. Bianco, G. P. Drago, M. Marchesi, C. Martini, G. S. Mela, and S. Ridella, "Measurements of complex dielectric constant of human sera and erythrocytes, IEEE Trans. Instrum. Meas., Vol. IM-28, No. 4, pp 290-295, December 1979.

[23] M. A. Stuchly and S. S. Stuchly, "Coaxial line reflection methods for measuring dielectric properties of biological substances at radio and microwave frequencies - a review," IEEE Trans. Instrum. Meas., Vol. IM-29, No. 3, pp. 176-183, September 1980.

[24] J. R. Mosig, J. E. Besson, M. Gex-fabry, and F. E. Gardiol, "Reflection of an open-ended coaxial line and application to nondestructive measurements of materials," IEEE Trans. Instrum. Meas., Vol. IM-30, No. 1, pp. 46-51, March 1981.

[25] M. A. Stuchly, M. M. Brady, S. S. Stuchly and G. Gajda, "Equivalent circuit of an open-ended coaxial line in a lossy dielectric," IEEE Trans. Instrum. Meas., Vol. IM-31, No. 2, pp. 116-119, June 1982.

[26] A. Kraszewski and S. S. Stuchly, "Capacitance of open-ended dielectric-filled coaxial lines - experimental results," IEEE Trans Instrum. Meas., Vol. IM-32, No 4, pp. 517-519, December 1983.

[27] G. Gajda and S. S. Stuchly, "An equivalent circuit of an open-ended coaxial line," IEEE Trans. Instrum. Meas., Vol. IM-32, No. 4, pp. 506-508, December 1983.

[28] L. S. Anderson, G. B. Gajda, and S. S. Stuchly, "Analysis of an open-ended coaxial line sensor in layered dielectrics," IEEE Trans. Instrum. Meas., Vol. IM-35, No. 1, pp. 13-18, March 1986.

[29] E. C. Burdette, F. L. Cain and J. Seals, "In vivo probe measurement technique for determining dielectric properties at vhf through microwave frequencies," IEEE Trans. Microwave Theory Tech., Vol. MTT-28, No. 4, pp. 414-427, April 1980.

[30] D. Misra, M. Chabbra, B. Epstein, M. Mirotznik, and K. Foster, "Noninvasive electrical characterization of materials at microwave frequencies using an open-ended coaxial line: Test of an improved calibration technique," IEEE Trans. Microwave Theory Tech., Vol. 38, No. 1, pp. 8-13, January 1990.

[31] K. Staebell, M. Noffke and D. Misra, "On the in situ probe method for measuring the permittivity of materials at microwave frequencies," IEEE, pp. 28-31, 1990.

[32] K. Staebell and D. Misra, "An experimental technique for in vivo permittivity measurement of materials at microwave frequencies," IEEE Trans. Microwave Theory and Tech., Vol. 38, No. 3, pp. 337-339, March 1990.

[33] N. R. V. Nightingale, S. Szwarnowski, R. J. Sheppard and E. H. Grant, "A coaxial line cell for measuring the permittivity of medium to high loss liquids in the frequency range 2 to 15 ghz," J. Phys. E: Sci. Instrum., Vol. 14, pp. 156-160, 1981.

[34] L. P. Ligthart, "A fast computational technique for accurate permittivity determination using transmission line methods," IEEE Trans. Microwave Theory Tech., Vol. MTT-31, No. 3, pp. 249-254, March 1983.

[35] M. Steel, R. J. Sheppard and E. H. Grant, "A precision method for measuring the complex permittivity of solid tissue in the frequency domain between 2 and 18 ghz," J. Phys. E: Sci. Instrum., Vol. 17, pp. 30-34, 1984.

[36] S. Chao, "An uncertainty analysis for the measurement of microwave conductivity and dielectric constant by the short-circuited line method," IEEE Trans. Instrum. Meas., Vol. IM-35, No. 1, pp. 36-41, March 1986.

[37] B. B. Szendrenyi, K. Kazi and I. Mojzes, "An alternative broadband method for automatic measurement of the complex permeability and permittivity of materials at microwave frequencies," IEEE MTT-S Digest, Vol. II, pp. 743-746, May 1988.

[38] M. F. Iskander and S. S. Stuchly, "A time-domain technique for measurement of the dielectric properties of biological substances," IEEE Trans. Instrum. Meas., Vol. IM-21, No. 4, pp. 425-429, November 1972.

[39] G. Voss and H. Happ, "Time domain spectroscopy (tds) of dielectric properties up to 15 ghz with voltage pulses. Application to solids and liquids," J. Phys. E: Sci. Instrum., Vol. 17, pp. 981-983, 1984.

[40] S. S. Stuchly and M. F. Iskander, "Permittivity measurements at microwave frequencies using lumped elements," IEEE Trans. Instrum. Meas., Vol. IM-23, No. 1, pp. 56-62, March 1974.

[41] M. A. Rzepecka and S. S. Stuchly, "A lumped capacitance method for the measurement of the permittivity and conductivity in the frequency and time domain - a further analysis," IEEE Trans. Instrum. Meas., Vol. IM-24, No. 1, pp. 27-32, March 1975.

[42] N. Belhadj-tahar, A. Fourrier-Lamer and H. De Chanterac, "Broad-band simultaneous measurement of complex permittivity and permeability using a coaxial discontinuity," IEEE Trans. Microwave Theory Tech., Vol. 38, No. 1, pp. 1-7, January 1990.

[43] S. Olson and M. F. Iskander, "A new in situ procedure for measuring the dielectric properties of low permittivity materials," IEEE Trans. Instrum. Meas., Vol. IM-35, No. 1, pp. 2-6, March 1986.

[44] G. S. Smith and J. D. Nordgard, "Measurement of the electrical constitutive parameters of materials using antennas," IEEE Trans. Antenna Propagat., Vol. 33, No. 7, pp. 783-792, July 1985.

[45] E. J. Kirkscether, "Ground constant measurements using a section of balanced two-wire transmission line," IRE Trans. Antenna Propagat., Vol. 8, No. 3, pp. 307-312, May 1960.

[46] P. N. Hill and H. E. Green, "In situ measurement of soil permittivity and permeability," J. Elec. Electron. Aus., Vol. 2, No. 4, pp. 202-208, December 1982.

[47] A. Sihvola and M. Tiuri, "Snow fork for field determination of the density and wetness profiles of a snow pack," IEEE Trans. Geosci. Remote Sensing, Vol. 24, No. 5, pp 717-721, September 1986.

[48] F. N. Dalton, W. N. Herkelrath, D. S. Rawlins, and J. D. Rhoades, "Time-domain reflectometry: Simultaneous measurement of soil water content and electrical conductivity with a single probe," Science, Vol. 224, pp. 989-990, June 1984.

[49] N. S. Nahman, "Introduction to time domain measurements and applications", Course Notes EE 593, The University of Colorado, Spring 1978.

[50] W. L. Gans and N. S. Nahman, "Continuous and discrete fourier transforms of steplike waveforms", IEEE Trans. Instrum. Meas., IM-31, pp. 97-101, June 1982.

[51] R. J. Vernon, and S. R. Seshadri, Proc. IEEE (Letters), vol. 57, pp. 101-102, January 1969.

[52] P. I. Somlo, and J. D. Hunter, "Condition for reflection coefficient magnitude greater than one for passive transmission line and passive load," IEEE Trans. Instrum. Meas., Vol. IM-30, No. 3, pp. 230-231, September 1981.

[53] R. L. Jesch, "Dielectric measurements of five different soil textural types as functions of frequency and moisture content," Technical Report NBSIR 78-896, National Bureau of Standards, Boulder, CO, October 1978.

[54] R. J. Lytle, "Measurement of earth medium electrical characteristics: Techniques, results, and applications," Technical Report VCRL-51479, Lawrence Livermore Laboratory, Livermore, CA, November 12, 1973.

[55] J. R. Birchak, C. G. Gardner, J. E. Hipp, and J. M. Victor, "High dielectric constant microwave probes for sensing soil moisture," Proc. IEEE, Vol. 62, No. 1, pp. 93-98, January 1974.

[56] W. R. Scott, Jr., and G. S. Smith, "Measured electrical constitutive parameters of soil as functions of frequency and moisture content," Georgia Institute of Technology, Atlanta, GA, 1991.

[57] P. I. Somlo, "The discontinuity capacitance and the effective position of a shielded open circuit in a coaxial line," Proc. Inst. Radio Elec. Eng. Australia, Vol. 28, pp. 7-9, January 1967.

[58] A. Stogryn, "Equations for calculating the dielectric constant of saline water," IEEE Trans. Microwave Theory Tech., Vol. MTT-19, pp. 733-736, August 1971.

[59] D. M. Kerns, Plane-wave scattering-matrix theory of antennas and antenna-antenna interactions, Nat. Bur. Stand. (U.S.) Monograph 162 (June 1981).

APPENDICES

APPENDIX A

PROGRAM TO DEEMBED TEFLON WASHER EFFECTS FROM TERMINATED COAXIAL SAMPLE HOLDER MEASUREMENTS

```
load va.fft; % Load Fourier transformed reflection waveform
load vs.fft; % Load Fourier transformed reflection
             % reference waveform
load vb.fft; % Load Fourier transformed transmission
             % waveform
load vi.fft; % Load Fourier transformed transmission
             % reference waveform
%
j=sqrt(-1);
va=va(:,1)+j*va(:,2); % Convert two column
vb=vb(:,1)+j*vb(:,2); % storage to Real +
vi=vi(:,1)+j*vi(:,2); % j*Imaginary
vs=vs(:,1)+j*vs(:,2);
%
s1c=-va./vs; % Evaluate S11 of teflon-sample-teflon
             % composite
%
for i=1:50;
```

```
jwc(i)=(-j*(2*i-1)*2*pi/299.792458);
end;
jwc=jwc.';
s2c2=(vb.*exp(2*.84*jwc))./vi; % Phase adjustment to
                               % evaluate S^2_21 of
                               % teflon-sample-teflon
                               % composite
%
s2c2=sqrt(s2c2);               % Evaluate square root
%
for i=2:50;                    % Make it continuous
if abs(s2c2(i-1)-s2c2(i)) > abs(s2c2(i-1)+s2c2(i)) ;
s2c2(i)=-s2c2(i);
end;
end;
%
u=ones(s1c);
rt=(1-sqrt(2.03))/(1+sqrt(2.03)); % Teflon reflection
                                  % coefficient
taut=exp(.2*sqrt(2.03)*jwc);      % Teflon propagation
                                  % constant
%
s1t=((u-taut.^2)*rt)./(u-(rt*taut).^2); % S11 of teflon
                                       % washer
```

```
s2t=((u-rt^2).*taut)./(u-(rt*taut).^2); % S21 of teflon
                                        % washer
%
for i=1:50;
tt=(1/s2t(i))*[s2t(i)^2-s1t(i)^2 s1t(i) ; -s1t(i) 1];
%
% T matrix for one teflon washer
%
ts=(1/s2c2(i))*[s2c2(i)^2-s1c(i)^2 s1c(i) ; -s1c(i) 1];
%
% T matrix for teflon-sample-teflon composite
%
td=inv(tt)*ts*inv(tt);  % Deembed teflon washers
%
s1(i)=td(1,2)/td(2,2);  % Recover sample S parameters
s2(i)=1.0/td(2,2);
%
end;
```

APPENDIX B

THE MODIFIED COLE'S METHOD

Cole points out in [7,8] that a section of uniform transmission line may be modeled as a symmetrical four terminal network with an input admittance of:

$$Y_{in} = \frac{Y_o + Y_d}{1 + Z_s Y_d} \qquad \text{(B.1)}$$

where Y_o is the open circuit admittance of the section, Z_s is the short circuit impedance, and Y_d is the terminating admittance of the section. It is also true that

$$Y_o = j\omega C_c d\epsilon^* \left(\frac{\tanh x}{x} \right) \qquad \text{(B.2)}$$

and

$$Z_s = j\omega L_c d \left(\frac{\tanh x}{x} \right) \qquad \text{(B.3)}$$

where L_c and C_c are geometric inductance and capacitance factors, and

$$x = j\omega d\sqrt{\epsilon^*}\sqrt{L_c C_c} = j\frac{\omega d\sqrt{\epsilon^*}}{C} \qquad \text{(B.4)}$$

since $C = \frac{1}{\sqrt{L_c C_c}}$.

It is also possible to relate the input admittance of the line section to the incident and reflected voltages seen at one end of the line. This gives

$$Y_{in} = G_c \frac{V - R}{V + R} \qquad G_c = \sqrt{\frac{C_c}{L_c}} \qquad \text{(B.5)}$$

These equations may be combined algebraically to give

$$\epsilon^* + \frac{Y_d}{j\omega C_c d} x \coth x = \frac{C}{j\omega d}\left(\frac{V - R}{V + R}\right)(x \coth x + j\omega L_c Y_d d) \qquad \text{(B.6)}$$

which produces

$$\epsilon^* = 1 - \frac{2C}{j\omega d}\left[\frac{R}{V + R}\right]\left[x \coth x + j\frac{\omega d}{C}\right] \qquad \text{(B.7)}$$

for the case of the matched line where $Y_d = G_c$.

The difficulty in the present experiment arises from the fact that the teflon washer which is present at the distal end of the sample forces

$$Y_d = G_c \sqrt{\epsilon_t} \left[\frac{1 + \sqrt{\epsilon_t} \tanh\left(j \frac{\omega l_t \sqrt{\epsilon_t}}{c}\right)}{\sqrt{\epsilon_t} + \tanh\left(j \frac{\omega l_t \sqrt{\epsilon_t}}{c}\right)} \right] \qquad \textbf{(B.8)}$$

$$= p\, G_c$$

where ϵ_t is the dielectric constant of teflon (2.03) and l_t is the thickness of the teflon washer (2 mm.). In addition, the teflon washer at the proximal end of the sample eliminates direct access to the incident and reflected waveforms. In this case one must rely instead on the admittance seen at the scope end of the teflon washer which may be transformed to the admittance which would be seen at the proximal end of the sample by using

$$Y_{sample} = G_c \sqrt{\epsilon_t} \left[\frac{Y_m - G_c \sqrt{\epsilon_t} \tanh\left(j \frac{\omega l_t \sqrt{\epsilon_t}}{c}\right)}{G_c \sqrt{\epsilon_t} - Y_m \tanh\left(j \frac{\omega l_t \sqrt{\epsilon_t}}{c}\right)} \right] \qquad \textbf{(B.9)}$$

where Y_m represents the admittance measured at the scope end of the proximal teflon washer and Y_{sample} is the admittance which would be measured at the sample plane.

The entire modified algorithm proceeds as follows:

1. Evaluate the admittance at the scope end of the

teflon washer by using $Y_m = G_c \frac{1 - \rho}{1 + \rho}$ where ρ is defined as the ratio of the Fourier transforms of the reflected response waveform and the transmitted excitation waveform.

2. Use equation B.9 to evaluate the admittance which would be seen at the proximal sample plane in the absence of the scope end teflon washer.

3. Use an iterative numerical root finding method to invert the modified Cole equation which is (after some algebraic manipulation):

$$\epsilon^* = \frac{(Y_{sample} - p)\sqrt{\epsilon^*}}{\tanh\left(j\frac{\omega d\sqrt{\epsilon^*}}{c}\right)} + Y_{sample}\, p \qquad \text{(B.10)}$$

where Y_{sample} is given by equation B.9.

APPENDIX C

ANALYSIS OF SHIELDED OPEN-CIRCUIT SAMPLE HOLDERS FOR DIELECTRIC AND MAGNETIC MEASUREMENTS *

James Baker-Jarvis
Electromagnetic Fields Division
National Institute of Standards and Technology
Division 813.02
Boulder, CO 80303-3328

Robert Stafford
Graduate Student - Department of Electrical Engineering
Virginia Polytechnic Institute and State University
Blacksburg, VA 24061

December 23, 1991

CONTENTS

ABSTRACT

The open-circuit sample holder is useful for measuring the permittivity and permeability of fluids and powders. Past theoretical formulations of the open-circuit holder used an admittance transformation through the various regions of the holder. In this report we express the problem in terms of a dominant mode scattering formulation and develop a single expression for the reflection coefficient in terms of bead and sample parameters. This formulation eliminates the need to transform through the various sections of the sample holder. We also extend the formulation to include magnetic measurements and present a differential uncertainty analysis. The uncertainty analysis indicates a decrease in relative uncertainty as a function of increasing sample length and as a function of frequency. The uncertainty in the lower frequency range places a limitation on the method. For lower frequencies there is a very small phase shift over the length of a sample. Therefore the real part of the permittivity at low frequencies is very sensitive to measured phase and sample length. For low-loss materials the imaginary part of the permittivity is not extremely sensitive to the sample length, whereas the real part of the permittivity is

sensitive. For high-loss materials both the real and the imaginary part of the permittivity are relatively sensitive to the sample lengths. The minima of the reflection coefficient for low-loss materials occurs at $n\lambda_m/2$, where $n = 1,2,3....$ These minima in the reflection coefficient correspond to regions of minimum uncertainty in the permittivity for low-loss materials. Therefore the minimum uncertainty for low-loss materials occurs at frequencies where there is maximal interaction of the fields with the sample.

Key words: Calibration; coaxial line; dielectric constant; loss factor; microwave measurements; permeability measurement; permittivity measurement; reflection method; short-circuit; transmission; uncertainty; waveguide.

APPENDIX D

HIGH ORDER MODE RESONANCES IN THE SHIELDED OPEN CIRCUITED COAXIAL SAMPLE HOLDER

The shielded open circuited coaxial sample holder (figure D.1) comprises two different transmission line structures, both of which must be analyzed with respect to non-TEM mode propagation and resonance. The first portion of the sample holder is a 14 mm. 50 ohm coaxial line of length 9.15 cm. which begins at a compensated teflon bead and is terminated in a circular waveguide structure. The second portion is a 14 mm. circular waveguide which is 4.83 cm. in length.

From [1] the characteristic impedance of an air filled coaxial line is

$$Z_0 = 60 \ln\left(\frac{r_o}{r_i}\right) \qquad \textbf{(D.1)}$$

where r_o and r_i represent the inner radius of the outer conductor and the radius of the inner conductor, respectively. Evaluating this equation for a 50 ohm line produces a value for the r_o/r_i ratio of 2.3 where r_0 in this

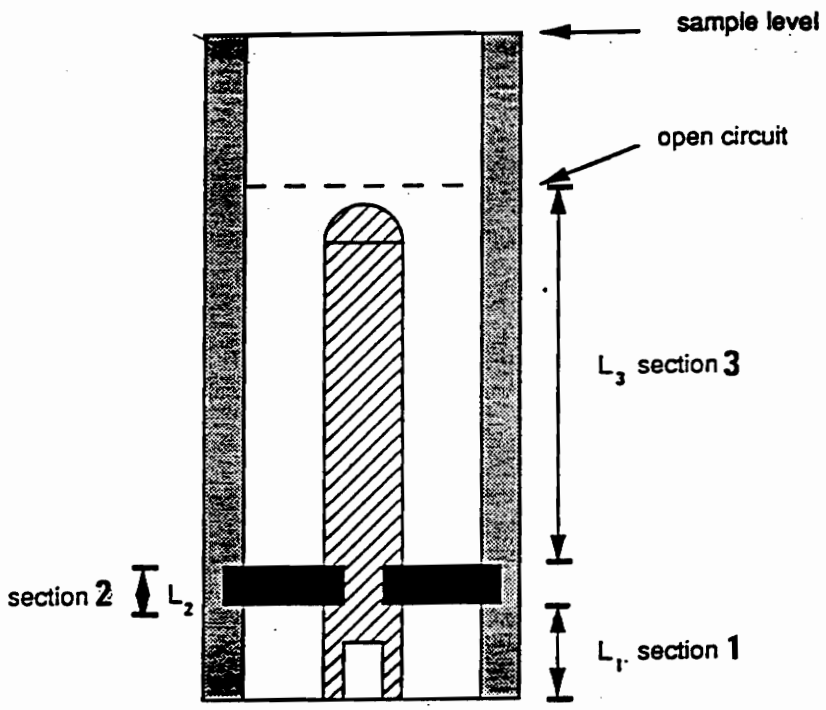

Figure D.1: The Shielded Open Circuited Coaxial Sample Holder

Table D.1: Coaxial Cutoff Frequencies

	air $\epsilon_R'=1.0$	dry sand $\epsilon_R'=3$	wet sand $\epsilon_R'=25$
TE_{11}	f_c=9.74 GHz.	f_c=5.62 GHz.	f_c=1.95 GHz.
TE_{21}	f_c=18.47 GHz.	f_c=10.66 GHz.	f_c=3.69 GHz.
TE_{31}	f_c=27.12 GHz.	f_c=15.66 GHz.	f_c=5.42 GHz.
TM_{01}	f_c=35.71 GHz.	f_c=20.62 GHz.	f_c=7.14 GHz.

Table D.2: Circular Waveguide Cutoff Frequencies

	air $\epsilon_R'=1.0$	dry sand $\epsilon_R'=3$	wet sand $\epsilon_R'=25$
TE_{11}	f_c=12.56 GHz.	f_c=7.25 GHz.	f_c=2.51 GHz.
TE_{21}	f_c=20.83 GHz.	f_c=12.03 GHz.	f_c=4.17 GHz.
TE_{01}	f_c=26.14 GHz.	f_c=15.09 GHz.	f_c=5.23 GHz.
TM_{01}	f_c=16.40 GHz.	f_c=9.47 GHz.	f_c=3.28 GHz.

It is clear from these tables that the cutoff frequencies for modes TE_{11} and TE_{21} in the coaxial portion of the line are exceeded in this experiment for the case where the sample is wet sand. Similarly, the circular waveguide portion of the sample holder can support propagation of the TE_{11}, TE_{21}, and TM_{01} modes in the wet sand samples at frequencies within the 5 GHz. upper limit of this investigation.

Previous experience indicates that high order mode effects are most noticeable at resonance, i.e. where the length of the waveguide represents an integer number of half guide wavelengths ($\lambda_g/2$). The lowest resonant frequency for a given mode will be that frequency at which $\lambda_g = 2\ l$ where l is the length of the guide. The guide wavelength for high order modes is given by

$$\lambda_g = \frac{\lambda}{\sqrt{1 - \left(\frac{\lambda}{\lambda_c}\right)^2}} \qquad \textbf{(D.2)}$$

where all values are for free space.

Setting $\lambda_g = 2\ l$ and $\lambda = c/f$ leads to a solution for the lowest resonant frequency at any mode

$$f_{resonance} = \sqrt{\left(\frac{c}{2l}\right)^2 + f_c^2} \qquad \textbf{(D.3)}$$

This resonant frequency is scaled by the square root of the real part of the permittivity to produce table D.3. It should be noted that the circular waveguide section of the sample holder looks like a capacitive load on the coaxial line section for frequencies below cutoff, and this effect will lower the resonant frequencies of the coaxial line slightly.

In any case, it is clear from table D.3 that no resonances are present which could account for the 600 MHz. oscillation in the sample holder. It is true that the TEM mode resonance of the coaxial portion of the sample holder occurs at 328 MHz when the dielectric is wet sand, but this effect is already accounted for in the equations used and thus could not be the cause of the oscillation in the derived permittivity data.

Table D.3: Resonant Frequencies for High Order Modes

	Coaxial Resonance l=9.15 cm.		Circular Resonance l=4.73 cm.	
	air	wet sand	air	wet sand
TE_{11}	f_{res}=9.88 GHz.	f_{res}=1.98 GHz.	f_{res}=12.95 GHz.	f_{res}=2.59 GHz.
TE_{21}	f_{res}=18.54 GHz.	f_{res}=3.71 GHz.	f_{res}=21.07 GHz.	f_{res}=4.21 GHz.
TM_{01}	f_{res}=35.75 GHz.	f_{res}=7.15 GHz.	f_{res}=16.70 GHz.	f_{res}=3.34 GHz.

REFERENCES

[1] Ramo, S., Whinnery, J. R., Van Duzer, T., Fields and Waves in Communication Electronics (John Wiley & Sons, Inc., New York, 1965).

[2] Moreno, T., Microwave Transmission Design Data (McGraw-Hill Book Company, Inc., New York, 1948).

VITA

Robert Bruce Stafford was born in Fremont, Ohio on December 19, 1952. He received the Bachelor of Science in Engineering and the Master of Science in Engineering degrees from the University of Central Florida, Orlando, FL in 1978 and 1979 respectively. He worked as a design engineer for Emerson Electric Company from 1980 to 1981. From 1981 to 1984 he worked as an instructor in the Bradley Department of Electrical Engineering, Virginia Polytechnic Institute and State University, Blacksburg, VA. He worked for the Electromagnetics Division, National Institute of Standards and Technology, Boulder, CO from 1986 to 1991 as an electrical engineer and guest researcher.

Robert B. Stafford